SYNTHESIS AND CURE CHARACTERIZATION OF HIGH TEMPERATURE POLYMERS FOR AEROSPACE APPLICATIONS

A Dissertation

by

YUNTAO LI

Submitted to the Office of Graduate Studies of
Texas A&M University
in partial fulfillment of the requirements for the degree of

DOCTOR OF PHILOSOPHY

December 2004

Major Subject: Materials Science and Engineering

SYNTHESIS AND CURE CHARACTERIZATION OF HIGH TEMPERATURE POLYMERS FOR AEROSPACE APPLICATIONS

A Dissertation

by

YUNTAO LI

Submitted to Texas A&M University
in partial fulfillment of the requirements
for the degree of

DOCTOR OF PHILOSOPHY

Approved as to style and content by:

Roger J. Morgan (Co-Chair of Committee)	Hung-Jue Sue (Co-Chair of Committee)
Steve Suh (Member)	Joseph H. Ross, Jr. (Chair of Materials Science and Engineering Faculty)
Michael A. Bevan (Member)	

December 2004

Major Subject: Materials Science and Engineering

ABSTRACT

Synthesis and Cure Characterization of High Temperature Polymers

for Aerospace Applications. (December 2004)

Yuntao Li, B.S., Lanzhou University; M.S., Lanzhou University

Co-Chairs of Advisory Committee: Dr. Roger J. Morgan
Dr. Hung-Jue Sue

The E-beam curable BMI resin systems and phenylethynyl terminated AFR-PEPA-4 oligomer together with an imide model compound N-phenyl-[4-(phenylethynyl) phthalimide] were synthesized and characterized.

E-beam exposure cannot propagate the polymerization of BMI system until the temperature goes up to 100^{o}C. However, a small amount of oligomers may be generated from solid-state cure reaction under low E-beam intensity radiation. Higher intensity E-beam at 40 kGy per pass can give above 75% reaction conversion of BMI with thermal cure mechanism involved.

NVP is a good reactive diluent for BMI resin. The cure extents of BMI/NVP increase with the increase of the dosage and applied dosage per pass. The reaction rate is much higher at the beginning of the E-beam cure and slows down after 2 dose passes due to diffusion control. Free radical initiator dicumyl peroxide can accelerate the reaction rate at the beginning of E-beam cure reaction but doesn't affect final cure conversion very much. According to the results from FT-IR, 200 kGy total dosage E-

beam exposure at 10 kGy per pass can give 70% reaction conversion of BMI/NVP with the temperature rise no more than 50^{o}C. The product has a T_g of 180^{o}C.

The predicted ultimate T_g of cured AFR-PEPA-4 polyimide is found to be 437.2^{o}C by simulation of DSC T_g as a function of cure. The activation energy of thermal cure reaction of AFR-PEPA-4 oligomer is 142.6 ± 10.0 kJ/mol with the kinetic order of 1 when the reaction conversion is less than 80%.

The kinetics analysis of the thermal cure of N-phenyl-[4-(phenylethynyl) phthalimide] was determined by FT-IR spectroscopy by following the absorbance of the phenylethynyl triple bond and conjugated bonds. The thermal crosslinking of N-phenyl-[4-(phenylethynyl) phthalimide] through phenylethynyl addition reaction has a reaction order of 0.95 and an activation energy of 173.5 ± 8.2 kJ/mol. The conjugated bond addition reactions have a lower reaction order of 0.94 and lower activation energy (102.7 ± 15.9 kJ/mol). The cure reaction of N-phenyl-[4-(phenylethynyl) phthalimide] can be described as a fast first-order reaction stage followed by a slow second stage that is kinetically controlled by diffusion.

ACKNOWLEDGEMENTS

Funding for this research was made primarily from the Air Force Office of Scientific Research (AFOSR) grant numbers F49620-01-1-0180 and FA 9550-04-1-0137, under Dr. Charles Lee. Their support was greatly appreciated by both colleagues and me who were funded by these resources.

I would like to thank my co-advisor, Dr. Roger J. Morgan. He has acted as a mentor and a source of knowledge, opinions, assistance, and guidance. I thank him for his help and support throughout my research and life during my studies in Texas A&M University. His loyalty to his students will leave a long-lasting impression on me. I would like to thank my co-advisor, Dr. Hung-Jue Sue. His continuous efforts to be on the edge of cutting technology motivates me to do the best that I can and to stay on the top of the latest developments in science and technology. His guidance and suggestions were extremely valuable to me throughout this research. I appreciate the numerous contributions from all members of my advisory committee, Dr. Steve Suh and Dr. Michael A. Bevan, in my learning experience during my study and research at Texas A&M University.

I would like to thank Francisco Tschen. His hard work and willingness during his undergraduate and graduate study helped a lot for this research. I am very grateful to the post-docs, graduate students and undergraduate students in the Polymer Technology Center. Especially to Dr. Jim Lu, Allan Moyse, Minhao Wong, Goyteck Lim, Lindsey

Murphy and Charles Tapp, for their assistance and friendship. Also special thanks to Kelly Strickland for her kind assistance on many aspects.

I would also like to thank Dr. Abraham Clearfield, Dr. Kim Dunbar and Dr. David. E. Bergbreiter in the Chemistry Department for allowing me to use their facilities. I am grateful to the help from Kang-Shyang Liao and Joy Heising. Their suggestions and instrumental analysis are very valuable for this research.

I would also like to express thanks to Dr. Jason Lincoln for his information and comments on my research.

I am very grateful to my parents, Deai Li and Yuqin Liu, for their willingness to provide an excellent education and continuous support for me. They taught me to be observant of the world around me and encourage me not only in science and math but also in the visual arts. I have so much gratitude towards my brother, Yunhai Li, who encourages and helps me all the time. I am also utterly thankful to my girlfriend, June Pan. Her love, support, patience and encouragement were so valuable to me. Finally, I would like to thank all my family and friends for their loyalty, support and company.

TABLE OF CONTENTS

Page

ABSTRACT iii

ACKNOWLEDGEMENTS v

TABLE OF CONTENTS vii

LIST OF FIGURES x

LIST OF TABLES xv

CHAPTER

I INTRODUCTION 1

1.1 Background 1
1.2 Research Goals 4

II LITERATURE REVIEW 7

2.1 Introduction 7
2.2 General Considerations of High-temperature Composite Materials 7
2.3 Present/Future Aerospace Applications 10
2.4 History and Classification of Polyimides 15
2.4.1 Kapton Polyimide 15
2.4.2 Avimid N Polyimide 16
2.4.3 Norbornyl End-capped Polyimides 17
2.4.4 Acetylene End-capped Polyimides 20
2.4.5 BMI Based Diels-Alder Systems 24
2.5 Fundamentals of Imide Synthesis 25
2.5.1 Formation of Poly(amic acid)s 25
2.5.2 Thermal Imidization 29
2.6 Fundamentals of Structure-Property Relationships of Polyimides 30
2.6.1 Degradation and Stability of Polyimides 31
2.6.2 Effect of Polyimide Structure on Crystallinity 37
2.6.3 Effect of Polyimide Structure on Solubility and Processability 39
2.7 Chemistry of Bismaleimides 42
2.7.1 Introduction 42
2.7.2 Backbone Modifications of BMIs 44
2.7.3 Cure Mechanism of BMPM/DABPA Bismaleimides 48

CHAPTER Page

2.8 Electron Beam Cure Technique for Space Applications 51
2.8.1 Introduction of Radiation Chemistry 51
2.8.2 Radiation Sources for Curing of Polymer Composites 53
2.8.3 Characteristics of E-beam Curing of Polymer Composites 55
2.8.4 Development of E-beam Curable Polymer Matrices for Aerospace Applications 58

III STUDY OF E-BEAM CURABLE BISMALEIMIDE RESINS 62

3.1 Introduction 62
3.2 Experimental 63
3.2.1 Materials 63
3.2.2 E-beam Curing 65
3.2.3 Characterizations 67
3.3 Results and Discussion 68
3.3.1 E-beam Curing of BMI Systems 68
3.3.2 E-beam Curing of BMI/NVP Systems 74
3.3.3 E-beam Curing of BMI/styrene Systems 81
3.3.4 The Effect of Reactive Diluent on E-beam Curing of BMI Resins 84
3.3.5 Cure Kinetics Study of BMI/NVP 50/50 Resins 89
3.3.6 High Intensity E-beam Curing 96
3.4 Conclusions 100

IV SYNTHESIS AND CURE CHARACTERIZATION OF PHENYLETHYNYL TERMINATED IMIDE OLIGOMERS 103

4.1 Introduction 103
4.2 Experimental 105
4.2.1 Materials 105
4.2.2 Syntheses 105
4.2.3 Characterizations 108
4.3 Results and Discussion 109
4.3.1 Characterization of AFR-PEPA-4 Oligomer 109
4.3.2 Cure Characterization of AFR-PEPA-4 Oligomer 112
4.3.3 Characterization of N-phenyl-[4-(phenylethynyl)-phthalimide] 124
4.3.4 Cure Kinetics of N-phenyl-[4-(phenylethynyl)-phthalimide] 130
4.4 Conclusions 139

V CONCLUSIONS 141

Page

5.1 Conclusions 141
5.2 Suggestions for Future Research 143

REFERENCES 145

VITA 154

LIST OF FIGURES

FIGURE		Page
1	Synthesis and Cure Characterization of High Temperature Polymers	6
2	End Groups of Polyimides	8
3	Temperatures Used for Resin Matrix Composites	9
4	Two Step Condensation Synthesis of Kapton^{TM} Polyimide	16
5	Avimid N Chemistry	17
6	PMR-15 Chemistry	18
7	Structure of AFR700B	19
8	Structure of Thermid 600 Polyimide	21
9	Structure of PETI-5 Polyimide	21
10	Synthesis of AFR-PEPA-N Imide Oligomers	22
11	Biphenylene End-capped Polyimides	23
12	Synthesis of Polyimide Based on the Reaction of Furan and Bismaleimide	25
13	Reaction Mechanism of Imide Formation	26
14	Stability Order for Polypyromellitimides at 400^{o}C as a Function of Diamine Structure	32
15	Effects of Dianhydride Structure on Polyimide Stability	32
16	Polymerization and Depolymerization of a Polyimide	35
17	Hydrolysis of (a) Anhydride (b) Amide Linkage	36
18	Interactions between Polyimide Chains (a) Charge Polarization; (b) Crystalline Interaction [56]	37

FIGURE Page

19 Chemical Structure of Bismaleimide 43

20 Chemical Structure of BMPM/DABPA System 45

21 Chemical Structure of BMPM / 4,4'-Diamino Diphenyl Methane Adduct 47

22 Chemical Structure of BMPM/DABPA Ene Adduct 49

23 Thermal Cure Reactions Involved in BMPM/DABPA BMI System 50

24 Scheme of Radiation Initiated Crosslinking 52

25 The Mechanism of E-beam Radiation Polymerization of Epoxy Resins..... 59

26 The Chemical Structures of the Components of BMI 5250-4 64

27 Scheme of E-beam Curing Setup 66

28 Temperature Rise of BMI Resins vs. Number of E-beam Exposure Passes (a) at 10 kGy per Pass; (b) at 20 kGy per Pass 69

29 FT-IR Spectra of BMI Systems..... 71

30 The Reaction Conversions of BMI Cured by Various E-beam Radiation Conditions from FT-IR Measurements..... 72

31 Temperature Rise of BMI/NVP vs. Number of E-beam Exposure Passes (a) at 10 kGy per Pass; (b) at 20 kGy per Pass 75

32 FT-IR Spectra of BMI/NVP 50/50 Systems 77

33 The reaction conversions of BMI/NVP 50/50 Cured by Various E-beam Radiation Conditions from FT-IR Measurements 78

34 Temperature Rise of BMI/Styrene vs. Number of E-beam Exposure Passes (a) at 10 kGy per Pass; (b) at 20 kGy per Pass..... 80

35 FT-IR Spectra of BMI/ Styrene 50/50 Systems 82

36 The Reaction Conversions of BMI/ Styrene 50/50 Cured by Various E-beam Radiation Conditions from FT-IR Measurements..... 82

FIGURE Page

37 The Appearance of E-beam Treated Samples 85

38 Temperature Data of Different BMI/NVP Systems during E-beam Curing at 10 kGy per Pass (Total 200 kGy Dosage) 86

39 The Dependence of Reaction Conversion of BMI/NVP Systems on Concentration of NVP (Dosage Applied: 200 kGy at 10kGy per Pass) 87

40 The Dependence of Degree of Crosslinking of BMI/NVP Systems on Concentration of NVP (Dosage applied: 200 kGy at 10kGy per pass) 88

41 The Dependence of Reaction Conversion of BMI/NVP 50/50 on Applied E-beam Dosage (10 kGy per Pass) 89

42 The Dependence of T_g of BMI/NVP 50/50 on Applied E-beam Dosage (10 kGy per Pass) 91

43 The Dependence of Degree of Crosslinking of BMI/NVP 50/50 on Applied E-beam Dosage (10 kGy per Pass) 91

44 The Dependence of Reaction Conversion of BMI/NVP 50/50 with 1% Dicumyl Peroxide on Applied E-beam Dosage (10 kGy per Pass) 93

45 Simulation of Cure Kinetics of E-beam Curing of BMI/NVP 50/50 (Dose Rate: 10 kGy per Pass) 96

46 Temperature Data of BMI and BMI/NVP 50/50 during E-beam Curing at 40 kGy per Pass (Total 400 kGy Dosage) 97

47 The Reaction Conversions of BMI Systems after High Intensity E-beam Radiation (Dosage Applied: 400 kGy at 40 kGy per Pass) 99

48 The Reaction Conversions of BMI/NVP Systems after High Intensity E-beam Radiation (Dosage Applied: 400 kGy at 40 kGy per Pass) 99

49 Reactions of Phenylethynyl Terminated Imide Monomers 104

50 Synthesis of AFR-PEPA-4 Oligomer 106

51 Synthesis of N-phenyl-[4-(phenylethynyl) phthalimide] 107

52 FT-IR Spectra of AFR-PEPA-4 Oligomer 111

FIGURE Page

53 DSC Curve of AFR-PEPA-4 Oligomer (Heating Rate: 20°C/min) 112

54 Reaction Conversion of AFR-PEPA-4 Oligomer vs. Cure Time at 350°C (Calculated from FT-IR Spectra) 113

55 Reaction Kinetic Plot of ln C≡C vs. Time for Thermal Cure of AFR-PEPA-4 at 350°C (Calculated from FT-IR) 115

56 T_g vs. Cure Time of AFR-PEPA-4 Oligomer Cured at 350°C in 1h..... 116

57 T_g vs. Reaction Conversion of AFR-PEPA-4 Oligomer Cured at 350°C in 1h 118

58 T_g vs. Cure Time of AFR-PEPA-4 Oligomer Cured at Various Temperatures 119

59 T_g as a Function of Reaction Conversion of Cured AFR-PEPA-4 Oligomer 120

60 Kinetic Plot of ln (1-α) vs. Time from DSC T_g Data..... 121

61 Kinetic Plots of ln k vs 1/T of the Cure Reaction of AFR-PEPA-4 Oligomer for First Order (Below 80% Cure) 122

62 Mass Spectrum of N-Phenyl-[4-(phenylethynyl) phthalimide] 126

63 ^{1}H n.m.r. Spectrum of N-Phenyl-[4-(phenylethynyl) phthalimide] 127

64 ^{13}C n.m.r. Spectrum of N-Phenyl-[4-(phenylethynyl) phthalimide] 128

65 FT-IR Spectrum of N-Phenyl-[4-(phenylethynyl) phthalimide] 129

66 DSC Curve of N-Phenyl-[4-(phenylethynyl) phthalimide]..... 130

67 The Dependence of IR Intensity on Cure Time for Thermal Curing of N-Phenyl-[4-(phenylethynyl) phthalimide] at 330°C in Air (a) Phenyl-ethynyl Group at 2216 cm^{-1}; (b) Conjugate Bonds at 1611 cm^{-1} 131

68 Reaction Conversion α vs. Cure Time of N-Phenyl-[4-(phenylethynyl) phthalimide] Cured at Various Temperatures from FT-IR Results (a) Phenylethynyl Group at 2216 cm^{-1}; (b) Conjugate Bonds at 1611 cm^{-1} 133

FIGURE Page

69 Kinetics Plots of ln k vs 1/T of the Cure Reaction of N-Phenyl-[4-(phenylethynyl) phthalimide] Calculated from FT-IR Conversion (a) Phenylethynyl Group at 2216 cm^{-1}; (b) Conjugate Bonds at 1611 cm^{-1} 136

70 Proposed Cure Products of N-Phenyl-[4-(phenylethynyl) phthalimide] 137

71 Proposed Structure of Cured AFR-PEPA-4 138

LIST OF TABLES

TABLE		Page
1	Electron Affinity of Aromatic Dianhydrides	27
2	Basicity (pK_a) Values of Diamines	28
3	Chemical Structure Related to Crystallinity [4]	39
4	T_gs and Reaction Conversions of BMI Resins Cured by Various Conditions	73
5	T_gs and Reaction Conversions of BMI/NVP 50/50 Systems Cured by Various Conditions	79
6	T_gs and Reaction Conversions of BMI/Styrene 50/50 Systems Cured by Various Conditions	83
7	Material Properties of Styrene and NVP	84
8	Element Analysis Results of AFR-PEPA-4 Oligomer	110
9	TGA Results of AFR-PEPA-4 Oligomer (Heating Rate: 10°C/min)	110
10	Kinetic Analysis of the Thermal Cure of AFR-PEPA-4 Oligomer by FT-IR	115
11	Kinetic Analysis of the Thermal Cure of AFR-PEPA-4 by DSC (Below 80% Cure)	120
12	Activation Energy of Thermal Cure Reaction of AFR-PEPA-4 Oligomer	123
13	TGA Results of Cured AFR-PEPA-4 Polyimide (Heating Rate: 10°C/min)	124
14	Element Analysis Results of N-Phenyl-[4-(Phenylethynyl)-phthalimide]	125
15	Kinetic Analysis of the Thermal Cure of N-Phenyl-[4-(phenylethynyl) phthalimide] by FT-IR 2216 cm^{-1}	134

TABLE Page

16 Kinetic Analysis of the Thermal Cure of N-Phenyl-[4-(phenylethynyl) phthalimide] by FT-IR 1611 cm^{-1} 134

17 Activation Energy of Thermal Cure Reaction of N-Phenyl-[4-(phenylethynyl) phthalimide] from FT-IR Calculation 135

CHAPTER I

INTRODUCTION

1.1 Background

High-temperature polymers have found a broad range of applications from structural materials in fiber-reinforced composites to thin films for use in electronics packaging and in emerging technologies such as photonic devices. In structural applications, fiber-reinforced high-temperature polymer matrix composites can offer significant advantages over other materials because of their low density and high specific strength. These composites are quite attractive for use in aerospace structural applications, e.g. aircraft engines, airframe, missiles, and rockets, where weight is critical [1].

The durability and reliability of materials used in aerospace components is a critical concern. Among the materials requirements for these applications are high glass-transition temperature, T_g, (at least 25°C higher than the intended use temperature), good high-temperature stability in a variety of environments, and good mechanical properties over a wide range of temperatures. In addition, a major requirement for any high-temperature polymers, regardless of their intended uses, is processability. Many monomers with multi-aromatic rings in structure are inherently stable and yield polymers with high T_g. However, they tend to produce polymers that have poor solubility in most organic solvents, very high melting or softening points, and melt

---

This dissertation follows the style and format of *Journal of Applied Polymer Science.*

viscosities that are too high to allow their processing by resin-injection molding or resin-transfer molding. Meanwhile, demands on large dimension structures for space vehicles eliminate expensive autoclave processing that has size limitations. Therefore, to improve the processability, stability, performance of high temperature polymer materials and an efficient non-autoclave processing is critical for development of future aerospace structures.

Fiber-reinforced high temperature polymer composites are and will be used for aerospace structural applications for a wide range of components that will be exposed to prolonged, extreme service conditions in military and commercial aircraft and hypersonic reusable space vehicles. These complex service environment conditions of stress, time, temperature, moisture, and chemical and gaseous environments required a thorough understanding of the physical, chemical and mechanical phenomena that control the most probable critical failure path of the composite component. Such an understanding of the fundamental aging mechanisms is necessary for credible, long-term composite performance predictions based on experimentally observed short-time service environment induced composite performance deterioration mechanisms.

There are two main categories of polymer matrices used for fiber-reinforced composites in aerospace applications: epoxy-based composites and imide-based composites [2, 3]. Epoxy resin based laminates have a great processability and provide a high strength/weight ratio. But epoxy based composites have drawbacks associated with a limited use temperature of 130^{o}C (relatively low T_g), moisture absorption and corresponding plasticization, and often a brittle mechanical response, especially after

exposure to severe environmental conditions. Crosslinked bismaleimides (BMIs) and Polyimides are leading high temperature polymer matrices for fiber reinforced composites. The need for bismaleimide arose because of the poor hot/wet performance of epoxies. And, BMI systems are able to be fabricated using epoxy-like conditions and are capable of performing at temperatures up to 230^{o}C. Polyimides have excellent mechanical properties, high T_g (up to 450^{o}C) and long term stabilities. However, one of the biggest drawbacks in the use of BMIs and polyimides is still processing difficulty due to their highly aromatic chemical structures. Meanwhile, BMI resins suffer from brittleness that leads to composite microcracking. Polyimides also have the toughness limitations and poor hydrolytic stabilities. As a result, present and future research related to Air Force aircraft and space applications involves determination of the critical damage mechanisms and thresholds for polyimides based on chemical structure, and new material development to balance the high temperature performance, high hydrolytic resistance and ease of processing [3].

Electron beam (E-beam) curing of polymer matrix composites is a nonthermal, nonautoclave curing method that offers the potential to fabricate large integrated structures for space vehicle applications. E-beam curing has many advantages over thermal curing, which include reduced curing time, lower tooling cost, shelf stable resin systems, low health risks because of fewer volatiles and hazardous chemicals, reduced thermal stresses and curing at controlled temperatures [4-10]. Electron beam curing of fiber-reinforced composites was explored over 30 years ago [7]. There are two factors contributing to the growing interest in the E-beam curing of composites: (i) The

development of high current, commercial industrial accelerators capable of attaining a high beam penetration; (ii) The development of radiation responsive resins or oligomers, initiators and formulation systems tailored for the needs of composite matrices.

The principal resin systems that have been widely studied as E-beam curable composites are epoxy resins, such as diglycidylether of bisphenol A epoxides (DGEBA) [11-14]. There are few reports on E-beam curing of BMI and polyimides yet. E-beam curing is found to be insufficient to cure BMI resin [15]. Marie-Florence et al. made an attempt at using N-vinylpyrrolidone (NVP) as a diluent for E-beam curing of BMI resins and found that the T_g of the related products are around 240^oC [15]. However, fundamental chemical and physical changes of BMI resins during E-beam curing are poorly understood (temperature evolution, gelation, vitrification, reaction mechanisms, kinetic analysis, processing-property relationships). NASA and subcontractors have been investigating E-beam curing for polyimides [16]. To date, there have been no known breakthroughs, but there has been encouraging progress toward understanding and resolving the barriers.

1.2 Research Goals

Structural polymer matrix composites used for aerospace applications are required to exhibit good high-temperature/high-moisture ('hot-wet') properties, processability and mechanical performance over a long period of time. An understanding of the fundamental cure reactions and aging mechanisms is necessary for credible long-term composite performance predictions based on experimentally observed short-time

service environment induced composite performance deterioration mechanisms. Meanwhile, there is a need for the development and characterization of new non-autoclave composite process for the future manufacture of large structures.

The overall objective of this dissertation is to characterize and develop polymer matrices that can be used for high temperature polymer composites in aerospace applications. The contribution from this dissertation involved two primary areas: (i) Characterization and development of E-beam curing of BMI resins, (ii) synthesis and cure characterization of imide oligomers.

The dissertation will specifically address several key issues:

- To gain fundamental understanding of the relations between processing parameters, the resultant physical and chemical structure and the performance of E-beam cured high temperature polymer matrices.
- To characterize the fundamental chemical mechanisms and kinetics of E-beam cured bismaleimide resins.
- To identify and characterize fundamental parameters that control imide oligomer synthesis and cure reaction and how such parameters affect the thermal properties of the cured polyimide resin.
- To characterize the cure reactions of acetylene compounds as the function of reaction conditions and parameters.

Figure 1 details the overall research approach that consists of resin processing, fundamental chemical factors and structure-property characterization of high temperature polymer matrices.

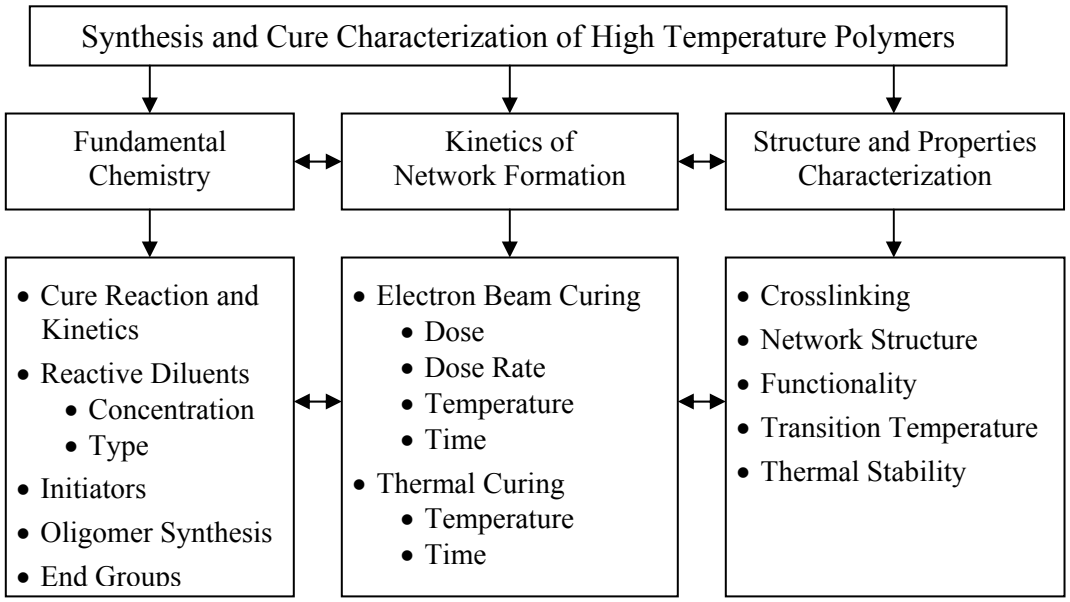

Figure 1 Synthesis and cure characterization of high temperature polymers.

CHAPTER II

LITERATURE REVIEW

2.1 Introduction

In this chapter, an overview of high temperature polymer composite matrices for aerospace applications is presented. The history of materials, chemical evolution, and the status of present problems will be focused. In more detailed terms, the synthesis and critical fundamental structure-property-processing relations of polyimides will be evaluated. The technique of E-beam curing of fiber reinforced composites, characterization of E-beam cure process and development of E-beam curable high temperature polymer matrices will also be discussed in detail.

2.2 General Considerations of High-temperature Composite Materials

The development of high-performance composite materials is based on the concept of taking advantage of the stiffness and strength of high performance fibers by dispersing them in a softer matrix, which acts as a binder and transfers forces across the fiber-matrix interface [17]. Specific properties can be tailored by placing or weaving the fibers into specific directions. Meanwhile, the matrix materials can be designed to fit complex requirements in aerospace structural applications.

Polyimides possess outstanding key properties such as high use temperature (above 300^{o}C), thermoxidative stability, high mechanical strength, high modulus, excellent electrical properties, and superior chemical resistance [18]. Because of these

merits, polyimides become one of the leading polymer materials for high temperature composites in aerospace structural applications. Although polyimides still suffer processing difficulty due to their highly aromatic chemical structures, the exploration of new compositions and new processing methods for polyimides is developed rapidly to balance the high temperature performance, high hydrolytic resistance and the processing ease of materials.

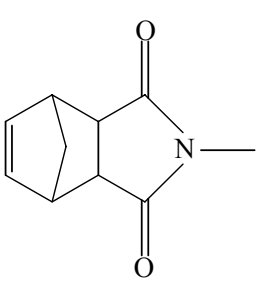

PMR Polyimides

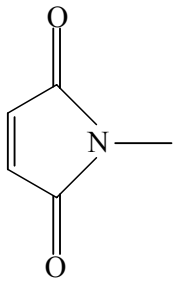

Bismaleimides

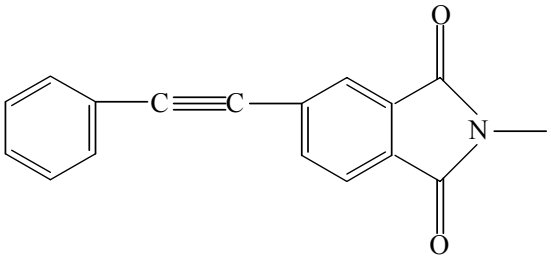

Phenylethynyl terminated imides

Figure 2 End groups of polyimides.

The primary focus of this dissertation lies in the area of aerospace grade polyimides used as composite matrices. These polyimides can be generally classified in terms of their reactive end groups, shown in Figure 2. PMR-type polyimides, BMI, and phenylethynyl terminated imides, are the most widely used in high temperature composites [19].

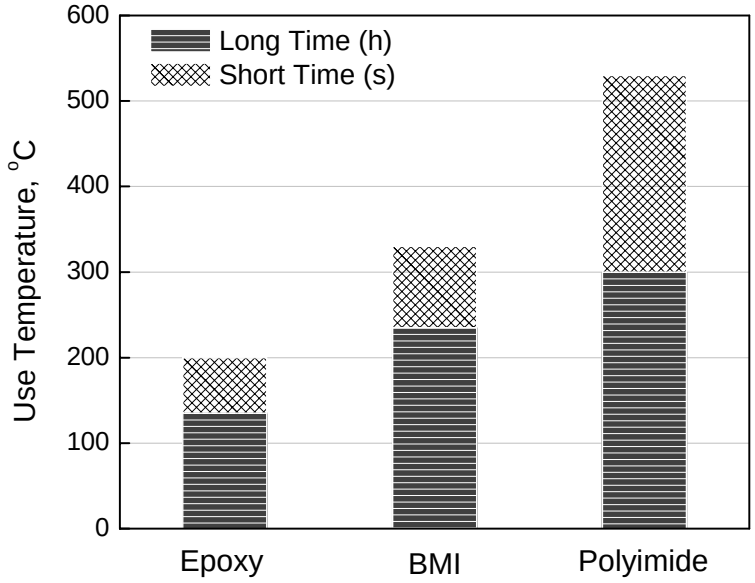

Figure 3 Temperatures used for resin matrix composites.

BMIs offer as an intermediate material in temperature performance between epoxies and polyimides (Figure 3) because of their capability of performing at temperatures up to 230°C and ability to be fabricated using epoxy-like conditions, without the evolution of void-producing volatiles [2]. The crosslinked BMI matrices

exhibit excellent hot/wet properties, which are required for aerospace applications. But BMIs have the drawback of brittleness. They are usually blended with the toughening agent or modified by adding toughening components in structure prior to manufacture of structural composites [20-22].

The majority of polyimides have extended rigid planar aromatic and heteroaromatic structures so that they are infusible and insoluble. The synthesis of polyimides usually begins with a diamine and a dianhydride which are added into a dipolar aprotic solvent. Poly (amic acid) will be formed, which can be transformed into polyimide by the process known as imidization. Imidization generally takes place in the solid state and occurs in the 250-350^{o}C temperature range, depending on the stability and T_g of the polymer. The reaction mechanisms are often complex and can be difficult to model [19]. The properties of obtained polyimide are affected by the imidization process and related reaction conditions. Also, the stability of polyimides is greatly dependent upon their chemical structure, chain packing, molecular weight, confirmation, and location of functional groups [18].

2.3 Present/Future Aerospace Applications

Composites for space applications have been developed rapidly over the past 20 years, being led by the US National Aeronautics and Space Administration (NASA) and the Air Force. Composites are now the leading candidate materials not just to save weight, but to increase system performance. Their high specific strength and stiffness, combined with low coefficient of thermal expansion, cryogenic stability, load

tailorability, and high specific damping capacity, make them particularly attractive for high-precision space structures.

The design lifetime of most early spacecraft is relatively short (5-7 years). However, the current trend toward longer lifetimes (ultimately to 20-25 years) has resulted in an interest in long-term durability of composites in the space environment. The exposure environments such as atomic oxygen, solar ultraviolet radiation, ionizing radiation, micro-meteoroids and man-made debris, and continuous thermal cycling place stringent durability demands upon materials [23]. A fundamental understanding of the synergistic effect of all these environmental conditions on composites is essential for design of long-life space structures.

Many of polyimides developed arose from the High Speed Civil Transport (HSCT) program. A part of the program, funded by NASA and Boeing Company, was to develop a commercial aircraft capable of Mach 2.4 (1600 mph) speeds, about the length of a football field in dimension, and capable of transporting up to 400 passengers for a length of 5000 nautical miles while flying at an altitude of 12 miles [19]. Under these conditions, the surface of the aircraft would be about 160^{o}C. But the program required material performance at 177^{o}C for 60,000h for safety. Some inner portions of the airplane, including fuel tanks in the wings, would also reach high temperatures [19].

In addition, polyimide composites are also widely used in present military aircraft, including Advanced Tactical Fighter (ATF), the F-117A stealth fighter, the Navy F-18 Strike Fighter, F-16XL, and AV-8B. The Air Force has had a continuing interest in the development of polyimides that (i) are large or complex shaped structures,

and (ii) exhibit superior thermal, mechanical properties with enhanced oxidative and hydrolytic resistance. As such, a fluorinated polyimide (AFR 700B) was formulated and developed at the Air Force in order to meet these requirements [24]. However, AFR 700B polyimide exhibits significant decreases in strength (~70%) and T_g (75°C) after 1000 hours at 160°C in a hygrothermal pressure bomb environment [25, 26]. It has been observed that phenylethynyl end capped based polyimides (developed by NASA Langley) exhibited considerably greater resistance to hydrolytic degradation [25].

Development of phenylethynyl end capped based polyimides AFR-PEPA-N at Air Force Research Laboratories [19] resulted in resins that exhibited only a 3-5% decrease in dry T_g for a range of oligomer molecular weights after hygrothermal exposure, compared to a 20% decrease for AFR 700B under similar exposure conditions [27]. In addition, AFR-PEPA-N exhibited (i) extremely high T_g's (435 - 455°C), (ii) significantly improved mechanical properties at 300°C compared to AFR 700B, (iii) the potential to be processed by resin transfer molding (RTM), (iv) high ductility for a high temperature polyimide (ambient temperature elongation to break of 5%), and (v) slightly lower thermo-oxidative stability compared to AFR 700B.

AFR-PEPA-N carbon fiber composites have already been deployed on the leading trailing edges of the stealth B-2 bomber. These ultra-high temperature light weight composites offer the potential to be used for aerospace structural applications for a whole range of components that will be exposed to extreme service environment conditions in military aircraft and future hypersonic reusable space vehicles. These complex service environment conditions of stress, time, temperature, moisture, and

chemical and gaseous environments, together with a range of different processing procedures require a through understanding of the structure-process-performance relations of these composites. Of critical importance are (i) the relations between the imide oligomer structure and morphology and the final cured resin and the composite properties, (ii) identification of relatively simple modifications of imide oligomer structure that leads to superior resin properties and enhanced versatile composite processing options, and (iii) characterization of composite damage growth mechanisms for future extreme service environment exposure conditions that range from cryogenic up to high temperatures.

Polyimides and BMIs are the most notable for high temperature applications. But BMIs are also being considered for cryogenic applications, such as liquid hydrogen (LH2) and liquid oxygen (LOX) cryogenic fuel tank containment structures needed for the Single Stage To Orbit (SSTO) launch vehicles in NASA's future space transportation systems. These load bearing primary composite structures will be large, i.e. 70 feet by 70 feet, which eliminates expensive autoclave processing which has presently available size limitations of approximately 20 feet by 10 feet. Hence, there is a need for the synthesis and characterization of new non-autoclave composite process for the future manufacture of such large structures.

E-beam curing provides a non-thermal, non-autoclave process for manufacturing space structures. Aerospatiale developed the first practical application of electron beam-cured structural composites for solid rocket motors using acrylated epoxy resins in 1990 [7]. However, these materials were found to be too brittle for manned and reusable

aerostructures. A Cooperative Research and Development Agreement (CRADA), sponsored by the Department of Energy Defense Programs and 10 industrial partners, was established to advanced E-beam curing of composites in 1994. Hundreds of E-beam curable resin systems, including toughened formulations, are now commercial available.

The US Air Force and its prime contractors also began to evaluate E-beam curing technology for military aircraft in the Composites Affordability Initiative in the 90's. Prototypical manufacture of Long FOG missile bodies was achieved using E-beam curing in 1996 [7]. Prototypical manufacture of a T-38 trainer aircraft windshield frame was also achieved using E-beam curing in 1998 [28]. The arch was a laminate construction of 36 thin stainless steel strips, with E-beam curable adhesive in between the strips. This stainless steel laminate was then overwrapped with fiberglass reinforcement. The frame was E-beam cured with the arch being irradiated using E-beam generated X-rays to ensure curing of the adhesive between the metal strips. E-beam curing processes for three-dimensional braided structures were developed for use in aircraft ducting applications in 1998 [29, 30]. E-beam curing has been also applied in numerous filament winding applications including flywheels, tactical rocket motor cases and helicopter drive shafts [7].

NASA is investigating E-beam curing technology for application in the curing of composites to be used in cryogenic piping, tanks [31], and as repair pieces of space structures under its Advanced Space Transportation Program [7]. NASA also successfully fabricated a scaled prototype of an overwrapped FASTRAC rocket nozzle,

in which material temperatures were held low to eliminate delamination attributable to high thermal stresses.

However, for many applications in the aerospace industries, E-beam processable resins currently available are epoxy systems, which do not meet the performance specifications (e.g. excellent thermal stability, high strength, and high toughness). Polyimides do not appear to be E-beam curable, possibly due to its high melt temperature. NASA and Air Force have been investigating the electron beam curing for polyimides and bismaleimides [16, 32, 33]. To date, there have been no known breakthroughs, but there has been encouraging progress toward understanding and resolving the barriers. Development of E-beam curable polyimide and bismaleimide resins is critical to aerospace applications.

2.4 History and Classification of Polyimides

2.4.1 Kapton Polyimide

Polyimides were originally developed at DuPont in 1950's and 1960's [34, 35]. These efforts revolved around the modification of nylon chemistry to produce polyimides in a two-step process [18] (Figure 4) that involved the condensation of an aromatic diamine (a), and dianhydride (b), to form poly(amic acid) (c), followed by cyclodehydration to the polyimide (d). Research at DuPont led to the development of Pyralin^{TM} soluble polyimides for use as wire coatings and Kapton-H^{TM} polyimide films. Since that time, a variety of condensation polyimides have been developed by researchers in the United States, Japan, Europe, and the former USSR [36].

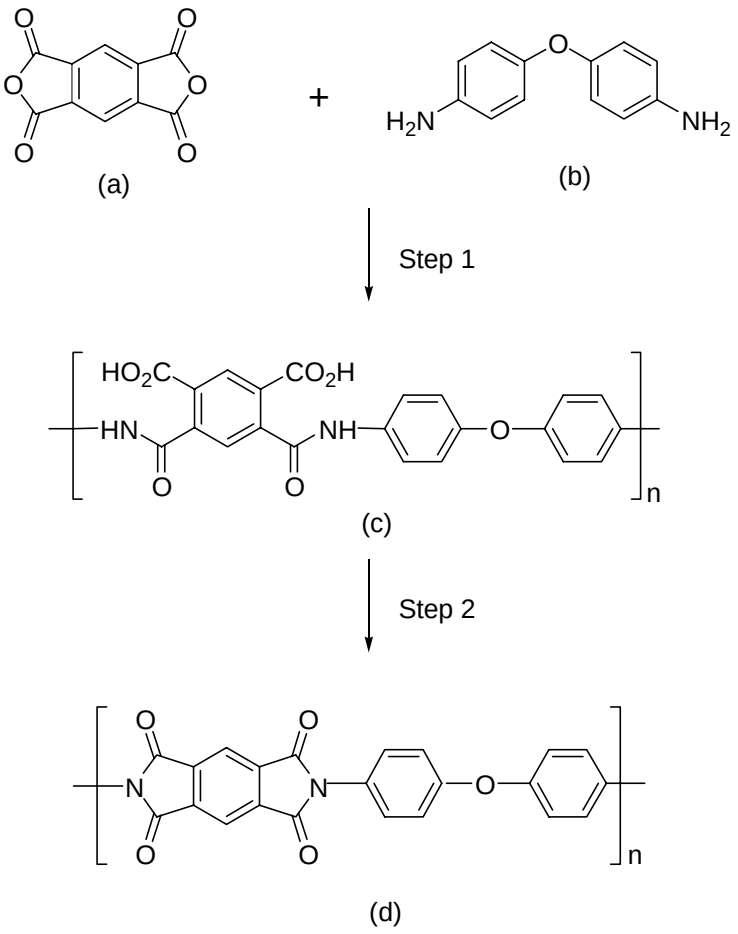

Figure 4 Two step condensation synthesis of Kapton™ polyimide.

2.4.2 Avimid N Polyimide

Condensation polyimides were mainly used as thin films in electronics packaging, wire insulation, and gas separator membranes. However, condensation polyimides have also been used as composite matrix resins, for example, DuPont's Avimid N (Figure 5)

[37]. Avimid N has a T_g close to 360°C, low weight loss, and good retention of mechanical properties after 100h aging in air at 371°C. However, the evolution of volatile condensation by-products (H_2O) and the low flow of this system make it difficult to process.

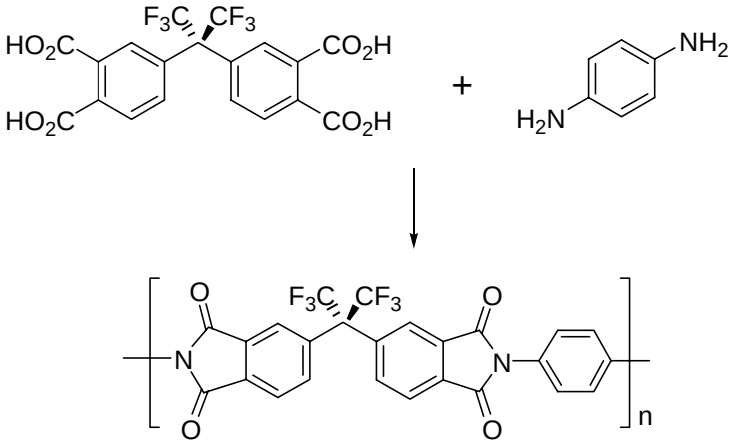

Figure 5 Avimid N chemistry.

2.4.3 Norbornyl End-capped Polyimides

PMR Polyimides

Addition-curing polyimides were synthesized to improve the processability of condensation polyimides without adversely affecting their stability and high-temperature performance in 1970's. The Polymerization of Monomer Reactant (PMR) family of polyimides, in particular PMR-15, developed at the NASA Lewis Research Center (Figure 6) [38]. Reinforcement fibers are impregnated with a solution of the dialkyl ester

of 3,3',4,4'-benzophenone tetracarboxylic acid (BTDE), methylene dianiline (MDA), and the monoalkyl ester of 5-norbornene-2,3-dicarboxylic acid (NE), in a low boiling solvent, typically methanol or ethanol. In the first step of this process, these monomers undergo imidization at temperatures around 200°C to yield short-chain norbornyl end-capped polyimide oligomers ($MW_{theoretical}$ = 1500 for PMR-15). At temperatures above 300°C, these oligomers undergo a cross-linking reaction involving the norbornyl end-cap (Step 2).

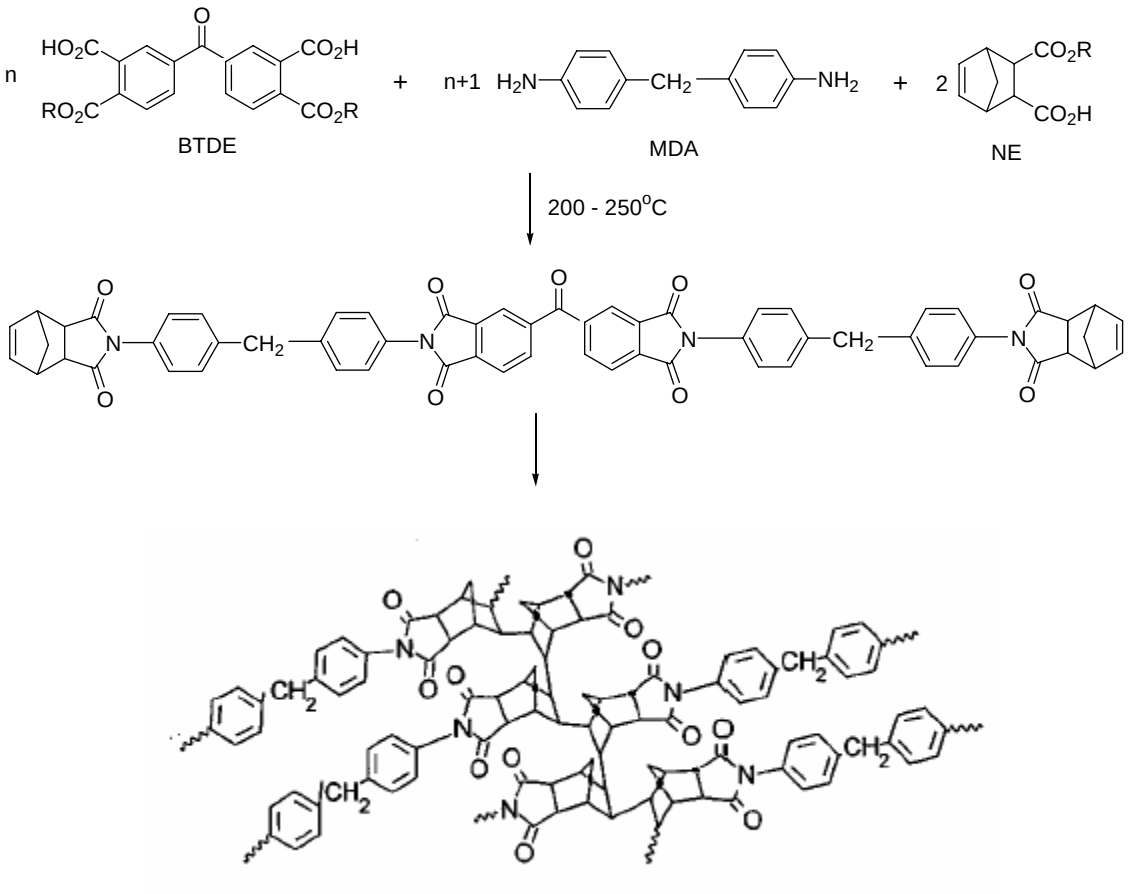

Fully crosslinked PMR-15

Figure 6 PMR-15 chemistry.

PMR-15 has a T_g after post-cure of 365°C and shows good retention of mechanical properties and low weight losses in air for long exposure times (>10,000 h) at temperatures up to 230°C and for shorter times at temperatures as high as 316°C. Because of its good high-temperature performance and processability, PMR-15 is widely used in composites and adhesives for a variety of aircraft engine applications. However, two draw backs limit its applications: (i) concern over the mutagenicity of MDA, and (ii) the high cost of fabricating PMR-15 engine components due to processing limitations [1].

AFR-700B Polyimide

Other norbornyl end-capped resins, such as LaRC-160, PMR-II, and AFR-700, have been developed provide materials with improved handling and/or better high-temperature performance than PMR-15 [1].

AFR-700B was created by the Air Force with an elevated service temperature at 371^{o}C. Compared to the structure of PMR-15, the backbone of AFR-700B consists of 2,2'-bis (3,4-dicarboxyphenyl) hexafluoropropane dianhydride (6FDA) and 1,4-diaminobenzene (p-PDA) instead of BTDE and MDA. Only one end of the chain was capped with NE, with an amine on the other end of the chain as seen in Figure 7.

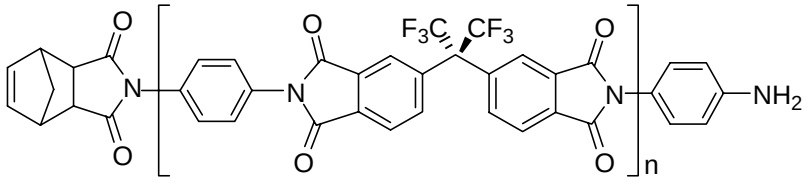

Figure 7 Structure of AFR700B.

AFR-700B has a T_g greater than 400^oC. It was used immediately on the fuselage trailing edges on the F-117A Stealth Fighter. Unfortunately AFR-700B was found not to perform well in a hygrothermal environment, although it had an excellent thermooxidative resistance. The polyimide experienced a significant amount of hydrolysis, which lead to a large drop in T_g and mechanical properties [19].

2.4.4 Acetylene End-capped Polyimides

Although norbornyl end-capped polyimides have been used successfully in many space applications, there are some drawbacks to their use. The thermal-oxidative stability of the norbornene ring is poor due to the large amount of saturated carbons present in this structure. The cross-linking often becomes the oxidative weak link when norbornyl end-capped polyimides are used. Moreover, processing problems can be encountered with norbornyl end-capped polymers due to the potential for formation of cyclopentadiene during cross-linking [39]. These deficiencies have prompted the search for new addition-curable end-caps for polyimides.

Thermid 600 Polyimide

Acetylenes are used widely as reactive end-caps in synthesis of polyimides. Most of the early research in this area was done by Landis and co-workers [40]. Acetylene-terminated imides (ATI resins) such as Thermid 600 (Figure 8) have high T_gs (370°C) and good thermal-oxidative stability at temperatures as high as 316°C. However, the acetylene group in these systems polymerizes at 195°C, which is too close to the imidization temperature to allow for complete removal of condensation by-products.

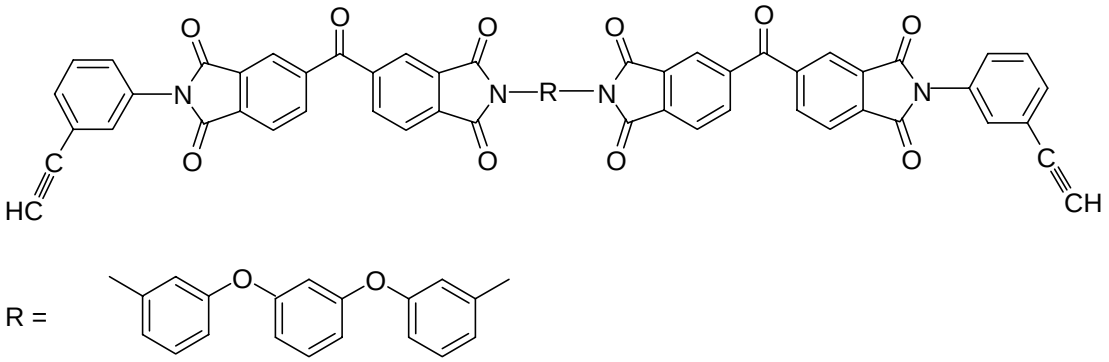

Figure 8 Structure of Thermid 600 polyimide.

Phenylethynyl Capped Polyimides

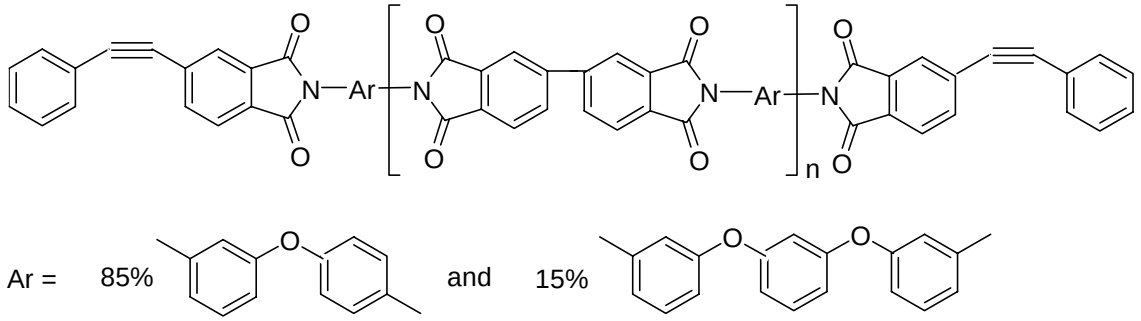

Figure 9 Structure of PETI-5 polyimide.

It is found that the polymerization temperature of acetylene end-caps can be increased more than 100°C through the introduction of a second phenyl ring on the acetylene groups [41]. The use of these phenylethynyl groups as the capping groups for polyimides attracted more interests recently [42-44]. Among them, 4-phenylethynyl-

phthalic anhydride (PEPA) is a successful case. One of PEPA-terminated polyimides, PETI-5 (Figure 9), is currently under evaluation for use in airframe applications for the High Speed Civil Transport [45]. It has been found to have excellent mechanical strength and toughness with a glass transition temperature at 270°C. It crosslinks between 320°C to 371°C range and at a pressure of 1MPa and can be easily processed by resin transfer molding [45].

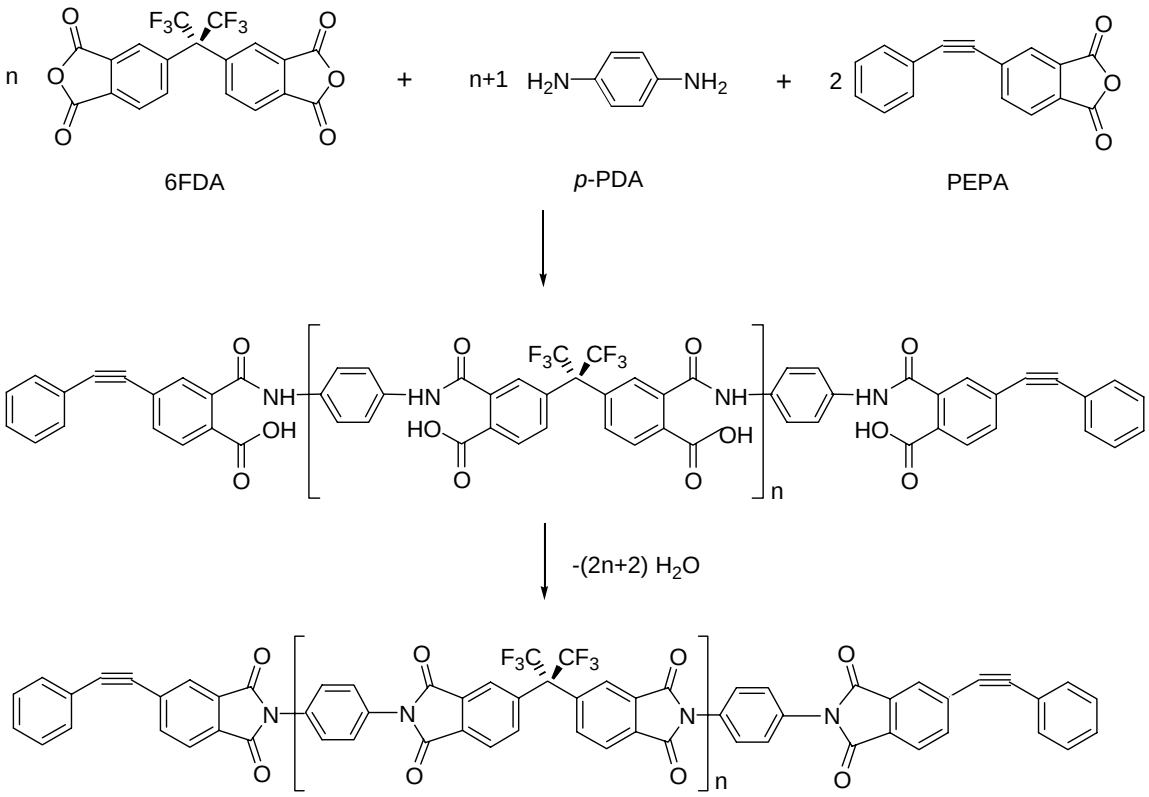

Figure 10 Synthesis of AFR-PEPA-N imide oligomers.

AFR700C polyimide was also synthesized to combine the thermooxidative abilities of AFR700B with the hydrolytic stability of PETI-5 [19]. The imide oligomer, AFR-700C, was termed AFR-PEPA-N due to that it is terminated on both chain ends with 4-phenylethynylphthalic anhydride (PEPA). In the synthesis of AFR-PEPA-N oligomer, 4-phenylethynylphthalic anhydride (PEPA), 2,2'-bis(3,4-dicarboxyphenyl)-hexafluoropropane dianhydride (6FDA) and 1,4-diaminobenzene (p-PDA) were reacted together in N-methylpyrrolidone (NMP) (Figure 10).

Biphenylene End-capped Polyimides

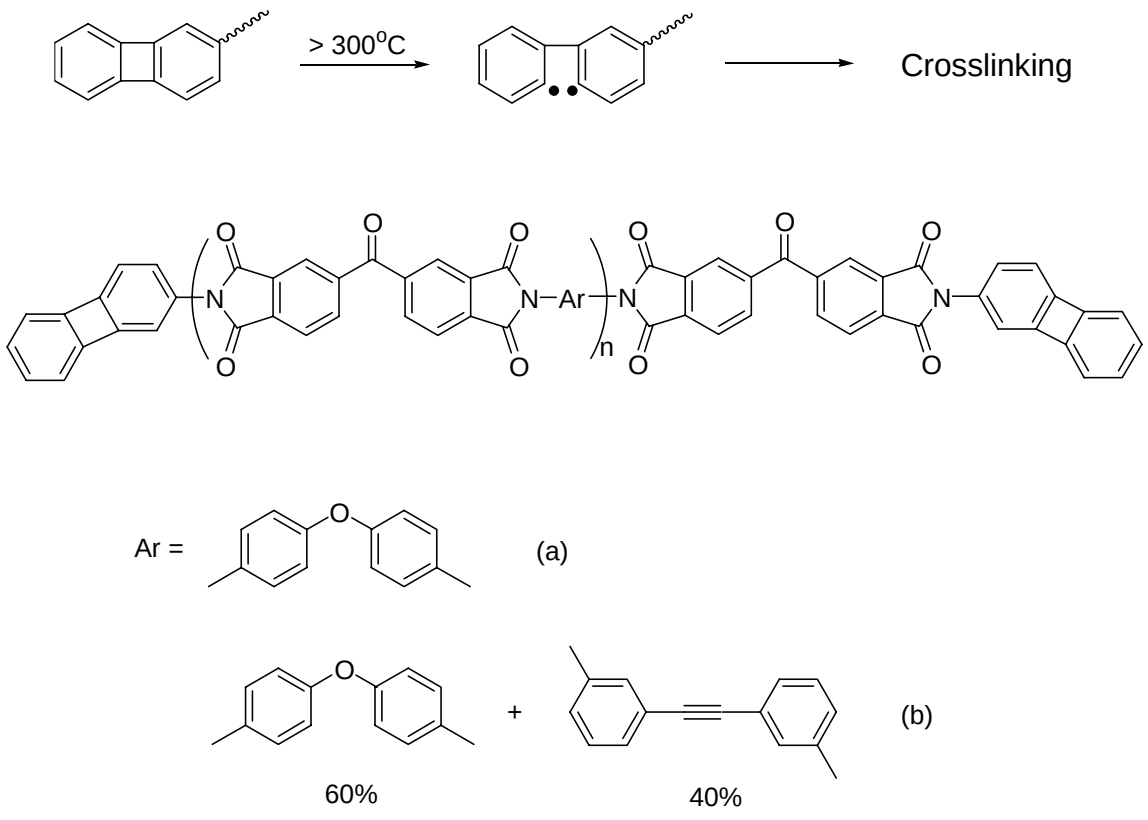

Figure 11 Biphenylene end-capped polyimides.

Stille and co-workers reported that biphenylene could be used as reactive end-caps for polyimide oligomers [46, 47]. When heated above 300°C, biphenylene undergoes a ring-opening reaction to produce a biradical that can couple and then cross-link (Figure 11). Cured films of biphenylene-terminated polyimides such as (a) have modest T_g (261°C). Biphenylene end-capped polyimides with an internal acetylene unit have much higher T_g [48]. Polyimide (b) (Figure 2.10) prepared from a 40/60 mixture of bis(3-aminophenyl)acetylene/4,4'-ODA (DP = 11) and cured at 350°C had a T_g of 347°C and good stability in air (5% weight loss at 520°C by TGA). Celion 6000 graphite-reinforced composites were also prepared with biphenylene end-capped polyimides containing internal acetylene groups [49]. Biphenylene end-capped polyimide is one of those polyimides with highest thermal and oxidative stabilities.

2.4.5 BMI Based Diels-Alder Systems

Diels-Alder cycloaddition reactions such as the reaction of BMI with some type of stable bisdiene, including bis(*o*-allylphenoxy)phthalimide, bispyrone, bisfuran, or polyfuran [1, 50-52], can also be used in synthesis of thermosetting polyimides. For example, Diels-Alder cycloaddition can be utilized to produce polyimide between bis(furyl)imide and BMI (Figure 12) [1]. HMS carbon fiber-reinforced composites made with this type of polyimide, which show modest thermal-oxidative stability. The samples had an 18% weight loss when they were aged in air for 1000h at 316°C. Flexural strengths of these composites dropped from 172 to 66 Ksi after aging under these conditions [1].

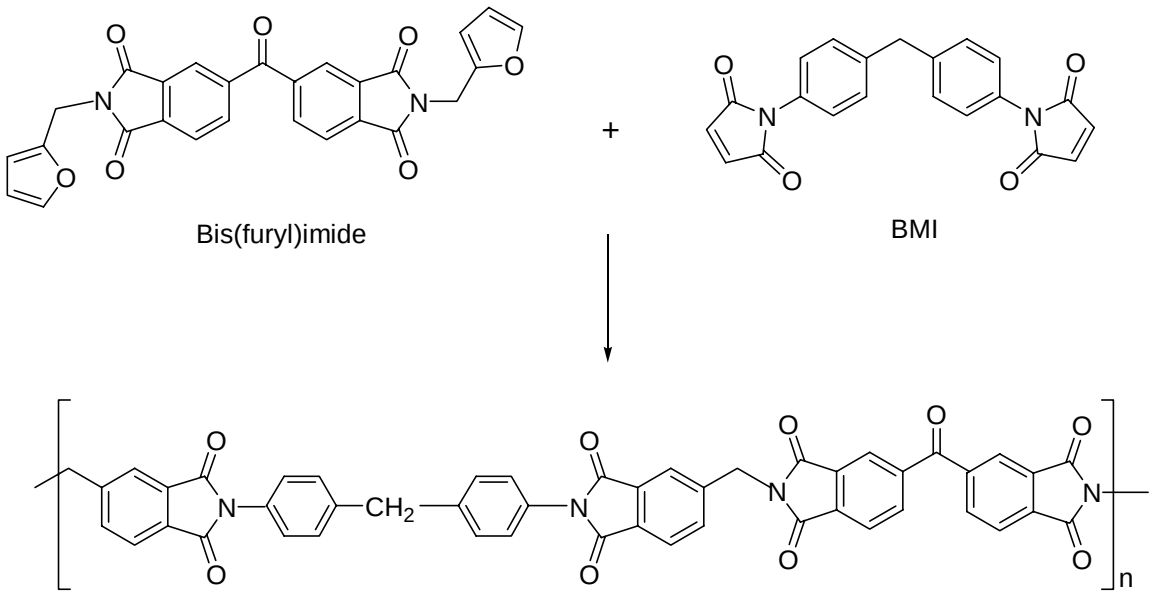

Figure 12 Synthesis of polyimide based on the reaction of furan and bismaleimide.

2.5 Fundamentals of Imide Synthesis

As mentioned earlier, most of the syntheses of polyimides start from the formation of poly(amic acid), which is formed by adding a diamine and a dianhydride into a dipolar aprotic solvent. And then the obtained poly(amid acid) can be converted into the final polyimide by thermal or chemical imidization. Therefore, the monomers, solvents, imidization process and other reaction parameters are very important factors for polyimide synthesis.

2.5.1 Formation of Poly(amic acid)s

The reaction mechanism of formation of poly(amic acid) involves the nucleophilic attack of the amino group on the carbonyl carbon of the anhydride group,

followed by the opening of the anhydride ring to form amic acid group as illustrated in Figure 13 [18].

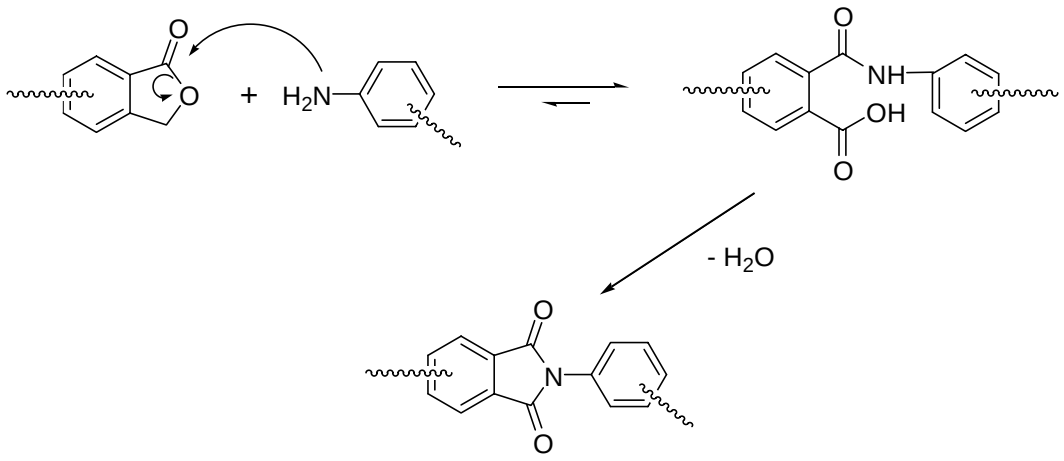

Figure 13 Reaction mechanism of imide formation.

Generally, this equilibrium reaction is irreversible because a poly(amic acid) with high molecular weight can be easily formed as long as the pure reagents are used. Therefore, the driving forces should favor the forward reaction over the reverse reaction. There are two factors need to be noted: (i) the acrylation reaction of amines is an exothermic reaction and the equilibrium is favored at lower temperatures; (ii) the forward reaction in dipolar solvents is a second-order reaction and the reverse reaction is a first-order reaction. Therefore, the equilibrium is favored at high monomer concentrations to form poly(amic acid)s with higher molecular weight [18].

Monomers

TABLE 1
Electron Affinity of Aromatic Dianhydrides

Dianhydrides	E_a, *eV*
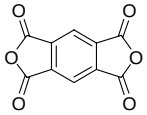	1.90
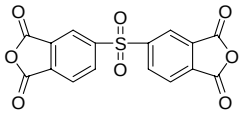	1.57
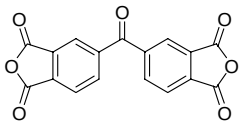	1.55
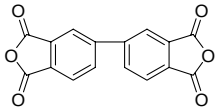	1.38
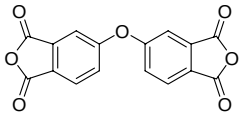	1.30
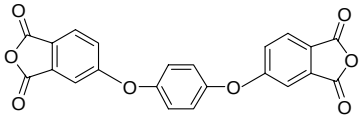	1.19
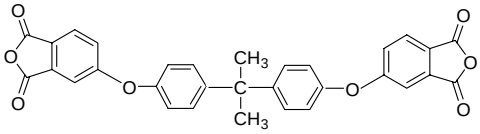	1.12
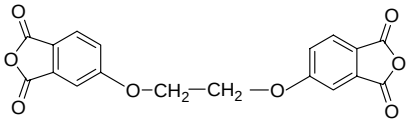	1.10

Based on the mechanism shown in Figure 13, the reaction rate is dependent on the elctrophilicity of the carbonyl groups of the dianhydride and the nucleophilicity of the amino nitrogen atom of the diamine. The elctrophilicity of the carbonyl groups of the dianhydride can be measured in terms of the electron affinity (E_a), a tendency to accept an electron. The dianhydride with higher E_a shows higher reactivity. Table 1 lists the electron affinity of various aromatic dianhydrides [18].

TABLE 2
Basicity (pK_a) Values of Diamines

Diamines	pK_a
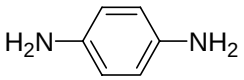	6.08
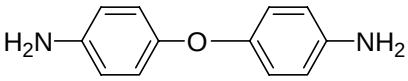	5.20
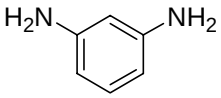	4.80
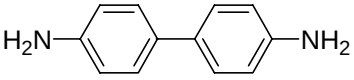	4.60
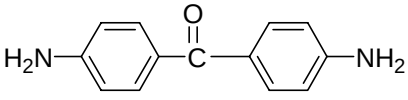	3.10

Unlike the dianhydride, the nature of the diamine is of extreme importance for imide formation. Highly basic diamines, e.g. aliphatic diamines, are not suitable for the

reaction due to their high tendency to form salts during the initial stages of the reaction [36]. The formation of the salt prevents the amine groups from reacting with the anhydride, therefore changes the stoichoimetry of the initial monomer charge, which is not favorable to form high molecular weight poly(amic acid). On the other hand, the reactivity of diamines is dependent on its basicity (pK_a). Diamines of low basicity do not exhibit sufficient nucleophilic character to allow them to enter into a polymer-forming reaction with the anhydride. Ideally, the diamine should have a pK_a of 4.5-6 [53]. The basicity (pK_a) values of several common diamines are listed in Table 2 [18].

Solvents

The most commonly used solvents are dipolar aprotic amide solvents such as N,N-dimethylformamide (DMF), N,N-dimethylacetamide (DMAc), N-methyl-pyrrolidone (NMP), and tetramethylurea (TMU). Sulfoxides such as Dimethylsulfoxide (DMSO) can also be used. The strong acid-base interaction between the amic acid and the amide solvent is a major source of exothermicity of the reaction and one of the most important driving forces. Thus, it is expected that the rate of poly(amic acid) formation is faster in more basic and more polar solvents. On the other hand, thermal stability of the solvent and ease to be removed in the following imidization process also need to be concerned [18].

2.5.2 Thermal Imidization

There are two ways to achieve imidization. One is the direct thermal cyclodehydration of the poly(amic acid) by heating the mixture to around 300^{o}C, depending upon the stability and T_g of the polymer. Another is to add a chemical

dehydration agent to poly(amic acid) and then followed by a thermal imidization. Thermal process is the most cost-effective way and can be controlled with high precision. Thus, it is the most practical approach to imidization, especially for commercial applications.

By monitoring of cure profile of a typical poly(amic acid)/NMP system from Mass spectrometry, the thermal imidization process can be described as following steps [36]: (i) In the temperature regime from ambient temperature to approximately 150^{o}C mostly solvent is evolved; (ii) In the region from 150^{o}C to 250^{o}C both solvent evolution and maximum evolution of water from imidization takes place; (iii) From 250^{o}C and up solvent removal is virtually complete and the final imidization is completed.

The imidization rate was found to be faster in the presence of dipolar amide solvents [18]. However, the thermal imidization reaction is complex, which has not been possible to be described by simple kinetic expression. The imidization proceeds rapidly at the initial stage and tapers off at a plateau, which is a typical diffusion-limited kinetic process. As the degree of imidization increases, the T_g or stiffness of the polymer chain increases. When the T_g reaches the reaction temperature, the imidization rate slows down remarkably.

2.6 Fundamentals of Structure-Property Relationships of Polyimides

For high temperature polymers, their thermal stabilities and processability are the most critical properties to study. There are increasing demands on composite matrix

resins with the use temperature as high as 371^{o}C (700^{o}F) having good hydrolytic stability, chemical stability, and mechanical properties of polyimides.

2.6.1 Degradation and Stability of Polyimides

Effect of Monomer Structure on Stability

The thermal stability of polyimide backbone is determined by the strength of its weakest bond. In an oxidizing atmosphere, the structure that affects the inherent oxidation potential of the system is also important. It is not just the bonding energies that determine the ability to resist degradation but much more complicated system of mechanisms that are involved, such as the chain packing, density, molecular weight, conformation, and location of functional groups. These characteristics can control the opportunity of degradation initiation and the rate of degradation of the polyimide [18].

The types of diamines, dianhydrides, and end-groups may determine how the polyimide will degrade at a certain rate. It was found that the diamine structure can be more of an influence upon polyimide stability than dianhydride [18]. Because the diamine has a higher electron density compared to the rest of the structure, the diamine can be a likely point of oxidation and 'weakest' link. It is known that electron-deficient diamines form more oxidatively stable polyimides than electron-rich diamines. It was observed that the stability of polypyromellitimides at 400^{o}C is dependent on the function of diamine structure (Figure 14) [54]. Also the amount of fused rings in the diamine affects the stability of the polyimides. The greater the amount of rings, the higher the probability of instability is [18]. The fluorinated diamine was reported to form polyimides with excellent stability [55].

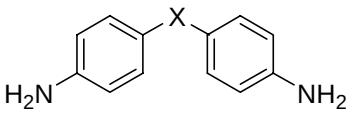

Stability order for X: $C(CF_3)_2 > SO > SO_2 > CH_2 > O$

Figure 14 Stability order for polypyromellitimides at 400°C as a function of diamine structure.

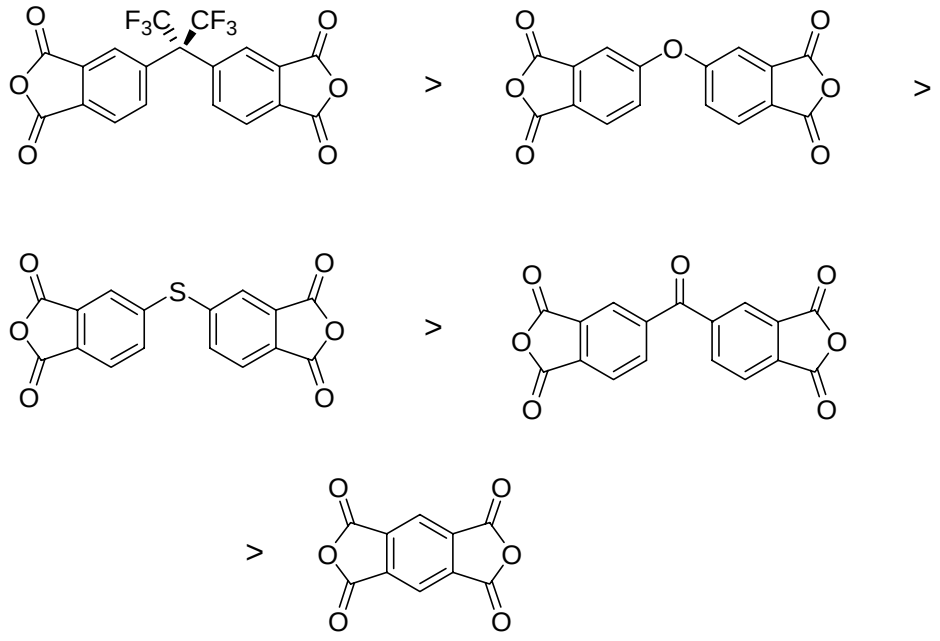

Figure 15 Effects of dianhydride structure on polyimide stability.

From the results of isothermal TGA (thermogravimetry analysis) at 371°C in Air, the effects of dianhydride structure on polyimide stability can be shown in Figure 15 [37]. It was found that 6FDA, with the structure of perfluoromethyl substituents, has the

highest use temperature and stability.

We can notice that both fluorinated diamine and fluorinated dianhydride form polyimides with better stability. The fluorine atom is the second smallest atom, and its 2s and 2d electrons are close to the nucleus. Its electric polarity is therefore small, and it is the most electronegative of all the elements. This high electronegativity results in strong bonds between carbon and fluorine atoms, giving fluorocarbon materials high thermal and chemical stability. The low polarity of fluorine gives fluorocarbons a low refractive index and low dielectric constant, and the low cohesive energy and surface free energy. It will reduce the permeability of water and/or oxygen.

If the polyimide chains are not terminated, the chains will have either an amine or an anhydride at the end of each chain. These amine or anhydride groups can be highly reactive with surrounding conditions that can decrease the stability of polyimides. A chain ending with an anhydride can cause hydrolytic degradation. The amine is even more active than anhydride so that a chain ending with an amine group can be considerably more detrimental than a chain ended with an anhydride. Therefore, It is better to have a slightly higher amount of dianhydride relative to the amount of diamine during the formation of poly(amic acid) [56].

Adding reactive end-groups to both ends of the polyimide chains is a very good way to increase the stability of the polyimide. End-groups can also limit the molecular weight of the polyimide, which aids in the processing capabilities and melt stability of the polyimide. Several reactive end-caps that are implemented are maleimide, nadimines, acetylenes, and biphenylenes. It was found that acetylene and biphenylenes offer higher

thermal and oxidative stability relative to the malic and nadic anhydrides [18]. A study of various aliphatic cross-linkable compositions suggested a stability order acerylene > norbornene > propargyl as measured by retention of adhesive properties after 1000h at 232^{o}C [57].

The trends noted above for structure-stability relationships in polyimides can be confirmed by the studies on those most successfully developed polyimides in high temperature aerospace applications. Compared to the structure of PMR-15, the backbone of AFR700B consists of 6FDA and *p*-PDA instead of BTDE and MDA. The fluorinated backbone makes AFR700B much more thermooxidative stable than PMR-15 for high temperature use up to 400^{o}C. However, AFR700B was found not to perform well in a hydrothermal environment because only one end of AFR700B's chain is capped with NE, with an amine on the other end of the chain. AFR700B polyimide exhibited significant decreases in strength (~70%) and T_g (75°C) after 1000 hours at 160°C in a hygrothermal pressure bomb environment [25, 58]. Such hygrothermal-induced property deterioration was identified with hydrolytic chain scission of the AFR700B the norbornene based crosslinks [59]. PETI-5, which is end-capped by phenylethynyl groups, exhibits 10^{13} times lower hydrolytical degradation rate than AFR700B [19, 60]. But it has a very low T_g at 270^{o}C due to the lack of flexible linkages in the structure. AFR-PEPA-N polyimides have both fluorinated backbone and phenylethynyl end-capper in structure. They have T_gs up to 435-455^{o}C, with much improved hydrolytic stability compared to AFR700B [19].

Hygrothermal Degradation

Many polyimides chemically degrade when exposed to water, leading to extremely deleterious and often irreversible damage to the composite. There is a rapid imide hydrolysis followed by thermal decomposition of the resulting amide acid intermediate. Hydrolytic attack of the imide ring reverses the formation of poly(amic acid) (Figure 16) [19], leading to chain scission and associated molecular weight and strength decreases.

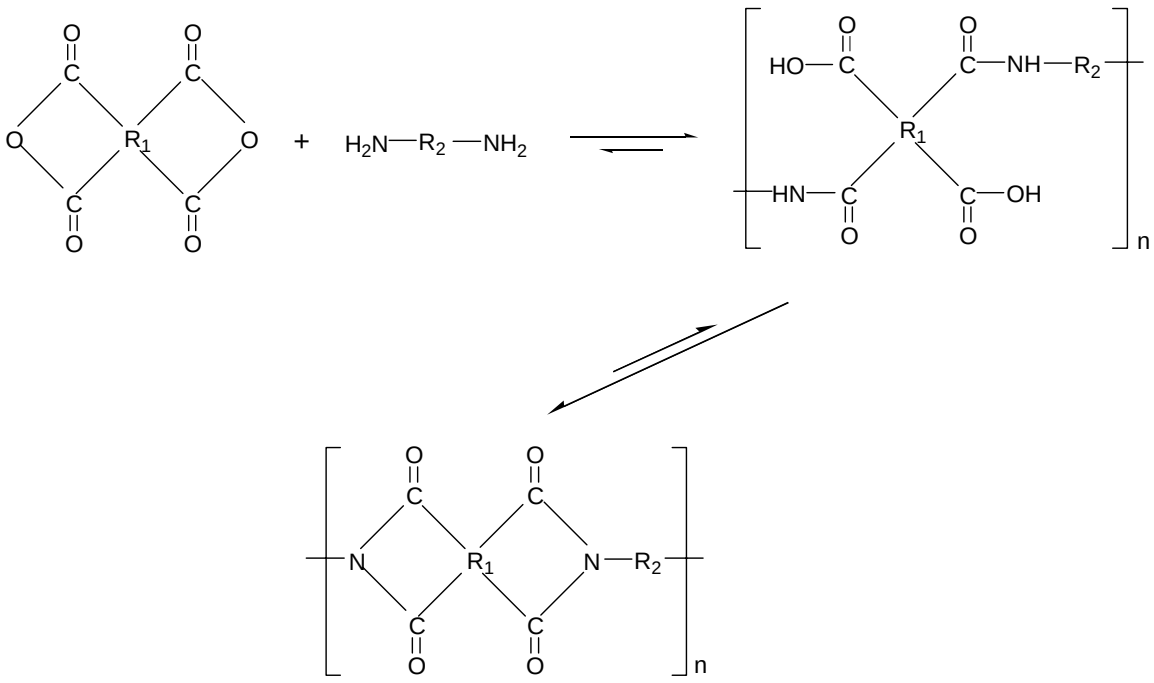

Figure 16 Polymerization and depolymerization of a polyimide.

The hydrolytic degradation of amide linkages at high temperatures has been well studied [18]. Anhydride groups are also susceptible to hydrolysis followed by

decarbocylation at elevated temperatures (Figure 17) [18].

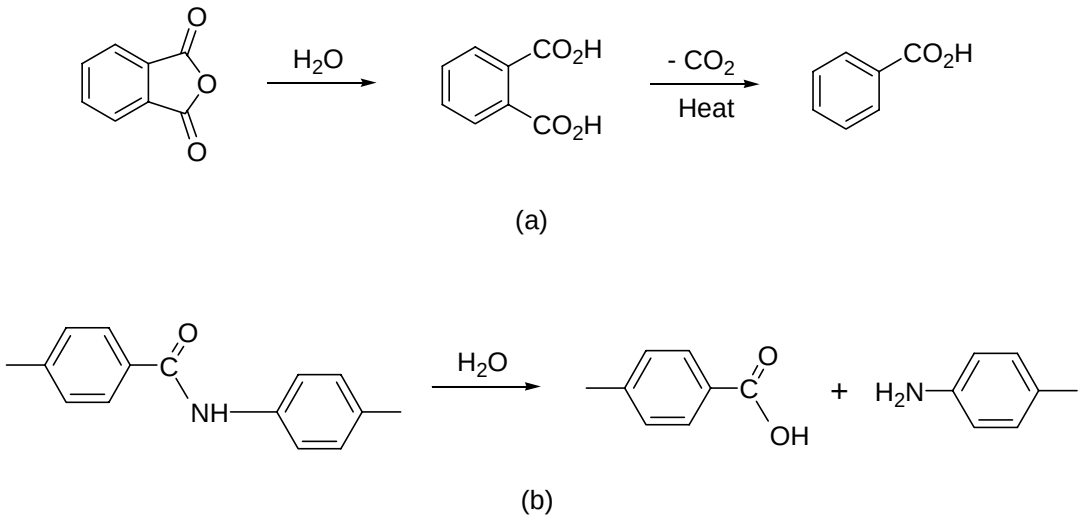

Figure 17 Hydrolysis of (a) anhydride (b) amide linkage.

Other Factors

The gaseous environment is also an important factor to affect polyimide degradation. Most aromatic polyimides do not lose weight severely when heated in a vacuum or an inert atmosphere at 350-400^{o}C for several hours. But they degrade at a noticeable rate in air and decompose faster in moist air.

Trace impurities such as alkali metal salts and trace metals Co, Cu, and Ni in polyimide can accelerate degradation significantly at elevated temperatures [18]. These salts and trace metals are always difficult to avoid because they are inherent in processes used in the synthesis of dianhydride monomers for polyimides or in solvents. The solvents used for polyimide synthesis are mainly dipolar aprotic solvents with high

boiling points. Therefore, solvents themselves can be detrimental to polyimide stability if they are not completely removed during the synthesis.

The physical state of the sample, for example, powder, film, molded part or composite, will also affect the degradation rate of polyimides. It was reported that the thicker film has the better weight retention than the thin one, which is probably due to surface area and diffusion rate of small molecules [18].

2.6.2 Effect of Polyimide Structure on Crystallinity

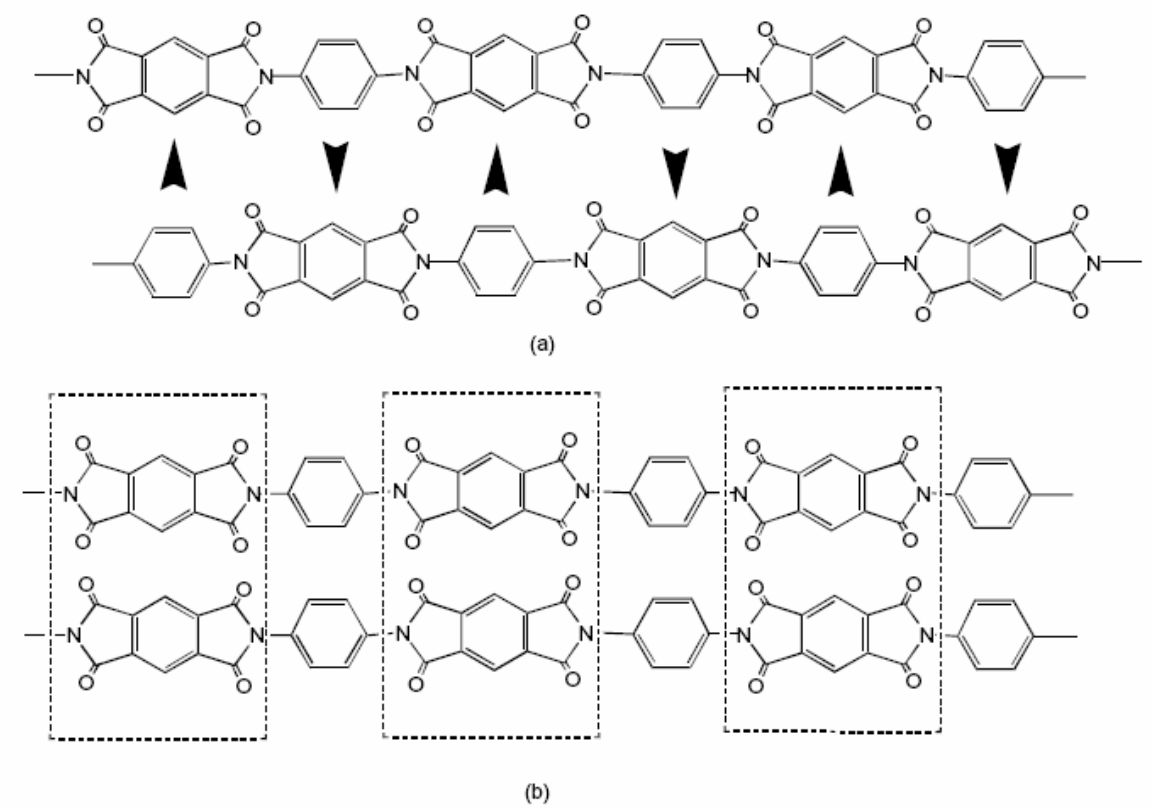

Figure 18 Interactions between polyimide chains (a) charge polarization; (b) crystalline interaction [56].

Polyimides have been observed to exhibit crystallinity in many instances. It is expected that electronic polarization occurs between electron-rich diamine and electron-deficient dianhydride regions in aromatic polyimide chains. Intermolecular charge polarization occurs when a group in one chain donates some of its electron density to an electron-deficient group in another chain [56]. This phenomenon is called "charge transfer complexation". Due to the stiffness of linear rigid-rod and segmented rigid-rod polyimides, chain-chain interactions can occur over several consecutive repeat units. Consequently, the segments become aligned along their axes. It is believed that this alignment contributes to the formation of short-range order and crystallinity [56]. An accurate physical picture has not yet been developed for chain-chain interactions comprising charge-transfer and crystalline-type interactions. There are two abbreviated idealized depictions shown in Figure 18 [56].

Polyimides containing amorphous and crystalline (or "ordered") regions are known as two-phase or semi-crystalline polymers. Two-phase linear thermoplastic polyimides are known for high T_gs, excellent solvent resistance and resistance to thermal /mechanical distortion at temperatures just above T_g [61-63]. X-ray diffraction, FTIR, and optical methods have been used to observe the semi-crystalline morphology.

Kapton-H polyimide from pyromellitic dianhydride/4,4-oxydianiline (PMDA/ ODA) is a widely studied semicrystalline polyimide system. It was found that biphenyl dianhydride (BPDA) and ODPA (3,3',4,4'-oxydiphthalic dianhydride) did not have very significant levels of crystallinity. However, BTDA (3,3',4,4'-benzophenone tetracarboxylic dianhydride) and PMDA backbones created a high amount of

crystallinity in the polyimide [56]. The crystalline behavior of some polyimide systems is listed in Table 3 [18]. The more linear and stiff the polyimide backbone is, there will be a higher amount of chain orientation within the material [18].

TABLE 3
Chemical Structure Related to Crystallinity [4]

Polyimide Name	Physical Structure	Crystalline / Amorphous
BPDA/PPD	Stiff/Rigid	Semi-crystalline
PMDA/ODA	Rigid/Flexible	Semi-crystalline
BPDA/ODA	Stiff/Flexible	Semi-crystalline
BTDA/PPD	Flexible/Rigid	Semi-crystalline
BTDA/ODA	Flexible/Flexible	Amorphous
ODPA/ODA	Flexible/Flexible	Amorphous

2.6.3 Effect of Polyimide Structure on Solubility and Processability

When crystallinity develops in polyimide, the solubility and processability of the polyimide will decrease. It has been hypothesized that crystals act as physical crosslink sites, which inhibit dissolution. This has been observed when partially imidized polyimides swell, but do not dissolve, when exposed to an organic solvent. It has also been suggested that partially imidized polyimides may contain quasi- crosslinks. These crosslinks would disappear after further imidization [64].

Incorporation of flexible linkages such as -O-, -CH_2-, -SO_2- and hexafluoro-

isopropylidene (6F) groups into the backbone of polyimides can decrease the rigidity of the backbone and inhibit packing, thus reduce the interchain interactions and H-bonging and enhance solubility and processability [65]. Bulky substituents can also decrease crystallinity and packing efficiency by distortion of backbone symmetry. Introducing bulky substituents into polyimide structure can increase T_g and thermooxidative stability while providing good solubility, especially with non-symmetrical or flexible units in the backbone [66-70]. The effect depends on the number, size and polarity of the substituents.

Monomers with twisted, kinked, or crankshaft-like structures and cage or bicyclic structures have also been used to enhance polymer solubility and processability. Meador reviewed the related efforts in detail [1]. Branching and starred structures also have been incorporated in polyimides to increase the solubility and T_g. Jensen [71] reported that PETI-5 modified by the inclusion of small amounts of a trifunctional monomer, triaminopyrimidine, had a significantly lower melt viscosity (600 poise at 335°C versus 10,000 poise for PETI-5 at 371°C). The T_g of the modified system is higher than PETI-5 (291°C versus 263°C), and the mechanical properties of films prepared with this polyimide are better.

It should be noted that to have a processable polyimide without sacrificing its inherent high temperature characteristics is a big challenge. There is a balance between stabilities of polyimides and their solubility and processability since the same structural feature that enhances one but decreases the other.

AFR-PEPA-N polyimides balance those properties for aerospace applications very well. The introduction of hexafluoro-isopropylidene (6F) group into the structure enhances the solubility and processability of the polyimides. Meanwhile, fluorinated backbone gives the polyimides higher thermal and chemical stability. The use of end group, phenylethynyl, also contributes to higher thermal and hydrolytic stability.

Characterization of the structure-property relations of AFR-PEPA-N oligomers and their crosslinked polyimides has been conducted recently by Lincoln [19]. The oligomers with different molecular weights (n = 2, 4, and 8) were synthesized. The n = 2 oligomer exhibited a broad molecular weight distribution whereas in the case of n = 4 and n = 8 oligomers the distributions were narrow. Rheological studies of these oligomers revealed AFR-PEPA-2 was borderline processable and the n = 8 oligomer was not processable due to its high viscosity, η, (40,000 poise) in the cure temperature range of 360 – 370°C. A plot of T_g versus degree of cure of AFR-PEPA-2 oligomer illustrates T_g's of over 400°C are achievable. Thermal stability of polyimides in N_2 was predicted. The Young's modulus, tensile strength and failure strain of some partially cured AFR-PEPA-N polyimides were given. However, no studies, as yet, have been performed to characterize the network structure and the effects of thermal history (free volume, degree and type of cure in air versus nitrogen). Cure reactions of different oligomer systems and related property characterization need to be investigated to further understand the structure-property-processing relations of AFR-PEPA-N polyimides.

Meanwhile, cure characteristics of 4-phenylethynyl phthalic anhydride (PEPA) derivates, the end-capper of AFR-PEPA-N, need to be studied in detail. To understand

the cure reactions of PEPA derivates as the function of reaction conditions and parameters is very important for understanding the fundamental chemistry of AFR-PEPA-N based composites.

2.7 Chemistry of Bismaleimides

2.7.1 Introduction

BMI resins are a leading class of thermosetting polyimides. Their good processability and balance of thermal and mechanical properties have made them attractive in advanced composites and electronics. BMIs also have many advantages such as low moisture absorption, low cost and they are nonvolatile. The major application of BMI structural composites are in aero-engines and military aircraft. However, BMIs have exhibited brittle mechanical response [2, 3].

The chemical structure of BMIs is shown in Figure 19. They were firstly synthesized from pyromellitic acid dianhydride, aromatic amine and endcapper maleic acid anhydride in dimethylformamide (DMF) [2]. The solution of the poly(amic acid) was heated to 70-120^{o}C to undergo the cyclohydration reaction. BMIs based on aromatic diamines are crystalline materials with high melting points. There is a wide variety of BMIs has been synthesized from various aromatic amines. 4,4'-biamaleimido diphenyl methane (BMPM) is the most often used among them due to its low cost and excellent thermal stability of the related BMIs [72]. Other BMI systems based on M-phenylene bismaleimide, 2,4-bismaleimido toluene, 2,4-bismaleimidoanisole, 1,5-bismaleimido-naphthaline have also been synthesized [2]. But many of them are too expensive so that

they are not used in commercial resin formulations.

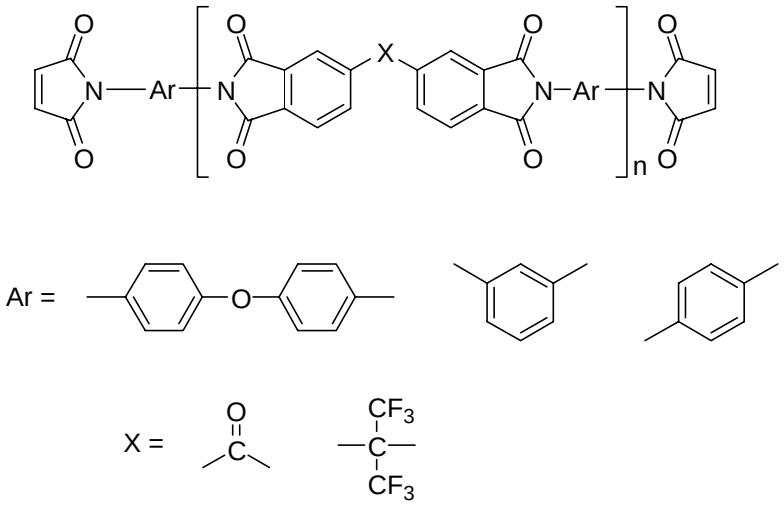

Figure 19 Chemical structure of bismaleimide.

The outstanding property of N-substituted maleimide is the reactivity of the maleimide double bond. This high reactivity is from two adjacent electron-withdrawing carbonyl groups, which make the maleimide double bond very electron-deficient. When heated above their melting points, BMIs undergo a free radical polymerization reaction without the need for a catalyst, following first-order kinetic law up to a conversion of 30-40% [73]. The homopolymerization of maleimides has been well studied [74]. Polymerization of maleimides or copolymerization of maleimide and the monomers with active double bonds can also be initiated in presence of peroxides. Peroxide cure of maleimide formulations can be of interest for fast-curing molding compounds. Those free radical initiators with high decomposition temperature are suitable for BMIs

because many of BMIs have high melting points [2]. It was reported that the maleimide double bond can also be activated by ionic-type catalysts [73]. Diazabicyclooctane (DABCO) and 2-methyl imidazole are recommended as anionic catalysts for BMI resins [2].

In addition to homopolymerization and copolymerization, there are many other chemical reactions involved in BMI chemistry. For example, BMI can undergo Diels-Alder reaction with a suitable diene; Ene reaction with allyl compounds; Michael addition with primary and secondary amines; and other addition reactions with cyanates, isocyanates, azomethines and epoxies [2]. Although BMI has a brittle nature that limits their applications, the versatile reaction capability of maleimides provides the great possibilities to modify BMIs with reactive components such as reactive diluents, additives, comonomers and viscosity modifiers so that the BMI systems with desired properties can be developed.

2.7.2 Backbone Modifications of BMIs

Bismaleimide / Allyl Phenyl (Allyl Phenol) Copolymers

The rigid aromatic units tightly held by the short methylene linkages make the BMI matrix brittle. Therefore, a suitable reactive comonomer that can extend the chain of BMI will improve processability and toughness of BMIs. Allyl phenyl and allyl phenol compounds have been proved to be the good comonomers for BMI resins [22].

The mechanism of the reaction between allyl compounds with BMI has been studied in detail. The reaction between the two components proceeds via the Ene reaction at relatively low temperature at first. The unsaturated Ene adduct intermediate

can easily undergoes a further Diels-Alder type reaction with excess BMI to give the bis- and tris adducts. The intermediate step (Diels-Alder) is sometimes referred to as Wagner–Jauregg reaction too [75]. The total reaction sequence is also referred to as Alder-ene reaction. At very high temperatures, a retro-Diels-Alder reaction is also suggested [22]. The resulting copolymer network is much tougher than the BMI homopolymer. The molar ratios of allyl comonomer to BMI can be varied. Theoretically, a molar ratio 1:3 (allyl:maleimide) gives a maximum cross linking and enhanced thermal stability, but this could lead to brittle matrices. To add more allyl function in the system ensures the Ene structure-dominated, tough matrix with good flexural properties, but with reduced T_g and thermal capability [2]. In most of the commercial cases, a compromise of various properties is achieved at an allyl/BMI ratio of 1:2.

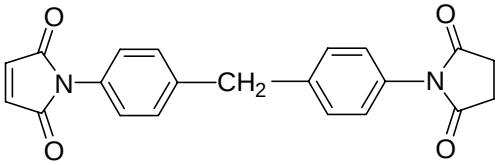

BMPM

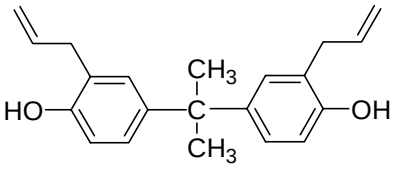

DABPA

Figure 20 Chemical structure of BMPM/DABPA system.

O,o'-diallylbisphenol-A (DABPA) and COMPIMIDE TM 121 are the most widely used allyl phenol and allyl phenyl comonomers for BMI resins. DABPA/BMPM (4,4′-bismaleimidodiphenyl methane) based BMI system (Figure 20) is one of the leading matrix resins for carbon fiber composite for advanced aerospace applications. With certain formulation and catalysts, these resin systems can give a high T_g (~315 °C) matrix [76]. Also, DABPA/BMPM based composites exhibit better heat and moisture resistance, which are desirable for cryogenic structures in aerospace applications. Therefore, one of the studied high temperature polymers in this dissertation will be DABPA/BMPM based matrix.

Bismaleimide / Diels-Alder Copolymers

BMI is a dienophile compound, which can react with a diene to form a ring-containing compound via Diels-Alder reaction. There are many dienes such as furanes [77], isobenzofuranes [78], cyclohexadienes [79], cyclopentadienones [79, 80] and pyrrones [81]. It was found that a prepolymer with maleimide ends can be formed if BMI and the bisdiene react nonstoichiometrically with BMI in excess, which can be crosslinked to obtain a heat resistant network [2].

Bismaleimide / Michael-Addition Copolymers

BMI can react with bis-nucleophilic species to form the crosslinking structure via Michael-Addition reaction. Dithiols and diamines are the favored bis-nucleophilic because they have high basicity [82-86]. One of the most important developments to thermosetting polyimides is the nonstoichiometric Michael-Addition reaction between BMI and aromatic diamine [2]. A typical adduct structure of prepolymer from BMPM

and 4,4'-diamino diphenyl methane is shown is Figure 21. The fracture and T_g were reported as the function of diamine content [2].

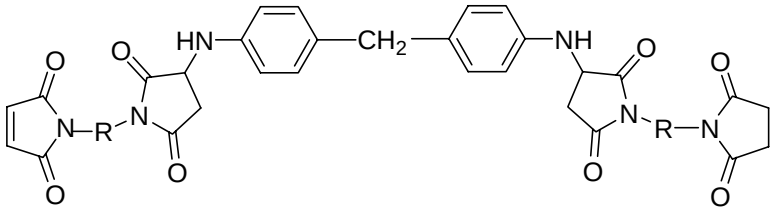

Figure 21 Chemical structure of BMPM / 4,4'-diamino diphenyl methane adduct.

Bismaleimide / Epoxy Copolymers

There are many efforts have been made to blend epoxy and BMI resins to achieve both high temperature performance and processing ease [87-89]. Introduction of epoxy backbone between the maleimide ends could improve the toughness of BMIs and have less sacrifice in thermo-oxidative stability. For example, Liu et al. prepared BMI with epoxy backbone linkages and various bridging groups through reacting 4-(N-maleimidophenyl)glycidylether with biphenol and silandiol compounds [89]. The BMIs with epoxy and silicon linkages or phosphorus groups exhibited good organosolubility, low melting points, and excellent processability. The cured polymers were found having high glass transition temperatures above 210°C and good thermal stability over 350°C [89].

Bismaleimide / Cyanate Copolymers

Copolymers of aromatic cyanate esters and bismaleimide have been realized to derive systems bearing good physicochemical attributes of the two components, i.e. the thermal characteristics of bismaleimide and the toughness of polycyanurates. Depending on the composition of the blend (generally from 10–60 wt% BMI), a variety of materials can be produced with melting points ranging from 70 to 110°C and T_g values around 230–290°C [90]. However, there is no report on detailed reaction mechanism of the copolymerization of maleimides with cyanate. Lin, et al. studied the cure reactions of BMPM with aromatic dicyanate esters and found the formation of pyrimidine and/or pyridine structures [91].

2.7.3 Cure Mechanism of BMPM/DABPA Bismaleimides

Most common BMIs, including those supplied by Cytec, Hexel, and others, contain 4,4'-bismaleimido diphenyl methane as one major component and an aromatic diamine, a diallyl alcohol, or another bismaleimide as the co-component. Cure reactions of BMI resins vary with different functional groups of such co-components. The major proposed reactions are: (i) Michael additions between maleimide and nucleophile groups such as amines and thiols; (ii) Ene or Diels-Alder reactions between maleimide and allyl, propenyl, cyanate or cyclobutene groups; (iii) Homopolymerization or copolymerization via active C=C double bonds of maleimide and allyl, propenyl or vinyl groups.

As mentioned in 2.7.2, DABPA (2,2’-diallylbisphenol A) is most commonly used as allyl co-component of BMI. DABPA/BMPM (4,4′-bismaleimidodiphenyl methane) based BMI system is one of the leading matrix resins for carbon fiber

composite for advanced aerospace applications. The thermal cure mechanisms of BMI/DABPA system have already been studied by DSC (Differential Scanning Calorimeter), FT-IR (Fourier Transform Infrared Spectrometry), Fluorescence, UV-Reflection Spectrometry and Fiber Optic Near-Infrared Spectrometry [92-96]. Morgan et al. concluded the cure reactions of the BMPM/DABPA BMI resin system as a function of temperature-time cure conditions:

1) In the 100-200^{o}C range, the BMPM and DABPA monomers react via Ene reaction to form Ene adduct (Figure 22). The Ene adduct is pentafunctional as a result of three carbon-carbon double bonds, capable of chain extension and crosslinking. In addition, two hydroxyl groups undergo etherification by hydroxyl dehydration.

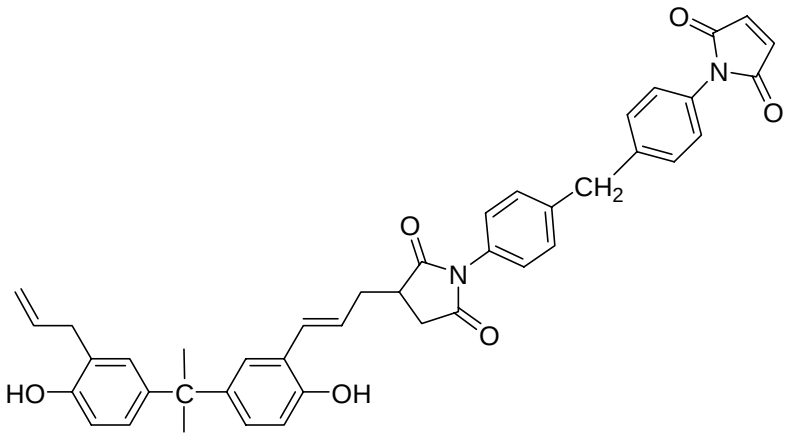

Figure 22 Chemical structure of BMPM/DABPA Ene adduct.

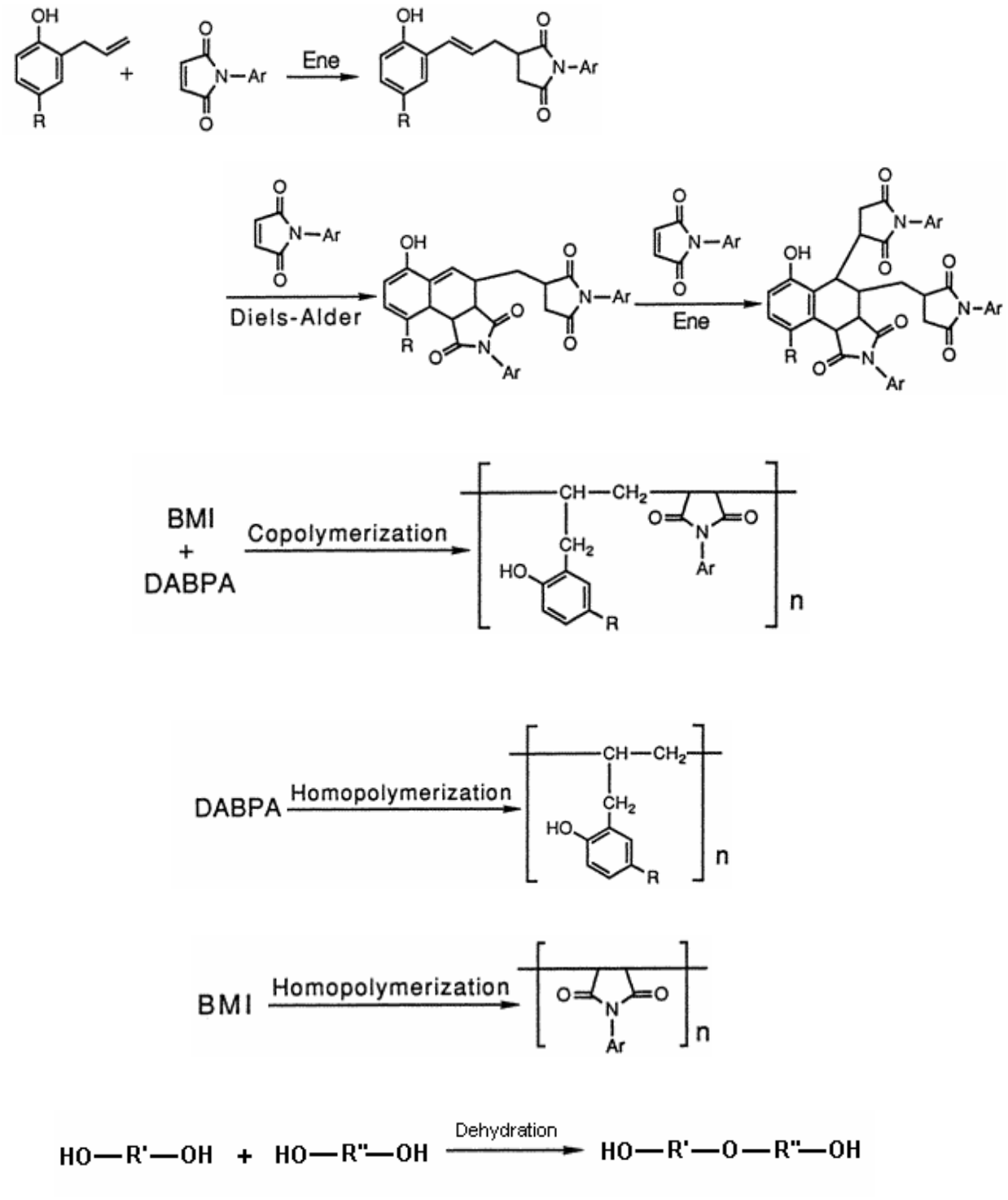

Figure 23 Thermal cure reactions involved in BMPM/DABPA BMI system.

2) The principal cure reactions occur in the 200-300^{o}C range via the carbon-carbon double bonds together with etherification occurring above 240^{o}C.
3) Cure was incomplete due to glassy-state diffusion restrictions at 250^{o}C and further cure at 300^{o}C for 1 or 2h produced a constant T_g near 350^{o}C.

The related formulas of reactions are listed in Figure 23.

2.8 Electron Beam Cure Technique for Space Applications

2.8.1 Introduction of Radiation Chemistry

Radiation chemistry is concerned with the interaction of energetic charges particles (electrons, protons, alpha and other heavy particles) and high energy photos (x-rays and γ rays) with matter. There interactions result in ionization (along with some excitation) of the medium. Visible or ultraviolet photons interact with matter by predominantly producing excited states (even though ionization can also be produced if there is enough energy in the photons). Therefore, charged particles, x-rays, and γ rays are called "ionizing radiations"; visible and ultraviolet photons are called "nonionizing radiations" [97]. The radiation sources can also be classified into "non-particulate radiation" including microwave, infrared, light energies, x-rays, and γ rays; and "particulate radiation" including α particles, β particles, high energy electrons, protons, deuterons, neutrons etc.

Absorption of high-energy radiation by polymers produces excitation and ionization and these excited and ionized species are the initial chemical reactants. There are two major categories for irradiation on polymer materials. One is to modify the

existing polymers either by chain scission or by crosslinking. Another is for radiation initiation of ionic or radical polymerization. Crosslinking is the intermolecular bond formation of polymer chains. The degree of crosslinking is proportional to the radiation dose. The polymerization and crosslinking reactions of reactive monomers, oligomers, or polymers can be initiated by radiation (Figure 24).

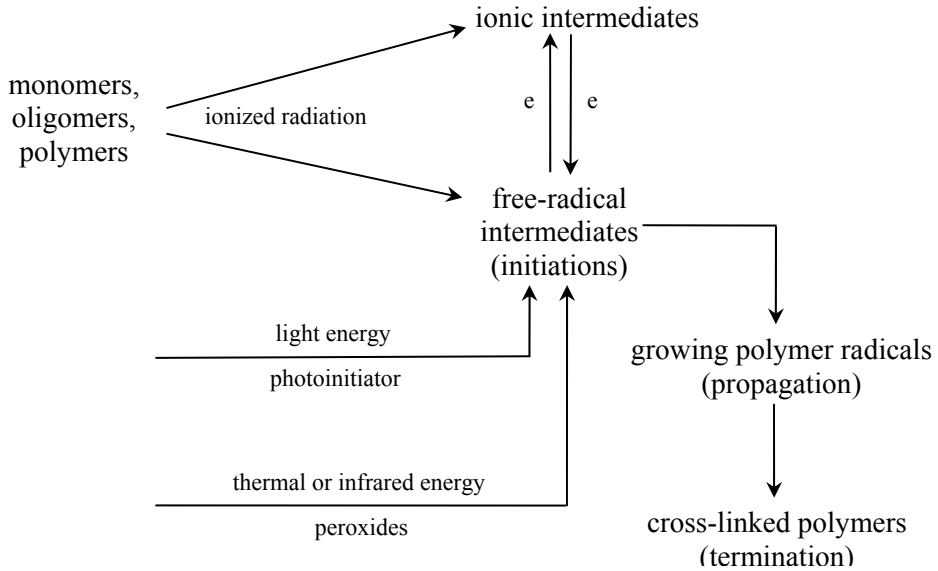

Figure 24 Scheme of radiation initiated crosslinking.

Although the mechanism of crosslinking by radiation has been studied since its initial discovery, there is still no widespread agreement on its exact nature. Generally, the mechanism of radiation initiated crosslinking involves the cleavage of a C-H bond on one polymer chain to form a hydrogen atom, followed by abstraction of a second

hydrogen atom from a neighboring chain to produce molecular hydrogen. Then the two adjacent polymeric radicals combine to form a crosslink [98]. The molecular weight of the polymer steadily increases with radiation dose, leading to branched chains, until a three-dimensional polymer network is formed when each polymer chain is linked to another chain. Often these reactions can also be obtained with thermal or chemical initiation. However, radiation process has some unique advantages over those thermal and chemical processes.

Radiation processes have many advantages over other conventional methods. In initiation processes, no catalyst or additives are required to initiate the reaction so that the purity of the processed products can be maintained. Chemical initiation is limited by the concentration and purity of the initiators. In radiation processing, the dose rate of the radiation can be varied widely and thus the reaction can be better controlled. Chemical initiation often brings about problems arising from local overheating of the initiator. But in the radiation-induced process, the formation of free radical sites on the polymer is not dependent on temperature but is only dependent on the absorption of the penetrating high-energy radiation by the polymer matrix. However, nuclear radiation energy is expensive though very efficient in bringing about chemical reactions. The unit cost of installed radiation energy is much higher than that of conventional heat or electrical energy.

2.8.2 Radiation Sources for Curing of Polymer Composites

The most commonly used radiation sources for polymerization and crosslinking reactions are cobalt-60, low and high energy electron accelerators, light energy

(ultraviolet-visible), infrared source of energy, and plasma or glow-discharge energy sources (microwave- or radio-frequency range).

The radioactive isotopes cobalt-60 and cesium-137 are the main sources of gamma radiation with deep penetration. Gamma-ray radiation has been used in curing of epoxy based polymer composites [11, 99]. Nho et al. [11] compared the effect of an Electron beam and Gamma-ray radiation on the curing of epoxy resins diglycidyl ether of bisphenol-F(DGEBF) and found the gel fraction of DGEBF irradiated by Gamma-ray was higher than that of the epoxy irradiated by E-beam at the same dosage. However, being a "live" source, gamma ray is inherently dangerous and faces severe liability problems.

Electron irradiation is normally obtained from electron accelerators to give beams with energies in the MeV range. The corresponding penetration depths are in the mm range. Lower energy x-radiation is produced by electron bombard of suitable metal targets with electron beams or in a synchrotron. E-beam and x-ray irradiation are the mainly used sources for radiation curing of thermosetting polymer composites [4-14], which will be summarized in the next section.

Classical sources for ultraviolet radiation include mercury and xenon arc lamps, which have the advantage of road band excitation for spectroscopic studies, but suffer from the corresponding broad monochromator controlled bandwidth. UV radiation is widely used for fast curing of polymer coatings, adhesives and thin films [100, 101], but its penetration is not deep enough for curing of structural composites. Infrared radiation

can also be used for curing of polymer coatings and thin films by heating effect. It will depend on the thermal conductivity of the system [102].

Plasma radiation sources fall into three categories: thermal plasma produced by gas arcs under atmosphere pressure in the 5,000-50,000 K region; cold plasma produced by glow discharges; and hybrid plasma generated from corona or ozone dischargers. However, the interaction of polymer solid with plasma radiation usually results in very thin (100nm) surface films containing crosslinked structures [103].

Microwaves heating have been investigated as an efficient alternative energy source for polymers and composites processing. Microwave processing offers several advantages over conventional thermal processing method such as fast and volumetric heating, enhancement of fiber/matrix adhesion [104-106].

2.8.3 Characteristics of E-beam Curing of Polymer Composites

The Merits of E-beam Technique

E-beam curing is a non-thermal method that uses high-energy electrons and /or X-rays as ionizing radiation to initiate polymerization and crosslinking reactions at controlled doses. For aerospace applications, the advantages of E-beam curing include:

- E-beam curing is faster than thermal processes. Curing time are minutes (versus hours in an autoclave).
- Curing is done near room temperature, allowing the use of low cost, low temperature tools such as wood, plastic or foam.
- Residual thermal stresses are reduced in low temperature curing.

- Co-boding and co-curing operations with E-beam curable adhesive allow fabrication of large, integrated structure.
- E-beam curable resins have long shelf-lives.
- Capital costs of E-beam curing systems (principally the electron accelerator and concrete radiation shielding) are similar to autoclave costs.
- Large parts are well suited to curing using E-beam

Processing and prototype development for E-beam cured aircraft and vehicle structures is currently conducted at a number of industrial and government laboratories [7].

Characteristics of E-beam Curing

The interaction of high energy electrons with condensed materials depends on both the kinetic energy of the electrons and the atomic composition of the irradiated materials. There is high level of variability that exists in the properties of E-beam cured systems cured at different facilities and under different cure conditions.

The important characteristics of E-beam facility are its energy and power. The power is proportional to the current for a given energy. Beam power determines the dose rate and the line speed of E-beam curing. Beam energy or accelerating voltage, typically expressed in MeV, controls penetration depth and determines the thickness of the resin that can be cured uniformly.

The penetration depth is the function of beam energy and product density, which is given by Equation (1):

$$d = \frac{0.4E - 1}{\rho} \quad (1)$$

Where E is the electronic energy in MeV, and ρ is the average density of the material in g/cm^3. We can estimate that the maximum resin thickness (suppose density is 1.6 g/cm^3) is 21mm for a 10 MeV E-beam. For greater penetration, the electron beam can be converted into X-rays, which have a penetration capability equivalent to gamma rays from cobalt-60.

Throughput is a function of the power of the E-beam. Theoretically, 1kW will process 3600 kGy kg per hour.

Radiation dose and dose rate are important parameters for controlling the cure extent and cure rate in E-beam systems. The dose is defined as the amount of energy absorbed by the material and is directly related to reaction conversion. It is reported that 100 KGy dosage can cure most composites completely. Dose rate is defined as the energy absorbed by exposed material per unit time, which controls the concentration of initiating species in addition to the time required attaining full cure during irradiation.

The application of E-beam dose to a resin part is a discontinuous process so that it is always expressed as kGy per pass. Several experiments show that the network structures and performances of cured resins vary with different cure schedules (different dose applied per pass) even if the final dose is same. Such differences associated with the cure schedules, in fact, are average dose rate and the temperature attained during polymerization.

The reaction rate always depends on temperature for any chemical reactions. E-beam radiation induces a temperature rise in all materials due to energy absorption:

$$\Delta T = \frac{D}{C_p} \tag{2}$$

Where D is dosage and C_p is specific heat coefficient of the materials. Thus, to investigate such temperature rise during radiation process and its effect on structure and properties of the products are critical for the program.

2.8.4 Development of E-beam Curable Polymer Matrices for Aerospace Applications

Work on E-beam curing of thermoset composites has been studied since 1970s. The principal resin systems that have been widely studied as E-beam curable resins are free radical polymerized acrylated epoxides [107] and $I^+SbF_6^-$ catalyzed Diglycidylether of Bisphenol A Epoxide (DGEBA) cationic polymerized resin [109, 110]. The mechanism of E-beam radiation polymerization of Epoxy is shown in Figure 25. It was found that initiator affects the effectiveness of E-beam curing polymerization. Generally, the cure effectiveness decreases in the order:

$$SbF_6^- > AsF_6^- > PF_6^- > BF_6^-$$

The $I^+SbF_6^-$ cationic catalyzed DGEBA epoxides resin-carbon fiber composites are the materials that have been studied by Air Force and NASA for their space applications. The studies on the E-beam curing of $I^+SbF_6^-$ - DGEBA resins and their carbon fiber composites have involved the effects of E-beam dose rate characteristics and $I^+SbF_6^-$ catalyst concentrations upon the resins T_g's [108, 109] and the composite

fiber matrix interface characteristics [110, 111]. However, epoxy based composites have drawbacks associated with a limited use temperature (relatively low T_g), moisture absorption and corresponding plasticization, and often a brittle mechanical response, especially after exposure to the synergistic exposure conditions. Thus, E-beam curable high performance polymer matrices need to be developed.

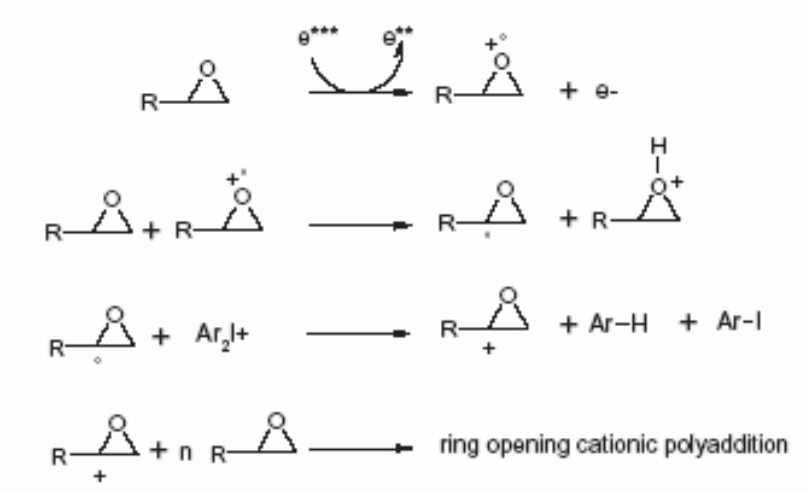

Figure 25 The mechanism of E-beam radiation polymerization of epoxy resins.

There are few reports on E-beam cure of imide oligomers or BMI probably due to their high melting point. E-Beam curing was found to be insufficient to cure BMI resin [15]. The addition of reactive diluents into the BMI resin system was proven to be feasible to increase the reactivity of BMI during E-beam curing. Reactive vinyl diluents, such as NVP, styrene, allylphenol, vinyl ethers, acrylonitriles, acrylates and methylacrylates, are widely used to assist BMI curing reactions [112-114]. Marie-

Florence et al. [15] made a successful attempt at using N-vinylpyrrolidone (NVP) as a diluent for E-beam curing of BMI resins. It has been reported that the percentages of residual maleimide functions in BMI/NVP systems are less than 10% and the T_g of the related products are around 240^{o}C after 400 kGy E-beam dosage E-beam at 50 kGy per pass [15]. Wang et al. used N,N-dimethyl acrylamide (DMAA) as a reactive diluent for BMI oligomer from 4, 4′-bis(maleimido)diphenyl methane and methylenedianiline [115]. The solution with a solid content up to 50-70% was irradiated by Cobolt-60 with the dose from 20 to 350 kGy at room temperature. The T_g before and after postcuring was around 100°C and 150-180°C, respectively. Styrene was used along with DMAA to decrease the water absorption for the copolymers [115].

However, fundamental chemical and physical changes of BMI resins during E-beam cure are poorly understood (gelation, vitrification, reaction mechanisms, kinetic analysis, processing-property relationships). In addition, it has always been found that the E-beam curing will increase the sample's temperature. Since the temperature factor plays a critical role in the cure rate and cure mechanisms, processing and the performance of final products, the studies of related temperature rise during E-beam curing are important. Unfortunately, there is no report on the temperature-time characteristic of E-beam curing of BMI systems.

NASA and Air Force have also been investigating the E-beam curing for polyimides [16, 32]. The idea is still to add reactive diluents or flexible components to reduce the viscosity of imide oligomers. Hay et al. synthesized a phenylethynyl terminated polydimethylsiloxane (PET-PDMS) [32], which is a viscous liquid at room

temperature due to the introduction of flexible polysiloxane backbone in the structure. It allows E-beam cure of the end-group without restricted mobility of the polymer chains. 73% of ethynyl bonds were consumed after 2 hours 25 keV E-beam curing. But the curing was performed on a thin film [32]. Hoyt also synthesized E-beam curable polyimide-siloxane oligomers. The oligomer has a T_g of 240-250^oC after being radiated at a total dose of 150 kGy [16].

A number of modeling approaches have been conducted in the area of the thermal cure processes of polymeric composite materials where the cure temperature is directly controlled by the oven temperature and heat transfer at the sample boundary [116]. Only a few studies have addressed the thermal modeling issue of the E-beam curing process by combining the experimental data and simulations. Boursereau et al. [117] reported their development of the finite element thermal analysis model that takes into account dose rate history, shape and nature of the sample, thermal absorption and transfer mechanisms. Moon et al. [118] developed a model that predict E-beam induced cure kinetics, local temperature and as a function of dose and catalyst concentration on $I^+SbF_6^-$ - DGEBA system. However, no modeling work has been done on E-beam curing of BMI systems.

Hence, if E-beam cured polymer matrix-carbon fiber composites are to confidently achieve their structural application goals for space vehicles, a fundamental standing of the relations between the processing parameters, the resultant physical and chemical structure and the performance of E-beam cured high temperature polymer matrices need to be addressed.

CHAPTER III

STUDY OF E-BEAM CURABLE BISMALEIMIDE RESINS*

3.1 Introduction

The ideal resin system for this research should be E-beam curable, readily available at low cost and has excellent thermal (cryogenic) and mechanical performance so that the resin can meet the requirement for aerospace applications. Meanwhile, thermal cure mechanisms of such system should be well studied. BMI resins have been shown to exhibit great potential in aerospace applications because of their high thermal stability which enables them to bridge the gap between epoxy and high temperature polyimide resins. BMI also has many advantages such as low moisture absorption, low cost, it is nonvolatile, and can be easily processed [2, 3].

Thermal cure reactions of BMI systems [92, 95, 96, 119-121] and related resin modifications [122-128] and structure-property characterization of BMI and BMI composites have already been widely studied [129-136]. However, E-Beam curing is found to be unable to fully cure BMI resin [15]. Although BMI can also be cured via anionic polymerization in presence of catalyst such as DABCO (diazabicyclooctane) and imidazole, the basis of E-beam cure mechanism of BMI in this research is that high energy of electrons transfer to molecular bonds, such as C-H bonds, causing rupture of the bonds with formation of excited carbon atom free radicals and then initiate and

*Part of the data reported in this chapter is reprinted with permission from "Electron Beam Curing of Bismaleimide-Reactive Diluent Resins" by Yuntao Li, Roger J. Morgan, Francisco Tschen, H.- J. Sue and Vince Lopata , 2004, Journal of Applied Polymer Science, 94(6), 2407-2416, Copyright 2004 by John Wiley & Sons, Inc.

propagate the related free radical reactions. Since ene reaction, homo- and co-polymerization between C=C bonds can all undergo free radical mechanism favorably, allyl compounds are suitable to be selected as the co-component of BMI resin for chain extension. The addition of reactive vinyl diluents, such as NVP, styrene, allylphenol, vinyl ethers, acrylonitriles, acrylates and methylacrylates, into the BMI resin system can increase the reactivity of BMI during E-beam curing.

E-beam radiation absorption will raise the temperature of the samples together with the resin cure exotherm. Since the temperature factor plays a critical role in the cure rate and cure mechanisms processing and the performance of final products, the studies of the corresponding temperature rise during E-beam curing are important. Unfortunately, there is no report on the temperature-time characteristic of E-beam curing of BMI systems.

In this chapter a basic study on E-beam curing of BMI, BMI/styrene and BMI/NVP systems with in-situ temperature monitoring has been investigated in order to understand how temperature rises, dosage, diluent concentrations, and catalyst affect E-beam cure reaction of BMI. This will lead to an understanding of the involved reactions and mechanisms, while controlling the optimum processing and performance of final products more easily.

3.2 Experimental

3.2.1 Materials

A modified BMI system, CYTEC 5250-4 RTM was utilized. It is a tri-component resin system comprised of 4,4'-Bismaleimidodiphenylmethane (BMPM),

BMI-1,3-tolyl and o,o'-diallylbisphenol A (DABPA) with the molar ratio of 6:4:5 (Figure 26). Thus, the overall molar ratio of BMI and DABPA is 2:1. This BMI resin is widely used in aerospace composites because of its superior mechanical and thermal properties [22-24]. It will be simply referred as "BMI" in the following discussion.

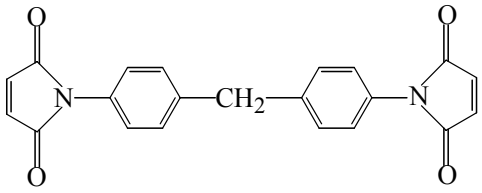

4,4'-Bismaleimidodiphenylmethane (BMPM)

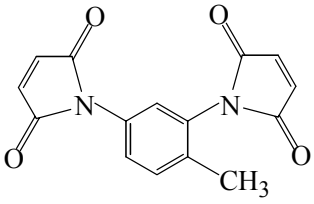

BMI-1,3-tolyl

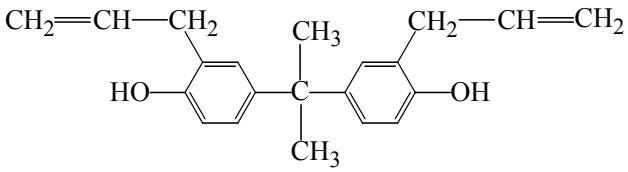

o,o'-Diallylbisphenol A (DABPA)

Figure 26 The chemical structures of the components of BMI 5250-4.

N-vinylpyrrolidone (NVP) and styrene were chosen as the reactive diluents because they have similar structural units as BMI and because the crosslinked products with good thermal and mechanical properties can be achieved. Both NVP and styrene were distilled for use. BMI/NVP 20/80, 40/60, 50/50 and 60/40 (wt./wt.) and BMI/styrene 50/50 (wt./wt.) solutions were prepared for E-beam curing.

To investigate the effect of catalyst on E-beam curing of BMI systems, dicumyl peroxide was used as a free radical initiator. After mixing and degassing, the samples of BMI, BMI/NVP and BMI/styrene with or without initiator were drawn into 1ml polypropylene syringes for low intensity E-beam exposures, with the intensity less than 20 kGy per pass. BMI resin was preheated at 75^{o}C in an oven until molten to be drawn into the syringes. For high intensity E-beam exposure with 400 kGy dosage at 40 kGy per pass, samples were stored in small glass vials with the diameter of 3 mm instead for E-beam curing because the plastic syringe will be melted due to high temperature rise from high intensity E-beam radiation.

N-vinylpyrrolidone, styrene, and dicumyl peroxide were obtained from Aldrich. N-vinylpyrrolidone and styrene were distilled before use.

3.2.2 E-beam Curing

E-beam curing of samples was carried out by a 10 MeV accelerator rated at 4 kW by Acsion Inc. The electron beam was scanned vertical over the samples. All the samples were lined up so that the samples would receive the dose in the same manner. The samples were passed across the vertical sweeping beam in the horizontal direction (Figure 27, (a)).

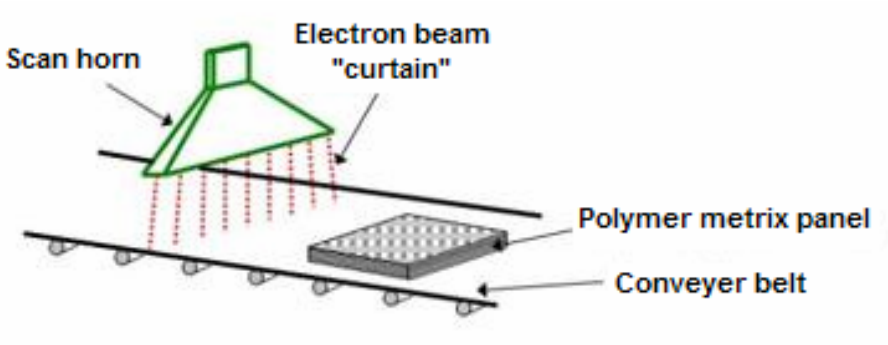

(a)

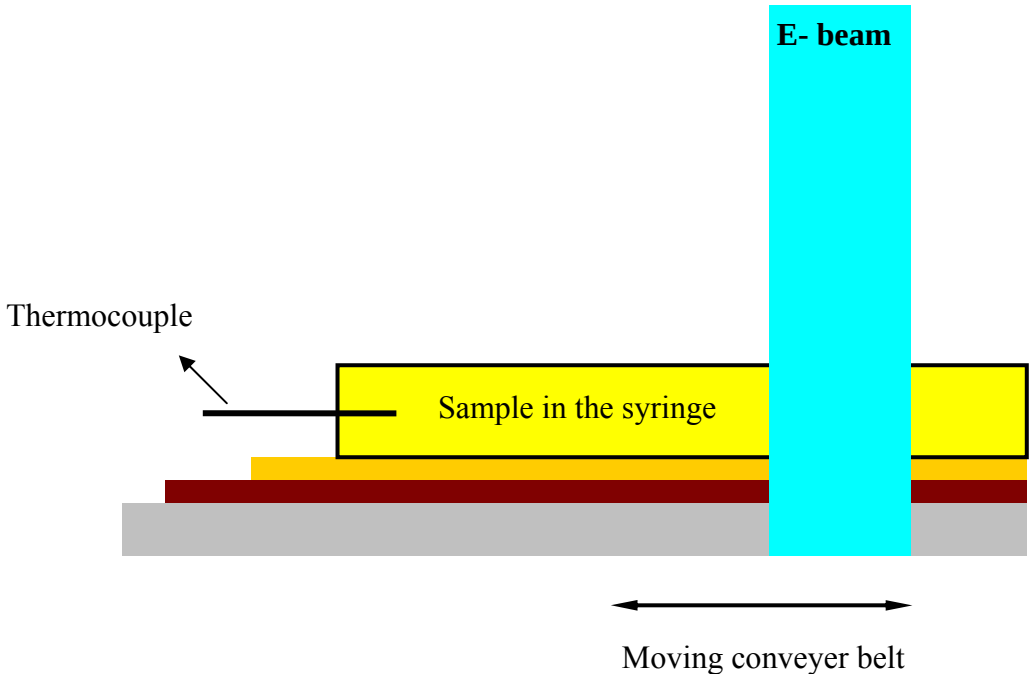

(b)

Figure 27 Scheme of E-beam curing setup.

As shown in Figure 27, (b), the samples were filled in 1 ml plastic syringes or small glass vials and placed on a polymer composite panel with a thickness of 3.175

mm. This panel was placed on an aluminum plate that was 6.35 mm thick, which was placed on a conveyor belt. The conveyor belt passed back-and-forth under the electron beam with certain speed to deliver the required total dose.

The thermocouples were placed about 3.175 mm into the resin in order to monitor the temperature of samples during exposure. A fully cured epoxy sample provided by Acsion Inc. was used as a reference during temperature monitoring to determine if the temperature rise is from exothermal chemical reactions or beam energy absorption only.

The dependence of reaction conversion on accumulated exposure dosage was investigated under the E-beam radiation at 10 kGy per pass. All of the samples were treated at the same time. Then, one of samples was removed after the first pass. The rest of the samples were subsequently treated by E-beam, and then, one of the samples was removed after each pass. The samples were treated and then removed one by one in this manner, producing samples with different dosage exposures.

3.2.3 Characterizations

The temperature profiles of BMI, BMI/styrene and BMI/NVP systems during E-beam curing were monitored in a range of experiment sets. To investigate the corresponding temperature rise on each radiation dose and reaction progress, the samples were cooled down to room temperature by applying a fan after each dose of E-beam exposure. In other experiments, the temperature profiles were obtained without a need to use a fan.

The glass transition temperatures, T_g, of the cured samples was measured by a Perkin Elmer DSC Pyris I system. Temperature was scanned from –50°C to 350°C at 10°C/min.

FT-IR analysis was used to measure the reaction conversion of BMI after E-beam curing. A Nicolet AVATAR 360 spectrometer was used in this study. BMI monomer and the cured samples were ground into the powder and then prepared as KBr pellets. For liquid samples such as NVP and styrene monomers or uncured mixture solutions, a drop of sample was placed between two KBr windows and then measured. The number of accumulations was set at 64 with a resolution of 2 cm^{-1}.

Degree of crosslinking (gel content) was measured by dissolution tests. A sample of approximately 0.1 g (m_1) was ground into powder form and then wrapped in a filter paper with known mass (m_2). The package was placed in a Soxhlet extraction apparatus and extracted by refluxed acetone for 48 hours. The package was then removed and dried in the vacuum oven at 80°C for 16 hours. The mass of the package (m_3) was then weighed. Degree of crosslinking was measured in terms of the percent of gel content, using the Equation (3):

$$Gel\ content\ (\%) = \frac{m_3 - m_2}{m_1} \times 100 \qquad (3)$$

3.3 Results and Discussion

3.3.1 E-beam Curing of BMI Systems

Temperature Profile

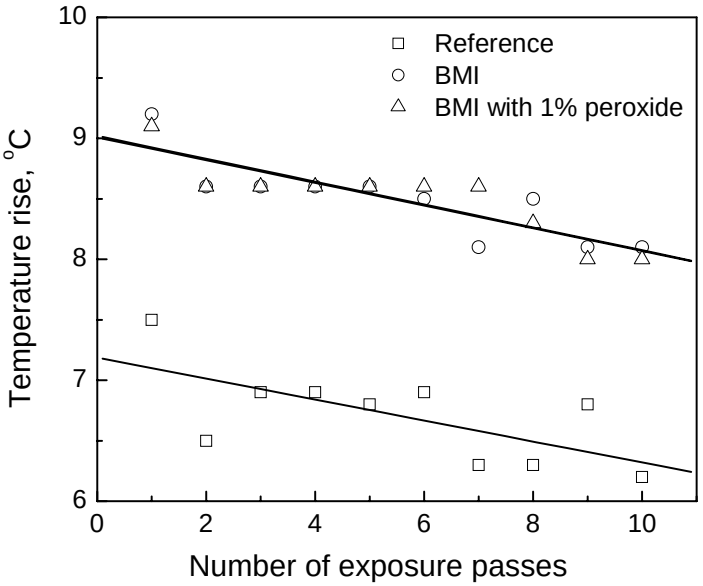

(a)

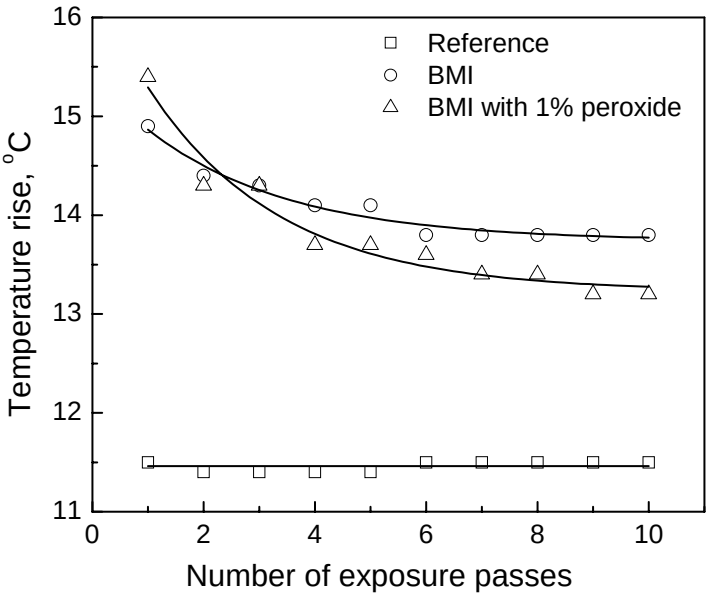

(b)

Figure 28 Temperature rise of BMI resins vs. number of E-beam exposure passes (a) at 10 kGy per pass; (b) at 20 kGy per pass.

BMI and BMI with 1% wt. dicumyl peroxide were cured by E-beam with various dose conditions. The conditions are: (i) 100 kGy total dose at 10 kGy per pass; (ii) 200 kGy total dose at 20 kGy per pass. Sample's temperature during the E-beam process was monitored along with the reference by thermocouples. During the experiment, the samples were cooled to room temperature after each dose and then treated by the next dose. The temperature rises of the samples during the exposure are shown in Figure 28.

As shown in Figure 28, the temperature rise of the samples is dependent on applied exposure dosage per pass. The corresponding rise values at 20 kGy per pass radiation are closed to twice those at 10 kGy per pass, which obeys the relation $\Delta T = D / C_p$, though the responses of BMI resins on different exposure dosage per pass are quite different. The temperature rise of BMI resins is slightly higher than that of fully cured epoxy reference sample, which may be due to the different specific heat of the materials. But they can also be caused from the solid-state reactions initiated by high energy E-beam radiation. The responses of BMI resin and that of BMI with dicumyl peroxide initiator on E-beam radiation are similar in term of temperature rise, indicating that the peroxide may not affect much on E-beam radiation process of BMI resin.

Cure Results of BMI Systems

Comparing the FT-IR spectra of uncured, thermal cured and E-beam cured BMI samples shown in Figure 29, the absorptions around 1150 cm^{-1} (ν_{C-N-C} in maleimide ring), 990 and 910 cm^{-1} ($\delta_{C=C-H}$ of allyl group), 825 cm^{-1}($\delta_{C=C}$ of maleimide double bond) and 690 cm^{-1} ($\delta_{C=C-H\ cis}$) decrease significantly after thermal cure. On the other hand, a new strong absorption at 1180 cm^{-1} (ν_{C-N-C} in succinimide ring) appears after thermal

cure. Therefore, the reaction conversion of BMI can be given by the consumption of double bonds through the calculation of the decreased intensities of the bands at 1150, 825 and 690 cm^{-1}. Since the absorption of 825 cm^{-1} is superimposed on a vibration band of the aromatic =C-H out-of-plane deformation, it never disappeared completely from the spectrum after thermal cure. We can assume that the reaction conversion of thermal cured BMI reaches 90% and then compare the intensity of 825 cm^{-1} absorption of E-beam cured samples with that of thermal cured BMI to obtain the relative reaction conversion. The absorption of benzene rings around 1511 cm^{-1}, inert from the reactions, was used as internal standard.

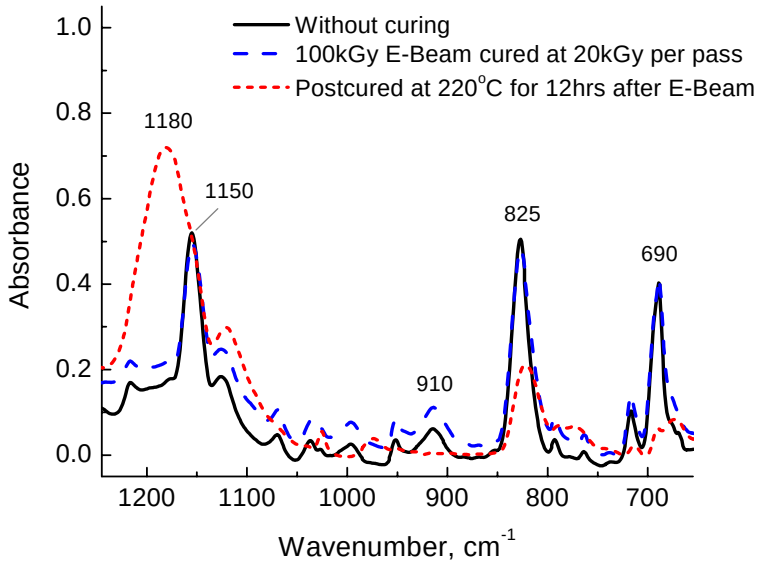

Figure 29 FT-IR spectra of BMI systems.

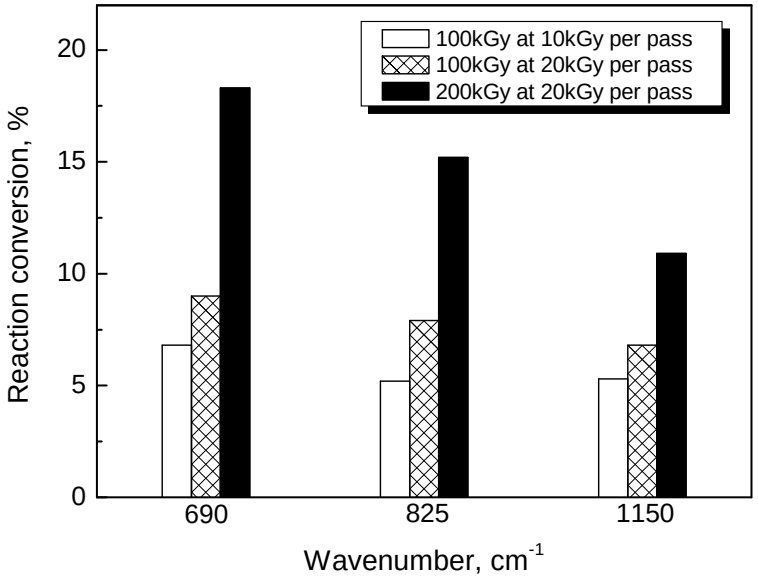

Figure 30 The reaction conversions of BMI cured by various E-beam radiation conditions from FT-IR measurements.

The reaction conversion can be calculated by relative intensity ratio compared between the intensity of the reaction involved peaks and that of internal standard. From the recorded intensity data, the consumption of functional groups, c, can be calculated by Equation (4):

$$c = 1 - \left(\frac{I_t}{I^{1511}} \Big/ \frac{I_0}{I^{1511}} \right) \tag{4}$$

where I_0, I_t are the relative intensities of reaction involved peak at time zero, and after a certain time interval, t, of the cure cycle. And then the reaction conversion α can be calculated by Equation (5):

$$\alpha = \left(\frac{I_t}{I^{1511}} - \frac{I_0}{I^{1511}} \right) \Big/ \left(\frac{I_\infty}{I^{1511}} - \frac{I_0}{I^{1511}} \right) \quad (5)$$

where I_∞ is the intensity at time of curing completion, $t=\infty$. It was assumed that the ultimate conversion ($t=\infty$) of reactive groups was reached after a postcuring-step at 220°C for 12h. The quantitative results are shown in Figure 30.

TABLE 4
T_gs and Reaction Conversions of BMI Resins Cured by Various Conditions

Cure condition	T_g [a], °C		Reaction conversion [b,c], %	
	BMI	BMI with 1% dicumyl peroxide	BMI	BMI with 1% dicumyl peroxide
1	9.8	10.1	0	0
2	10.2	10.6	5.7	5.7
3	14.3	15.7	7.9	8.1
4	19.8	18.3	14.8	15.9
5	231.6	224.2	100	100

a: T_g is obtained from DSC test with the heating rate of 10°C/min
b: Reaction conversion is obtained from FT-IR calculation. Average value of the reaction conversions of three peaks 690, 825 and 1150 cm^{-1}.
c: 100% reaction conversion is the case that the peaks are no longer detectable.

From the results of FT-IR, the reaction conversions of the BMI system are low and around 5-15% after E-beam treatment. The reaction conversions are increased with

the increase of the total dosage and applied dosage per pass as shown in Figure 30. DSC results showed that all the T_g's of the treated BMI samples are around 10-20^oC, which are very close to T_g of uncured BMI at 10^oC (Table 4). There are five cure conditions listed in Table 4: (1) Without curing; (2) E-beam curing with 100 kGy dosage at 10 kGy per pass; (3) E-beam curing with 100 kGy dosage at 20 kGy per pass; (4) E-beam curing with 200 kGy dosage at 20 kGy per pass; and (5) E-beam curing with 200 kGy dosage at 20 kGy per pass, followed by postcure at 220^oC for 12 hours. Since 5250-4 RTM BMI resin cannot flow below 70^oC, together with the cure temperature data (as shown in Figure 28) from E-beam curing which shows that the temperature of BMI didn't exceed 40^oC during the E-beam exposure, the BMI resin will remain in the solid state during E-beam exposure at 10 or 20 kGy per pass. Therefore, even if free radicals are generated by E-beam exposure at low temperatures, chain propagation is very difficult to occur. As a result, temperature rise of BMI samples under relatively low E-beam intensity radiation remains low and is mostly generated from beam energy absorption. However, the change of samples T_gs and the consumption of active double bonds indicate that the solid state polymerization of BMI does happen under the E-beam radiation, though the extent is very low.

3.3.2 E-beam Curing of BMI/NVP Systems

Temperature Profile

As shown in Figure 31, the temperature rise of BMI/NVP 50/50 samples is also dependent on applied dosage per pass. However, the temperature rise, ΔT, during each pass is quite different during the whole cure processing.

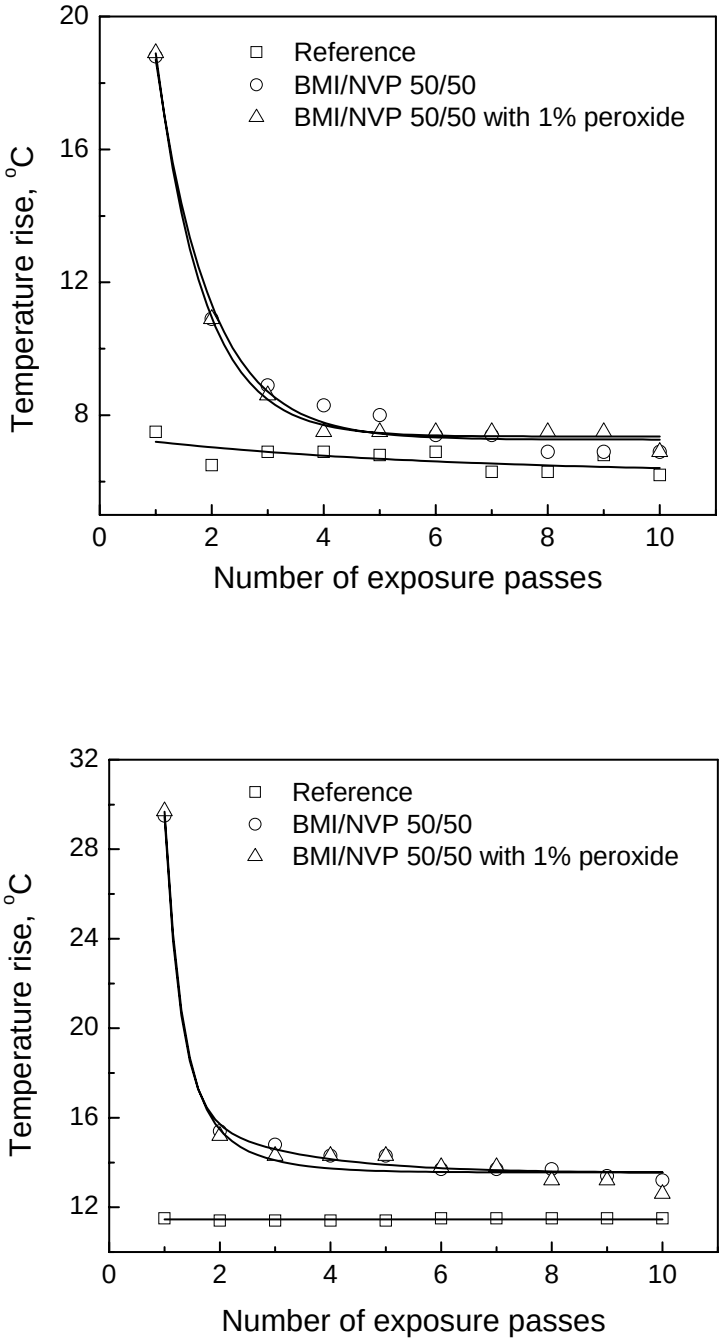

Figure 31 Temperature rise of BMI/NVP vs. number of E-beam exposure passes (a) at 10 kGy per pass; (b) at 20 kGy per pass.

For the BMI resin, the temperature rise during each pass did not change significantly (within 1-2^{o}C). However, for BMI/NVP systems, temperature rises of the samples during the first two passes were much higher than those during the rest of the passes. The temperature rises of the sample after the first pass are twice more than those after four passes (~ 19^{o}C vs. 8^{o}C at 10 kGy per pass and ~ 30^{o}C vs 14^{o}C at 20 kGy per pass). Temperature rise during E-beam radiation comes from both beam energy absorption and free radical induced exothermal cure reactions. The trend of temperature changes of BMI/NVP systems is due to the change of reaction rate during the E-beam radiation process. The cure reactions are slowed after the first two passes, as the concentration of unreacted species decreases. The reaction rate is the highest during the first radiation pass and then went smoothly thereafter. The diffusion control mechanism plays a role as the rising T_g reaches the cure temperature, which means the mobility of free radicals and molecular chains decreases due to the increase of viscosity of the systems so that the cure reactions take place more difficultly. Therefore, E-beam induced dissociation of the double bonds of NVP containing BMI took place easily than BMI itself. Meanwhile, material specific heat C_p will increase during the cure reactions, which also reduces the extent of temperature rise. In addition, it is found that the temperature rise of BMI/NVP with peroxide is similar to that of BMI/NVP system. The cure reactions need to be monitored in detail. The extent of cure reactions as monitored by FT-IR measurements substantiates the above explanations.

Cure Results of BMI/NVP Systems

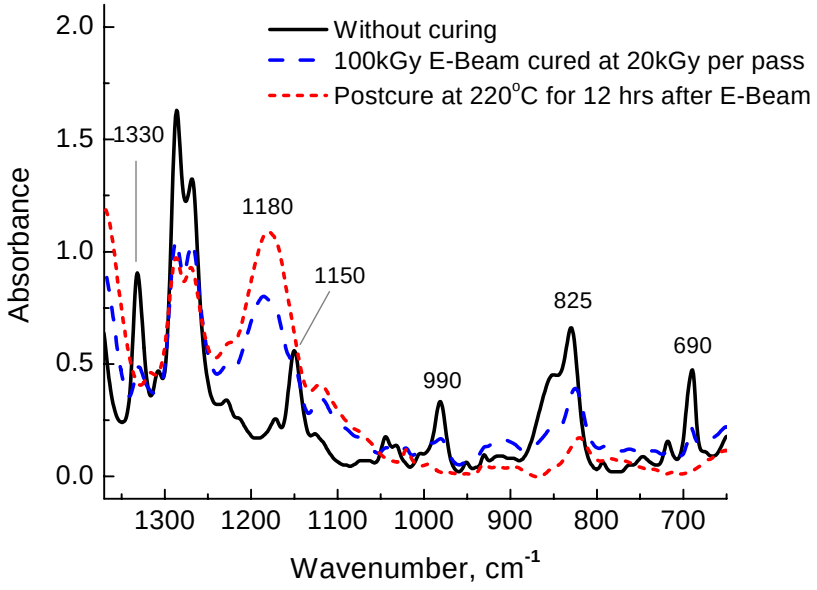

Figure 32 FT-IR spectra of BMI/NVP 50/50 systems.

Comparing the FT-IR spectra of uncured and thermal cured BMI/NVP 50/50 samples shown in Figure 32, the absorptions around 1330 cm^{-1} (in plane CH deformation vibrations of NVP vinyl group) together with 1150 cm^{-1}, 990 cm^{-1}, 825 cm^{-1} and 690 cm^{-1} decreases significantly after thermal cure. Meanwhile, 1180 cm^{-1} appears after thermal cure which is attributed to the structure of succinimide ring. The band of 990 cm^{-1} is attributed to the double bonds of both BMI and NVP so that it can be used to calculate the total consumption of allyl groups in the BMI/NVP system. The band of 1330 cm^{-1} is attributed to NVP only and the bands of 825 cm^{-1} and 690 cm^{-1} are attributed to BMI only so that the consumption of BMI and NVP can also be obtained

separately. The peak at 1511 cm^{-1} was used as an internal standard. From the quantitative data shown in Figure 33, the conversion results of BMI/NVP are similar to those of BMI/styrene. Above 50% reaction conversion can be achieved after 200 kGy dosage.

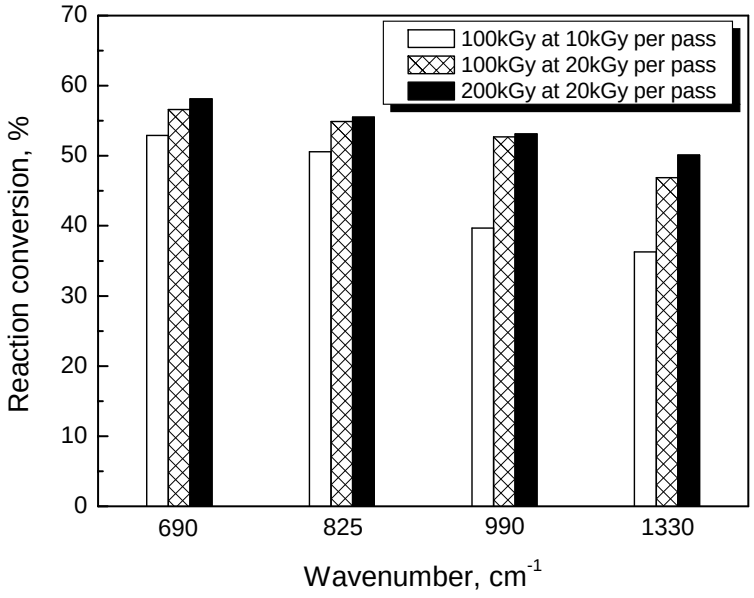

Figure 33 The reaction conversions of BMI/NVP 50/50 cured by various E-beam radiation conditions from FT-IR measurements.

The T_gs and reaction conversions of BMI/NVP 50/50 systems cured at various conditions are listed in Table 5. There are five cure conditions: (1) Without curing; (2) E-beam curing with 100 kGy dosage at 10 kGy per pass; (3) E-beam curing with 100 kGy dosage at 20 kGy per pass; (4) E-beam curing with 200 kGy dosage at 20 kGy per

pass; and (5) E-beam curing with 200 kGy dosage at 20 kGy per pass, followed by postcure at 220°C for 12 hours. A total 200 kGy E-beam radiation with 20 kGy per pass can give BMI/NVP 50/50 system above 50% reaction conversion with the T_g above 170°C. However, the T_g and reaction conversion of BMI/NVP with peroxide system are similar to those of BMI/NVP without any catalyst. Unlike the cationic catalysts for E-beam curing reaction of epoxy system, which have significant effect on cationic polymerization, free radical initiators do not play an important role in this E-beam initiated free radical polymerization.

TABLE 5
T_gs and Reaction Conversions of BMI/NVP 50/50 Systems Cured by Various Conditions

Cure condition	T_g [a], °C		Reaction conversion [b,c], %	
	BMI/NVP	BMI/NVP with 1% dicumyl peroxide	BMI/NVP	BMI/NVP with 1% dicumyl peroxide
1	-	-	0	0
2	148.3	150.5	44.9	45.4
3	169.4	168.2	52.8	51.7
4	174.6	175.9	54.2	52.7
5	206.3	200.1	100	100

a: T_g is obtained from DSC test with the heating rate of 10°C/min
b: Reaction conversion is obtained from FT-IR calculation. Average value of the reaction conversions of four peaks 690, 825, 990 and 1330 cm^{-1}.
c: 100% reaction conversion is the case that the peaks are no longer detectable.

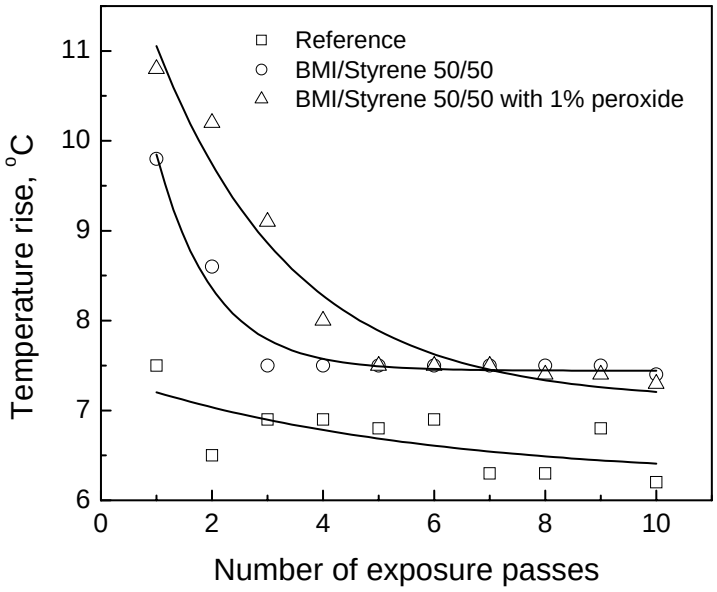

(a)

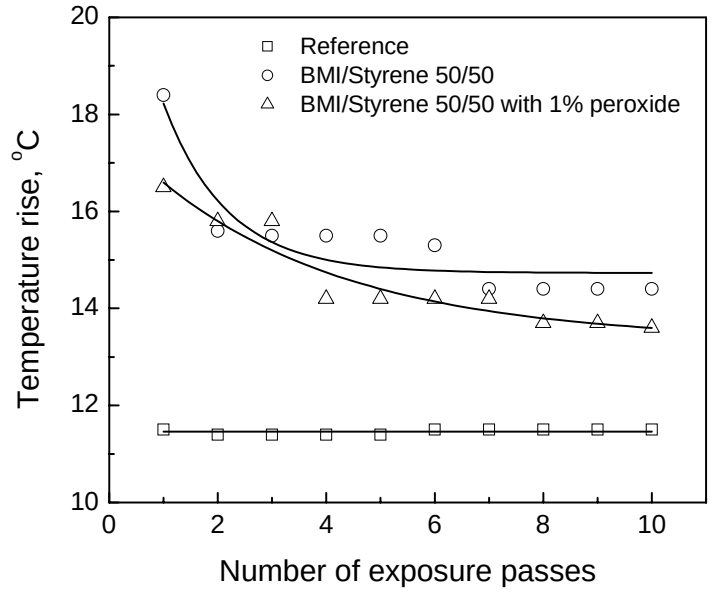

(b)

Figure 34 Temperature rise of BMI/styrene vs. number of E-beam exposure passes (a) at 10 kGy per pass; (b) at 20 kGy per pass.

3.3.3 E-beam Curing of BMI/styrene Systems

Temperature Profile

The temperature profile of BMI/styrene 50/50 was obtained by the same ways as that of BMI and BMI/NVP systems. As shown in Figure 34, the temperature rise of BMI/styrene 50/50 samples is also dependent on applied dosage per pass. In addition, temperature rises of the samples during the first two passes were higher than those during the rest of the passes, which was also taken place in the case of BMI/NVP system. However, the data of temperature rise of BMI/styrene system is much scatter than that of BMI and BMI/NVP samples, which is due to phase separation of BMI/styrene curing the E-beam cure process. Both E-beam cured and thermal cured BMI/styrene 50/50 samples showed yellow shell and white core appearance, which is due to high vapor pressure of styrene and unfavorable variation of the entropy of mixing [137].

Cure Results of BMI/Styrene Systems

Comparing the FT-IR spectra of uncured and thermal cured BMI/styrene 50/50 samples shown in Figure 35, the absorptions around 1150 cm^{-1}, 990 cm^{-1}, 910 cm^{-1}, 825 cm^{-1} and 690 cm^{-1} decrease significantly together with the appearance of 1180 cm^{-1} after thermal cure. Since both BMI and styrene have the IR absorption around 990 cm^{-1} and 690 cm^{-1}, the total consumption of allyl groups in BMI/styrene system can be calculated from the decreased intensities of these two bands with 1511 cm^{-1} as an internal standard. The band of 825 cm^{-1} is attributed to BMI only so that the reaction conversion of BMI in the system can also be obtained.

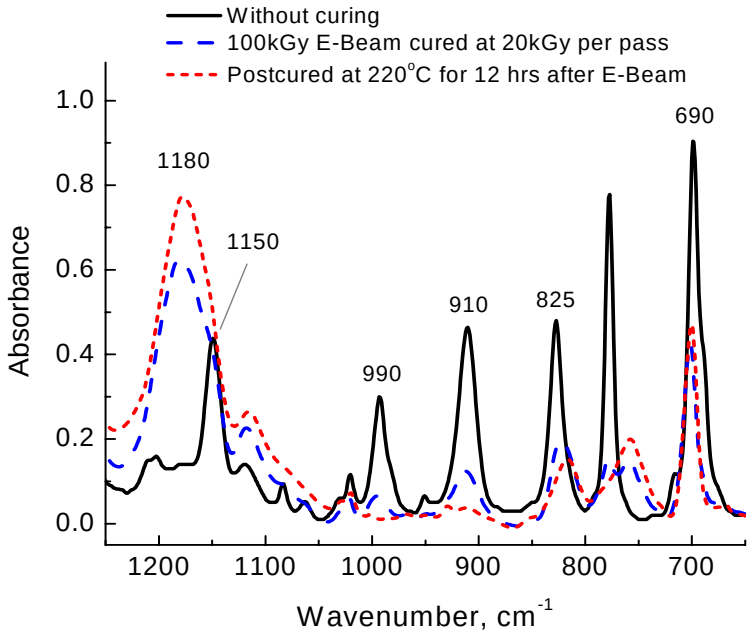

Figure 35 FT-IR spectra of BMI/Styrene 50/50 systems.

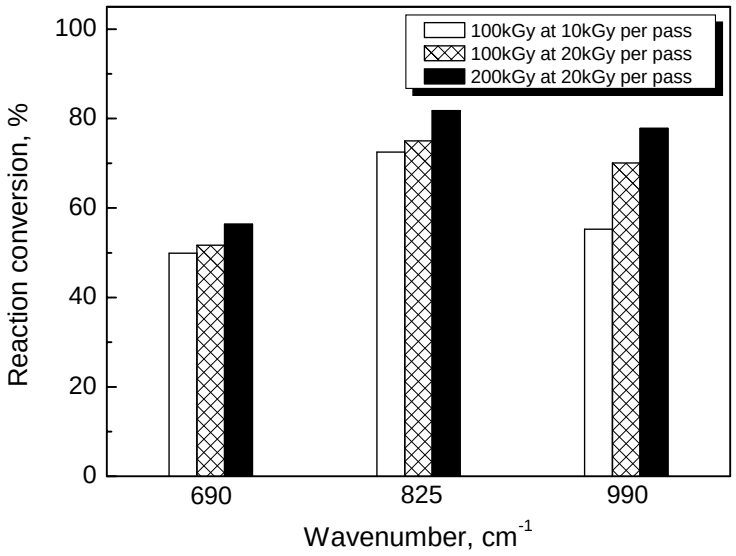

Figure 36 The reaction conversions of BMI/styrene 50/50 cured by various E-beam radiation conditions from FT-IR measurements

From these quantitative results shown in Figure 36, the reaction conversion of BMI/styrene system reaches above 70% after 200 kGy E-beam radiation. The conversion increases with the increase of applied dosage per pass and total applied dosage.

TABLE 6
T_gs and Reaction Conversions of BMI/Styrene 50/50 Systems Cured by Various Conditions

Cure condition	T_g [a], °C		Reaction conversion [b,c], %	
	BMI/ST	BMI/ST with 1% dicumyl peroxide	BMI/ST	BMI/ST with 1% dicumyl peroxide
1	-	-	0	0
2	128.7	132.6	59.2	63.6
3	149.5	154.3	65.6	71.0
4	161.0	163.2	72.0	73.1
5	195.0	187.6	94.1	93.0

a: T_g is obtained from DSC test with the heating rate of 10°C/min
b: Reaction conversion is obtained from FT-IR calculation. Average value of the reaction conversions of four peaks 690, 825, and 990 cm^{-1}.
c: 100% reaction conversion is the case that the peaks are no longer detectable.

The T_gs and reaction conversions of BMI/styrene 50/50 systems cured at various conditions are listed in Table 6. There are also five cure conditions used: (1) Without curing; (2) E-beam curing with 100 kGy dosage at 10 kGy per pass; (3) E-beam curing

with 100 kGy dosage at 20 kGy per pass; (4) E-beam curing with 200 kGy dosage at 20 kGy per pass; and (5) E-beam curing with 200 kGy dosage at 20 kGy per pass, followed by postcure at 220^{o}C for 12 hours. A total 200 kGy E-beam radiation with 20 kGy per pass can give BMI/styrene 50/50 system above 70% reaction conversion with the T_g above 160^{o}C. The use of peroxide didn't affect the reaction much.

3.3.4 The Effect of Reactive Diluent on E-beam Curing of BMI Resins

Obviously, the addition of reactive diluents into BMI resin can improve the reactivity of BMI system significantly. The increases of applied dosage per pass and total applied dosage lead to higher reaction conversion. However, the effects of NVP and styrene on E-beam curing of BMI are quite different. Material properties of NVP and styrene are listed in Table 7.

TABLE 7
Material Properties of Styrene and NVP

Materials	Structure	Molecular weight	Boiling point (^{o}C/760 mmHg)	Flush point (^{o}C)	Density (g/cm^3)
Styrene	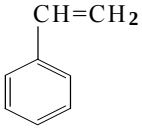	104.15	145	31	0.909
NVP	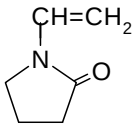	111.16	148	98	1.040

Although the structure, molecular weight, and the boiling point of styrene and NVP are similar, the flush point of styrene is much lower than that of NVP, which is due to styrene's higher vapor pressure. It makes styrene monomer easier to move toward the surface of BMI/styrene mixture solution, resulting in a serious phase separation during the polymerization (Figure 37). Compared to the density of styrene, the density of NVP is closer to that of cured BMI (1.25 g/cm^3), which may also favor to form uniform structure. Therefore, NVP was chosen as the reactive diluent of BMI resin for cure kinetics study; though styrene can give BMI higher cure conversion and better solubility.

Figure 37 The appearance of E-beam treated samples (Treated by 200kGy at 20kGy/pass. From left to right: 1. BMI/NVP 50/50 with 5% peroxide; 2. BMI/Styrene 50/50 without any catalyst; 3. BMI/Styrene 50/50 with 1% peroxide; 4. BMI/Styrene 50/50 with 5% peroxide).

Effects of Diluent Concentration

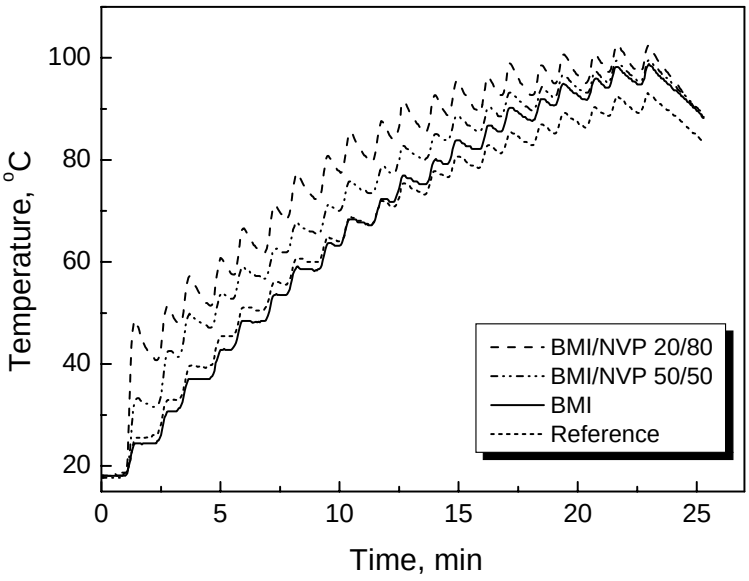

Figure 38 Temperature data of different BMI/NVP systems during E-beam curing at 10 kGy per pass (total 200kGy dosage).

To investigate the effects of diluent concentration on E-beam curing of BMI resins, BMI/NVP systems with different NVP concentrations were irradiated by total 200 kGy of E-beam exposure at 10 kGy per pass, with temperature being monitored. The temperature profiles are shown in Figure 38. Each peak in the plots corresponds with temperature rises during each radiation pass. The higher the concentration of NVP in BMI/NVP system, the higher the sample temperature is found during the E-beam radiation. The higher concentration of reactive diluents in the BMI system, the lower the viscosity and the system is more reactive, which cause higher temperature rise during the

cure reaction. It is also shown that the temperature rise of BMI tends to be close to that of BMI/NVP systems after the temperature of BMI reaches about 95°C, which is consistent with earlier observation from high intensity E-beam exposure. The temperature rises of BMI are similar to those of fully cured reference when the sample temperature is below 70°C and much higher than those of fully cured reference when the sample temperature is above 70°C, which confirm that the viscosity of the BMI resin plays a critical role in E-beam curing of BMI resins.

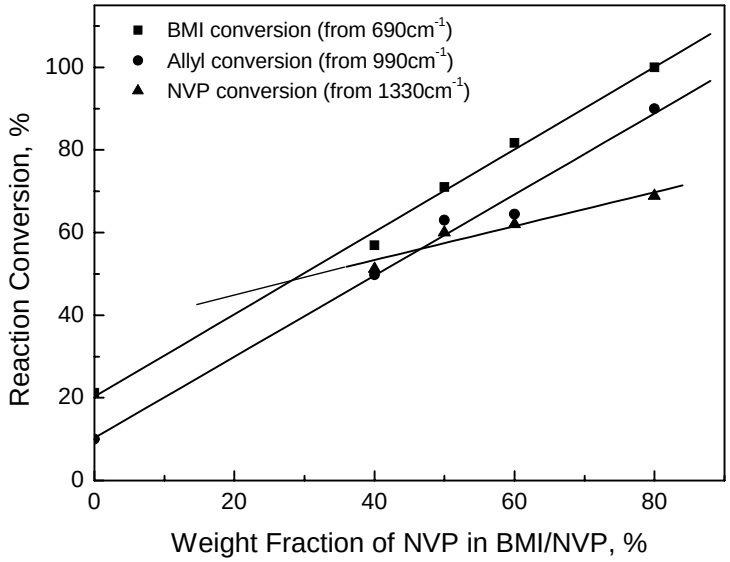

Figure 39 The dependence of reaction conversion of BMI/NVP systems on concentration of NVP (Dosage applied: 200 kGy at 10 kGy per pass).

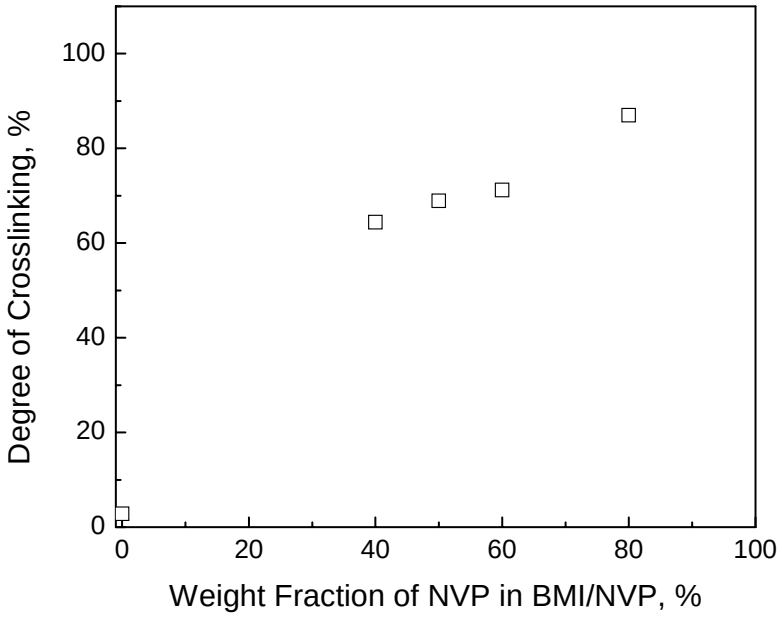

Figure 40 The dependence of degree of crosslinking of BMI/NVP systems on concentration of NVP (Dosage applied: 200 kGy at 10 kGy per pass).

Based on FT-IR measurements, the reaction conversions of BMI/NVP system increase almost linearly, with the increase of the concentration of NVP in the system (Figure 39). The degree of crosslinking of BMI/NVP 20/80 reaches to 87 % (Figure 40). The increase of NVP fractions in BMI/NVP system will decrease the viscosity of the BMI resin and activate the curing so that both the reaction conversion and degree of crosslinking are increased significantly. However, the increase of NVP fractions in the system does not increase the reaction conversion of NVP itself as much as that of BMI. It should be noted that NVP alone does not cure readily with E-beam radiation. Even NVP alone we can only get less than 80 % of conversion after E-beam radiation at the

same dosage condition. Free radical homopolymerization of NVP is well known and it is a readily polymerizable monomer. It would appear that the enhanced cure conversion observed with NVP as a diluent monomer are due to charge transfer complexes formed between NVP and BMI, which means the dilution and activation effects of NVP play the most important role in the interaction between BMI and NVP, and make BMI more reactive upon E-beam radiation.

3.3.5 Cure Kinetics Study of BMI/NVP 50/50 Resins

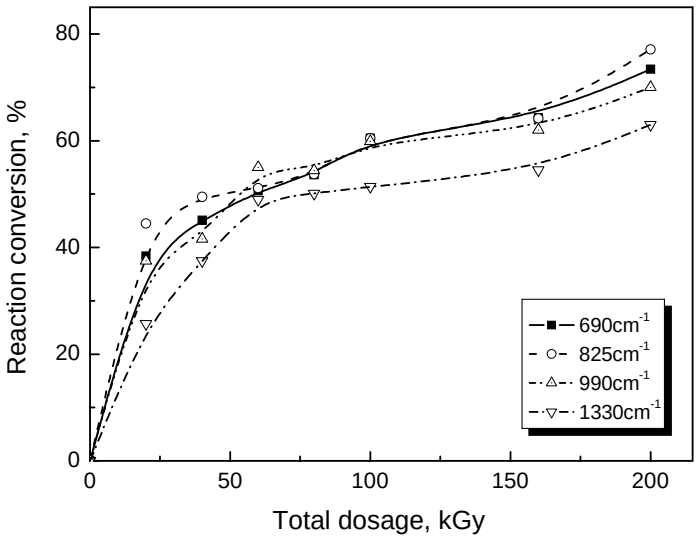

Figure 41 The dependence of reaction conversion of BMI/NVP 50/50 on applied E-beam dosage (10 kGy per pass).

The dependence of the reaction extents of these resin systems on dosage needs further investigation to characterize the diffusion control mechanism and cure kinetics

during E-beam radiation. A cure reaction study of BMI/NVP 50/50 system was investigated at 10 kGy per pass without sample cooling to investigate the effects of total applied E-beam exposure dosage on cure reaction conversion. From the temperature profiles, the maximum temperature recorded during the whole radiation exposure was 70^{o}C. The intensities of the absorption bands around 690 cm^{-1}, 825 cm^{-1} and 1330 cm^{-1} from FT-IR were used to calculate the consumption of BMI and NVP after E-beam exposure. Meanwhile, the consumption of allyl groups was calculated from the 990 cm^{-1} band.

From Figure 41, the trends of those curves obtained from the different IR absorptions are similar, which indicates the calculation of reaction conversion is quite reliable. It can be noted that the increase of total E-beam dosage increases the extents of cure reaction. After the first 20 kGy total dosage radiation, a glass-like product was obtained with the reaction conversion of 35% and the T_g of 130^{o}C. Subsequently, the reaction rates slowed down and the consumption of double bonds was about 70% after 10 single pass exposure of 10 kGy. Meanwhile, the T_g of the product increased to 180^{o}C. The dependence of T_g of BMI/NVP resins on total applied E-beam radiation dosage is shown in Figure 42. It is noticed that the reaction conversions and T_gs of sample in kinetics study are higher than those of cured BMI/NVP samples in 3.3.2. Since the cooling process was not applied in cure kinetics study, the reactions were carried out at higher temperature than cure reactions in 3.3.2. Therefore, the cure conversions of the final products are higher.

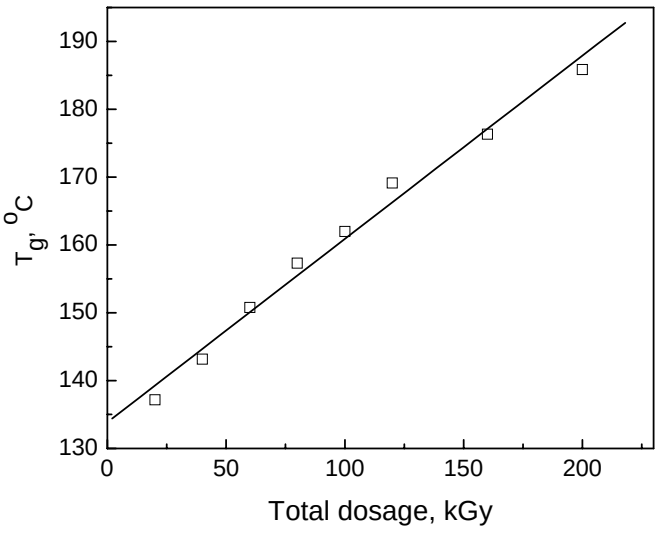

Figure 42 The dependence of T_g of BMI/NVP 50/50 on applied E-beam dosage (10 kGy per pass).

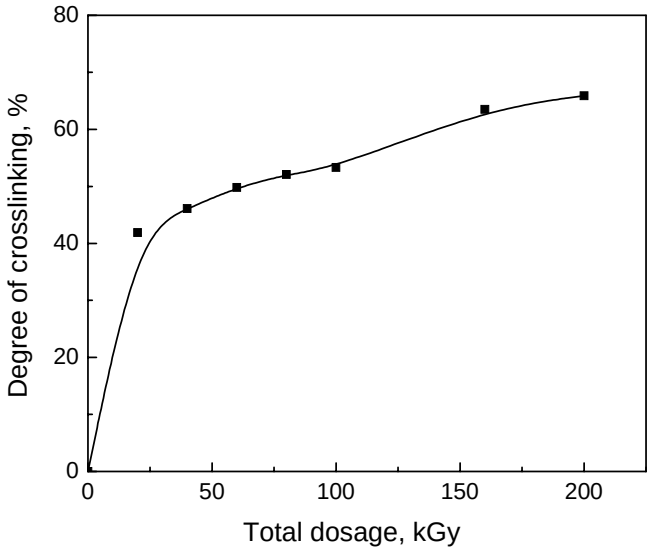

Figure 43 The dependence of degree of crosslinking of BMI/NVP 50/50 on applied E-beam dosage (10 kGy per pass).

The degree of crosslinking results shown in Figure 43 indicates that the sample's degree of crosslinking reached up to 40% right after the first 20 kGy total dosage radiation and then climbed slowly to 65% finally, which are similar to the results of reaction conversion obtained from FT-IR measurement.

Combined the above results with the observation we made earlier from Figure 31 that the temperature rise during the first two passes were much higher and then becomes stable, we may conclude that the vitrification of BMI/NVP 50/50 system took place during the first two E-beam radiation passes at 10 kGy per pass. After that, the cure reactions continue more slowly in the glassy state, as polymerization in the glassy state is diffusion controlled. However, compared to the BMI resin, a much higher solid-state reaction rate of BMI/NVP system can be achieved under E-beam radiation for similar radiation conditions. NVP increases the activity of BMI significantly due to charge transfer effects. Charge transfer complexes formed between NVP and BMI lower the energy required to cure the systems so that the cure rates and conversions are increased. It has been reported that cyclic amides form charge transfer complexes which enhance photochemical and free radical polymerization of maleic anhydride and methyl methacrylate [138].

The effect of dicumyl peroxide initiator on E-beam curing of BMI/NVP was investigated under same dosage exposures. And, the extents of reaction conversions of BMI/NVP 50/50 with those of BMI/NVP 50/50 with 1% dicumyl peroxide (Figure 44) were compared. The reaction conversions generally increase with the increase of applied E-beam radiation dosage, which is similar to BMI/NVP 50/50 system without peroxide.

However, higher reaction conversion of BMI/NVP is observed at the beginning of E-beam exposure in the presence of the initiator. And finally, the consumption of allyl groups in both systems tends to be very close. We can conclude that the initiator can increase the reaction rate at the beginning of E-beam curing of BMI/NVP system when the viscosity of the materials was still relatively low. After the cure reaction reached a certain level and the vitrification took place, initiators did not affect the glassy-state reaction rate much and neither affects the cure conversion to the final products.

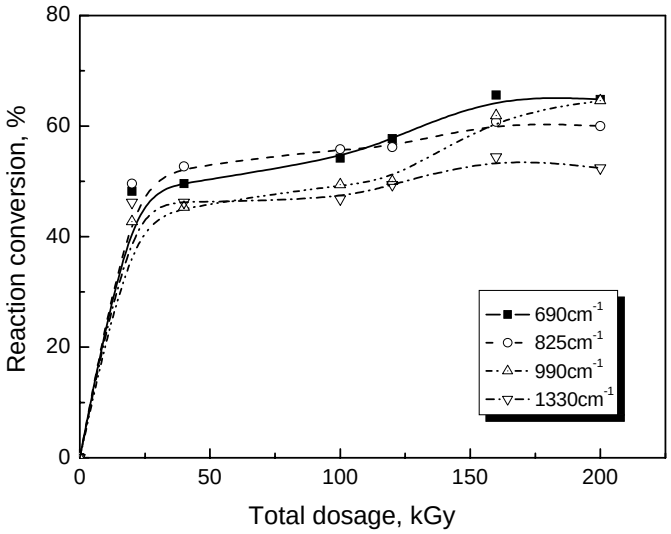

Figure 44 The dependence of reaction conversion of BMI/NVP 50/50 with 1% dicumyl peroxide on applied E-beam dosage (10 kGy per pass).

Photocalorimetry and real time infrared spectroscopy [139-142] have been used for several years to study the complex kinetics governing cross-linking

photopolymerization. The analysis and interpretation of the primary data with advanced kinetic models result in a better understanding of the mechanisms that control the overall behavior. These *in-situ* methods, however, have not been successfully used in high energy E-beam radiation due to many technical difficulties such as electromagnetic noise interference of electrical-based sensor signal, radiation heating of sensors, and darkening of glass in fiber-optic-based sensors. In this dissertation, the cure kinetics study does not produce real-time information. All the spectroscopic studies were carried out after the E-beam curing, which can not give the real structure and concentration of reaction intermediates.

The cure process is often represented analytically through existing models such as nth order and autocatalytic models. The general kinetics equations for these models are presented by Equation (6) and (7):

$$\frac{\partial \alpha}{\partial t} = k(1-\alpha)^n \tag{6}$$

$$\frac{\partial \alpha}{\partial t} = \left(k_1 + k_2 \alpha^m\right)\left(1-\alpha\right)^n \tag{7}$$

where α is the degree of cure, k is Arrhenius equation constant, m and n are reaction orders.

There are two characteristics for an n^{th} order type cure mechanism: the relationship between ln ($d\alpha/dt$) and ln (1-α) should be linear and the maximum cure rate ($d\alpha/dt$) should be reached at $\alpha = 0$. In an autocatalytic model, the products act as catalysts for further reaction and the reaction rate is thus affected by the amount of the

products as well. From the reaction conversion data in this research, the relationship between ln ($d\alpha/dt$) and ln (1-α) is linear and the maximum cure rate ($d\alpha/dt$) was reaches at the beginning of the cure, which matches the characteristics of n^{th} order reaction kinetics. However, the simulation based on *n*th order kinetics failed due to serious deviation, which implies that E-beam cured reactions of BMI resin may not follow the simple n^{th} order.

Defoort et al. [143] predicted numerically the time dependence of the temperature gradient in the sample depth on the effects of different dose rate and total heat of reaction for continuous E-beam radiation on the basis of general heat equation applied to a one-dimensional system. A time dependent phenomenological equation with adjustable parameters based on their experimental work was used to describe the cure kinetics in their one-dimensional model, which appeared more convenient than autocatalytic models:

$$\alpha = c_1 t + c_2 - \frac{1}{c_3 t + c_4} \tag{8}$$

where t is time and c_1 to c_4 are adjustable parameters.

Equation (8) is utilized to simulate the cure kinetic data for E-beam curing of BMI/NVP 50/50 system. It is found that this phenomenological equation simulates the kinetic data very well (Figure 45). c_1, c_2, c_3 and c_4 are 0.000139, 0.505282, 0.02785, and 1.97943, respectively. Although convenient, this equation shall be limited to the particular condition under which its adjustable parameters are to be determined.

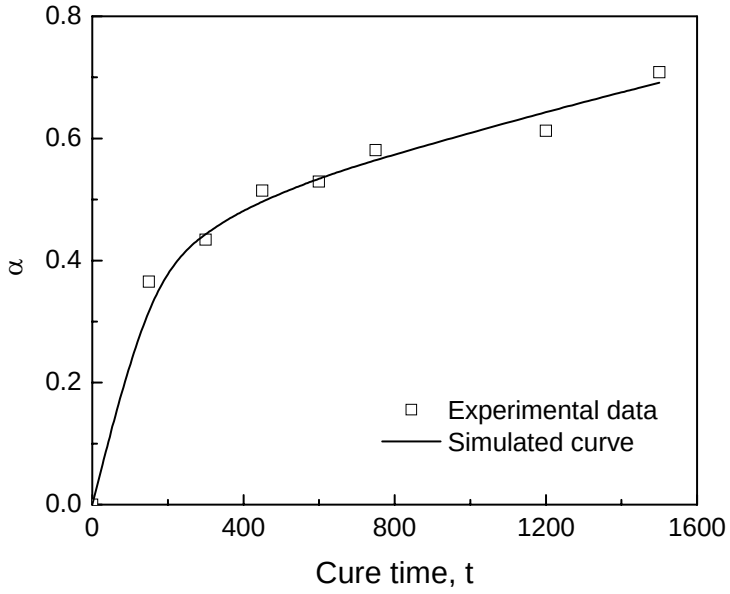

Figure 45 Simulation of cure kinetics of E-beam curing of BMI/NVP 50/50 (Dose rate: 10kGy per pass).

3.3.6 High Intensity E-beam Curing

To investigate the effects of high intensity E-beam radiation on BMI and BMI/NVP cure processes, a total 400 kGy E-beam exposure at 40 kGy per pass, without any sample cooling process, was applied for the curing of BMI and BMI/NVP 50/50 systems. The temperature profiles are shown in Figure 46. Each peak in the curve corresponds to the temperature rise during each radiation dose. The whole process took 20 minutes. We can observe that the high intensity E-beam radiation caused significant temperature rise. The temperature of BMI/NVP 50/50 sample rose to 62^{o}C after the first 40 kGy dosage and 190^{o}C after 10 passes. The temperature of BMI sample even reached

to 230°C after 10 passes. The following reaction types have been proposed to be involved in the thermally cure process of BMPM/DABPA based resin: Ene, Diels-Alder, homopolymerization, copolymerization, re-aromatization and etherification [92]. It is known that these reactions will not take place until the temperature reaches above 100°C [92]. Therefore, thermal cure mechanisms will occur in such a high intensity E-beam radiation process.

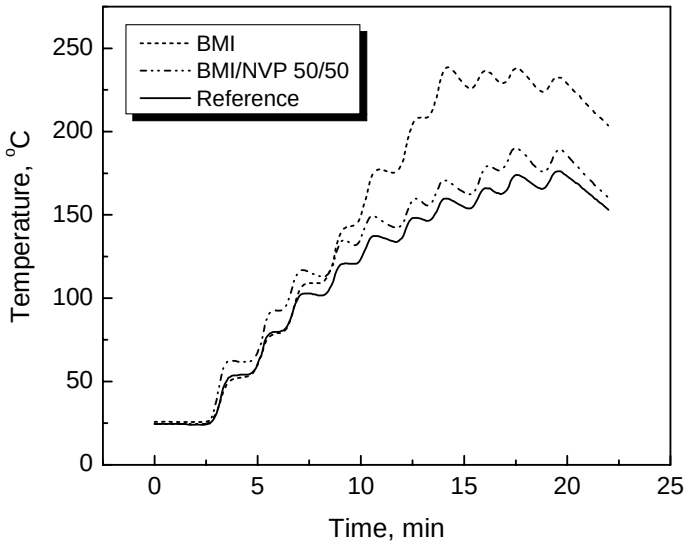

Figure 46 Temperature data of BMI and BMI/NVP 50/50 during E-beam curing at 40 kGy per pass (total 400 kGy dosage).

As shown earlier, E-beam radiation can initiate the polymerization of BMI/NVP even at low intensity and low temperature. Thus, the initial temperature rise of BMI/NVP was higher than the reference during the E-beam process because of the onset

of the cure reactions. However, the increases of temperature in BMI were very close to those of the reference sample during the first two doses, but much higher than those after the third dose, which indicate that E-beam curing alone cannot propagate the polymerization of BMI even at 40 kGy per pass until the three passes of 40 kGy radiation (total 120 kGy dosage) was applied. From Figure 46, the temperature of BMI during the third pass of E-beam radiation raise from 77 to 110^{o}C. The original three-component BMI resin can flow above 70^{o}C, and the viscosity of the resin is reduced significantly, which increases the chain mobility and the reactivity of the system. Meanwhile, the "ene" reaction and other thermal curing mechanisms were induced when the temperature of BMI exceeded 100^{o}C. The heats generated from these reactions further increased the temperature of BMI during E-Beam exposure. After 3 passes of exposure (total 120 kGy dosage), the temperatures of BMI were even much higher than those of BMI/NVP because a significant portion of the BMI/NVP cure has already occurred during the initial radiation exposure.

Based on the consumption of 690 and 825 cm^{-1} infrared bands from FT-IR measurements (Figure 47), the reaction conversions of BMI and BMI with 1 % dicumyl peroxide reach up to 80% after 400 kGy E-beam exposure at 40 kGy per pass and the T_g of the product is 215^{o}C. Obviously, the high intensity E-beam process increases the cure conversion significantly. However, the consequent fast temperature rise needs to be considered carefully because thermal stresses and induced shrinkage stresses could affect the final resin properties and diminish the advantages of E-beam curing.

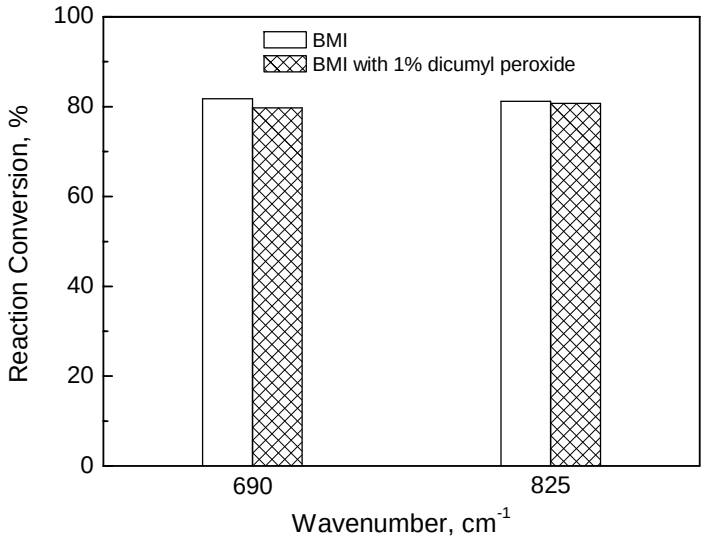

Figure 47 The reaction conversions of BMI systems after high intensity E-beam radiation (Dosage applied: 400 kGy at 40 kGy per pass).

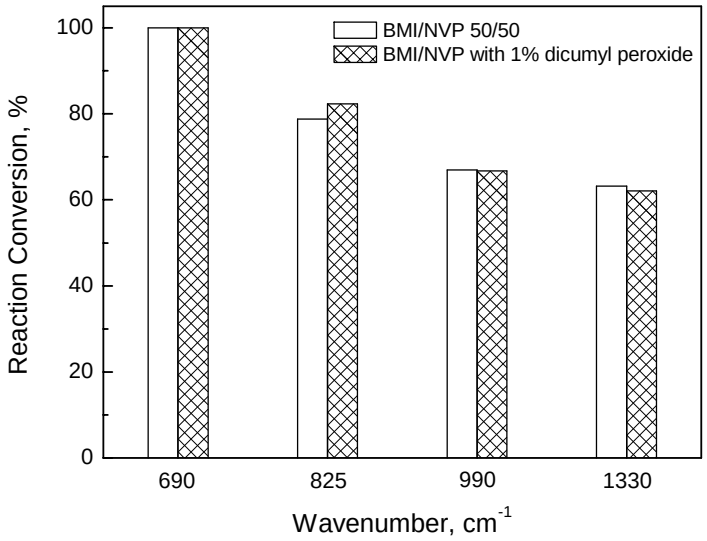

Figure 48 The reaction conversions of BMI/NVP systems after high intensity E-beam radiation (Dosage applied: 400 kGy at 40 kGy per pass)

Figure 48 shows the reaction conversions of BMI/NVP 50/50 and BMI/NVP 50/50 with 1% dicumyl peroxide systems after 400 kGy of E-beam exposure at 40 kGy per pass. It is shown that the conversion of BMI in the BMI/NVP system is above 80%, but the consumption of NVP and total allyl groups are only about 62% and 67%, respectively. The T_g of the final product is 200^oC. The above reaction conversions and T_g of BMI/NVP products are close to those reported by Marie-Florence et al. [15], who cured the modified BMI/NVP resin by 400 kGy at 50 kGy per step. Also, the conversion results support our earlier conclusion that initiators do not affect the cure conversion of the final products. We note that the effect of higher intensity E-beam radiation on the BMI system is much more significant than that on BMI/NVP system, which indicates that thermal cure is the dominant process in the BMI system during high intensity E-beam exposure. However, for BMI/NVP system, E-beam induced cure rather than thermal cure is dominant, which makes low intensity E-beam curing at low temperature possible.

3.4 Conclusions

According to the results of reaction conversion of BMI cured by different total E-beam radiation dosages at 10, 20 and 40 kGy per pass, E-beam exposure cannot propagate the polymerization of BMI system until the temperature goes up to 100^oC. However, solid-state cure reaction of BMI does occur to some extent and a small amount of oligomers may be generated under low E-beam intensity radiation, though the reaction conversion was low. Higher intensity E-beam at 40 kGy per pass can give high

reaction conversion of BMI above 75%. However, the temperature of BMI reached up to 250^{o}C, which induced normal thermal cure mechanism.

NVP is a good reactive diluent for BMI resin. It decreases the viscosity of BMI resin so that the reactivity of the system is increased significantly. The cure extents of BMI/NVP increase with the increase of the dosage and applied dosage per pass. The reaction conversion of BMI/NVP is up to 40% after the first two passes of 10 kGy dosage exposure. The reaction rate slows down after that due to diffusion control. According to the results from FT-IR, 200 kGy total dosage E-beam exposure at 10 kGy per pass can give 70% reaction conversion of BMI/NVP with the temperature rise no more than 50^{o}C. The product has a T_g of 180^{o}C. Free radical initiator dicumyl peroxide can accelerate the reaction rate at the beginning of E-beam cure reaction but doesn't affect final cure conversion very much.

Styrene can also used as a reactive diluent for BMI resin. BMI resin has better solubility in styrene than that in NVP. BMI/Styrene system has higher reaction conversion under E-beam radiation, which is up to 70% after 200 kGy dosage at 10 kGy per pass. However, BMI/Styrene system shows serious phase separation after E-beam curing due to high vapor pressure of styrene.

The effect of higher intensity E-beam radiation on BMI system is much more significant than that on BMI/NVP system, which indicates that thermal cure is the dominant process in BMI system during high intensity E-beam exposure. As to BMI/NVP system, E-beam induced cure rather than the normal thermal cure is dominant, which makes low intensity E-beam curing at low temperature possible. The increase of

the concentration of NVP in the system increases the reaction conversions almost linearly. The dilution and activation effects of NVP play the most important role in the interaction between BMI and NVP and make BMI have a more active response on E-beam radiation.

CHAPTER IV

SYNTHESIS AND CURE CHARACTERIZATION OF PHENYLETHYNYL TERMINATED IMIDE OLIGOMERS

4.1 Introduction

Aromatic polyimides prepared from the phenylethynyl terminated imide monomers or oligomers demonstrate many advantages in both favorable processability and good materials properties, and could provide high-performance composites with broad applications. The advantages of these materials are that (1) no volatiles are formed curing reaction, (2) the phenylethynyl group exhibits greater process control over the ethynyl group due to the larger processing window, and (3) improved thermal and thermo-oxidative stability over ethynyl-terminated imide oligomers. Also, phenylethynyl terminated imide monomer or oligomers can be used for the E-beam curing for polyimides [16, 32].

Several studies on the thermal cure of various ethynyl and phenylethynyl terminated imide monomers or oligomers in an attempt to understand the chemistry of the process have been also reported in recent years. The molecular structure of cured ethynyl-terminated polyimides was investigated by solid state ^{13}C-NMR. The crosslinking structure of phenylethynyl-terminated imide polymer was also proposed (Figure 49). Although the triple bonds of terminated phenylethynyl groups are expected to react by chain extension, crosslinking, and branching, the cure reaction mechanism is still poorly understood. The expected steric effect of the phenyl-ended functional groups,

relatively low concentration of phenylethynyl groups in the oligomers and insolubility of the cured products adds to the difficulties in elucidating the cure reaction mechanism.

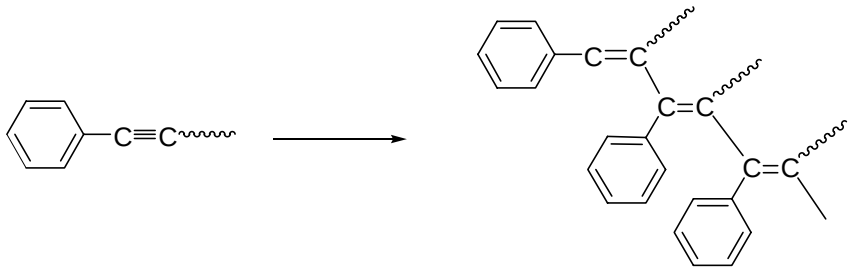

Figure 49 Reactions of phenylethynyl terminated imide monomers.

Generally speaking, crosslinking of a polymer causes an increase in the T_g; at a given temperature, T_g increases with the extent of cure until it reaches an ultimate value. A good estimate of the extent of cure or crosslinking, *x*, can be deduced from T_gs by the use of the DiBenedetto equation, which has been modified to investigate the cure reaction of thermosetting polymers.

In this research, AFR-PEPA-4 oligomer and an imide model compound N-phenyl-[4-(phenylethynyl) phthalimide] were synthesized and characterized for cure reaction study. Differential scanning calorimetry (DSC) was used in determining the cure kinetics of AFR-PEPA-4 oligomer by following the increase in T_g as a function of cure. The kinetics analysis of the thermal cure of N-phenyl-[4-(phenylethynyl)

phthalimide] was determined by FT-IR spectroscopy by following the absorbance of the phenylethynyl triple bond and conjugated bonds. The aim of this research is to determine the kinetics of the cure reaction of the phenylethynyl-terminated imide monomer or oligomers and to characterize the cure reaction and thermal stabilities of cured products in order to understand the cure mechanism and structure-property relations of phenylethynyl-terminated polyimides.

4.2 Experimental

4.2.1 Materials

2,2'-bis(3,4-dicarboxyphenyl)hexafluoropropane dianhydride (6-FDA), 1,4-diaminobenzene (*p*-PDA), 4-(phenylethynyl)phthalic anhydride (PEPA) were obtained from Performance Polymer Solutions Inc. N-methyl-2-pyrrolidinone (NMP), aniline, acetic acid and methanol were obtained from Aldrich. All chemicals were used as received.

4.2.2 Syntheses

AFR-PEPA-4 Oligomer

AFR-PEPA-4 oligomer was synthesized according to Figure 50.

p-PDA (7.034 g, 0.065 mol) was dissolved in 150 ml NMP in a 500 ml, three-neck round-bottom flask equipped with a Teflon stirring bar and a gas adaptor under a nitrogen atmosphere at room temperature. 6FDA (23.117 g, 0.052 mol) was dissolved in 150 ml NMP under a nitrogen atmosphere protection. The solution of 6FDA/NMP was then added in *p*-PDA/NMP solution three portions over 3h. Once all of the 6FDA

solution was added, stirring continued for 20h at room temperature. PEPA (6.459 g, 0.026 mol) was added as a solid and stirred until completely reacted (4 hours) under nitrogen. The NMP using is 10% solids by weight during the whole synthesis.

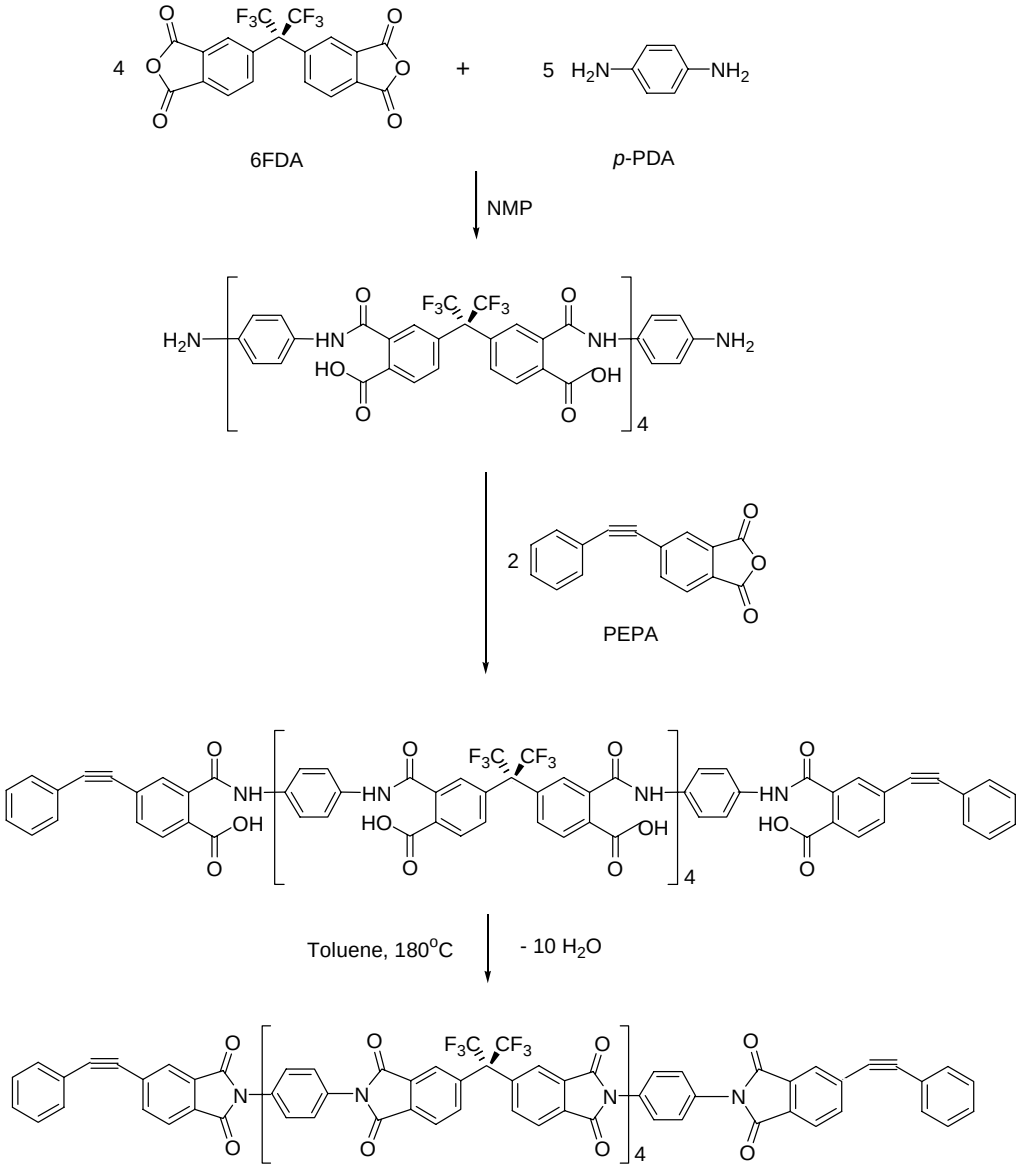

Figure 50 Synthesis of AFR-PEPA-4 oligomer.

Toluene was then added, and the resulting mixture was then imidized under reflux in 180^{o}C oil bath with the removal of water via azeotropic distillation. The reaction mixtures were finally added into distilled water, filtered, washed in boiling water and then in warm methanol to remove the NMP. This produced very fine yellow powders that were dried under vacuum for 24h at 160^{o}C. The yield was 33.387g (97.5%).

N-phenyl-[4-(phenylethynyl) phthalimide]

The model compound N-phenyl-[4-(phenylethynyl) phthalimide] was synthesized according to Figure 51.

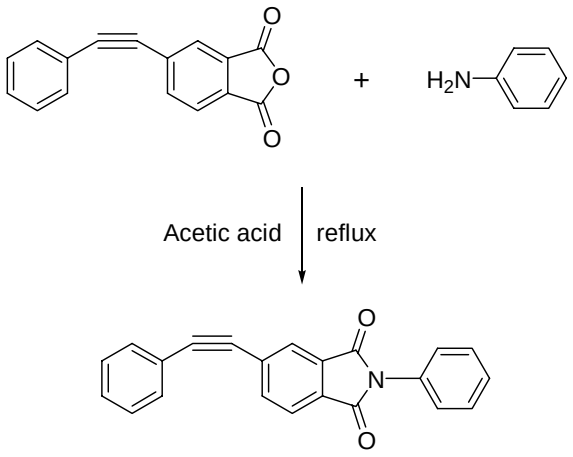

Figure 51 Synthesis of N-phenyl-[4-(phenylethynyl) phthalimide].

PEPA (31.029 g, 0.125 mol), aniline (12.200g, 0.131 mol) and 225 ml of acetic acid were placed in a 500 ml, three-necked flask. The mixture was stirred under nitrogen and heated to reflux for 1.5h. A total of 50 ml of water and acetic acid mixture was distilled off during the following 0.5h period. The reaction mixture was cooled and the

yellow crystalline solid was filtered. The product was washed with methanol and dried. The yield was 38.883 g (96.2%).

Polymerization

About 0.2 g oligomers were cured in small glass vials in a preheated furnace. The cure temperature was from 330^{o}C to 410^{o}C and the cure time was from 2 minutes to 8 hours. After cooling, the samples were removed from the vials for characterization.

4.2.3 Characterizations

Element Analysis

Element analyses of the synthesized materials were performed by Robertson Mocrolit Labs. The contents of C, H, N in the samples were determined by using Perkin Elmer 2400 CHN analyzer. The content of F was determined by using Ion Chromatography.

FT-IR

The IR spectra of AFR-PEPA-4, N-phenyl-[4-(phenylethynyl) phthalimide] and cured products were measured by using A Nicolet AVATAR 360 spectrometer. The samples were ground into the powder and then prepared as KBr pellets. The number of accumulations was set at 64 with a resolution of 2 cm^{-1}.

NMR

^{1}H and ^{13}C nuclear magnetic resonance (n.m.r.) spectroscopy was performed on an Inova-300 operating at 300 MHz. $CDCl_3$ was used as the solvent.

Mass Spectrometry

Mass Spectrometry was performed on a PE SCIEX QSTAR mass spectrometer with Electrospray Ionization (ESI). Methanol was used as the solvent.

Melting Points

Melting points were determined on a capillary melting point apparatus and are uncorrected.

TGA

Thermogravimetric analysis was performed on a TGA Q500 thermal analyzer. The heating atmospheres were air or nitrogen. The samples were heated to 800^{o}C. Heating rates are from 2^{o}C/min to 20^{o}C/min.

DSC

Differential scanning calorimetry was performed on Perkin Elemer Pyris 7 DSC. Heating rate is 20^{o}C/min.

4.3 Results and Discussion

4.3.1 Characterization of AFR-PEPA-4 Oligomer

The results for element analysis of synthesized AFR-PEPA-4 oligomer are listed in Table 8. The contents of C, H, F, N in synthesized AFR-PEPA-4 are very close to theoretical value. The temperatures for various weight losses of AFR-PEPA-4 oligomer calculated from TGA are list in Table 9. In nitrogen atmosphere, the temperatures for 1%, 2%, 5%, 10% and 20% weight losses of AFR-PEPA-4 oligomer are higher that those in air. The oligomer has less than 2% weight loss in both air and N_2 when the temperature is lower than 480^{o}C.

TABLE 8
Element Analysis Results of AFR-PEPA-4 Oligomer

Monomer or oligomer	Chemical formula	Molar mass (g/mole)	Composition (%)			
			C	H	F	N
6FDA	$C_{19}H_6F_6O_6$	444.24	51.37	1.36	25.66	
p-PDA	$C_6H_8N_2$	108.14	66.64	7.46		25.9
PEPA	$C_{16}H_8O_3$	248.23	77.42	3.25		
AFR-PEPA-4	$C_{138}H_{60}F_{24}N_{10}O_{20}$	2634.01	62.93	2.30	17.31	5.32
AFR-PEPA-4 (experimental)			62.69	2.55	17.17	5.36

TABLE 9
TGA Results of AFR-PEPA-4 Oligomer (Heating Rate: 10°C/min)

Weight loss (%)	Temperature (°C)	
	Air	N_2
1	339.6	342.8
2	480.1	488.6
5	524.2	527.4
10	543.8	548.7
20	564.8	584.5

The FT-IR spectrum of AFR-PEPA-4 oligomer is shown in Figure 52. The absorptions around 1726 cm^{-1} and 1785 cm^{-1} are attributed to symmetric stretching and asymmetric stretching of imide C=O bond, respectively. 1367 cm^{-1} is attributed to imide C-N stretching. 1517 cm^{-1} is from skeleton of benzene ring. The triple bond C≡C has absorption around 2214 cm^{-1}. Due to the relatively low concentration of phenylethynyl groups in AFR-PEPA-4 oligomer, the intensity of the peak 2214 cm^{-1} is relatively low.

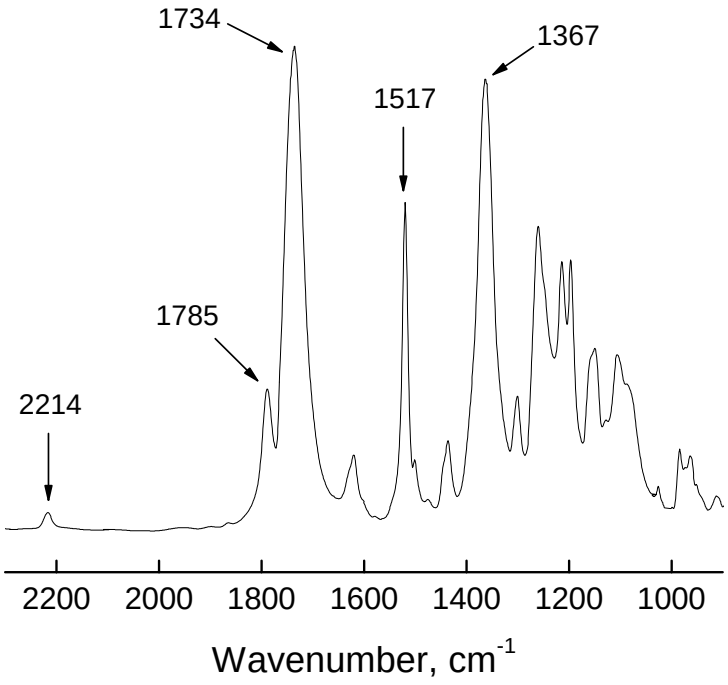

Figure 52 FT-IR spectra of AFR-PEPA-4 oligomer.

A DSC curve of AFR-PEPA-4 oligomer is shown in Figure 53. The T_g of the oligomer is 250°C, The melting point around 280°C indicates the presence of crystalline

structure in AFR-PEPA-4 oligomer. The reaction starts at 340°C and reaches to the peak at 410°C. Based on the thermal analysis results, the temperature window for thermal curing of AFR-PEPA-4 oligomer can be chosen from 340°C from 410°C to ensure the occurrence of crosslinking reaction without serious thermal degradation.

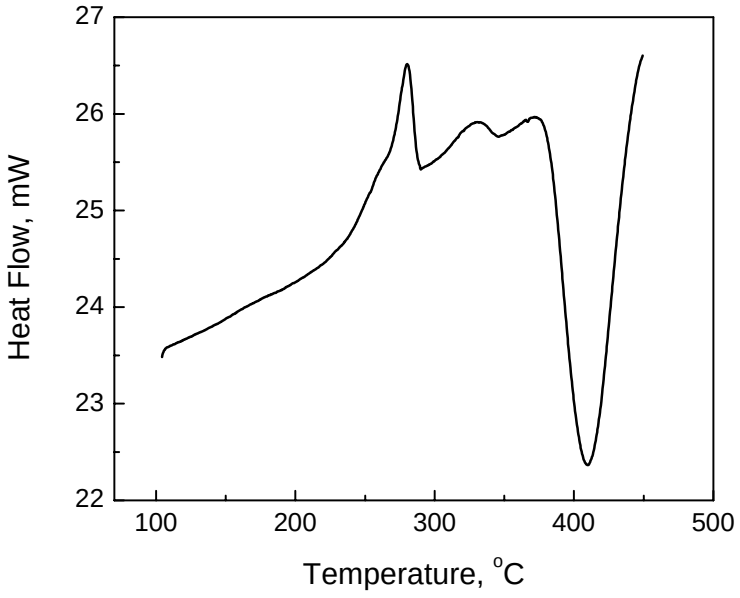

Figure 53 DSC curve of AFR-PEPA-4 oligomer (Heating rate: 20°C/min).

4.3.2 Cure Characterization of AFR-PEPA-4 Oligomer

Cure Reactions and Kinetics

Based on the thermal analysis results, the cure temperatures 350, 370, 390 and 410°C were chosen to study the effect of temperature on cure reactions of AFR-PEPA-4 oligomer.

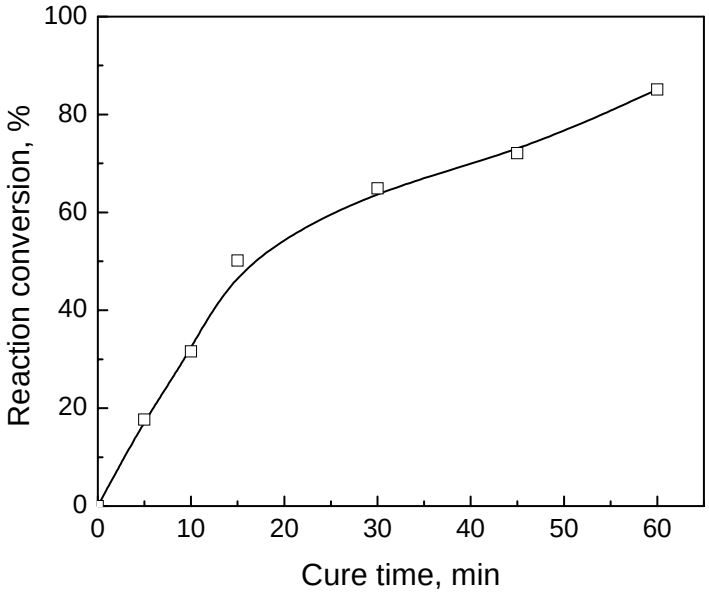

Figure 54 Reaction conversion of AFR-PEPA-4 oligomer vs. cure time at 350°C (calculated from FT-IR spectra).

The cure reactions of AFR-PEPA-4 oligomer can be monitored by FT-IR. Since the absorption around 2213 cm^{-1} is attributed to $\nu_{C\equiv C}$ in ethynyl group, the reaction conversion of AFR-PEPA-4 oligomer during the curing can be given by the consumption of C≡C triple bonds through the calculation of the decreased intensities of the bands at 2213 cm^{-1}. The absorption of imide C=O stretching around 1726cm^{-1} and 1785 cm^{-1}, inert from the reactions, can be used as internal standard. The reaction conversion can be calculated by relative intensity ratio compared between the intensity of the reaction involved peaks and that of internal standard. The reaction conversion α can be calculated by Equation (9), which is similar to Equation (5):

$$\alpha = \left(\frac{I_t}{I^{1785}} - \frac{I_0}{I^{1785}} \right) \Big/ \left(\frac{I_\infty}{I^{1785}} - \frac{I_0}{I^{1785}} \right) \tag{9}$$

The quantitative results are shown in Figure 54. The reaction conversion of AFR-PEPA-4 oligomers increased with the increase of cure time when they were cured at 350°C in air atmosphere. However, when the cure time is longer than 1h and the reaction conversion is more than 85%, FT-IR cannot detect the 2213 cm^{-1} band due to the limited resolution and the relatively low concentration of phenylethynyl groups in AFR-PEPA-4 oligomer. Based on the calculation from residual exothermal reaction ΔH in DSC test, the curing is not complete even over 8h cure at 350°C and the degree of cure is about 90%.

Assume the initial concentration of phenylethynyl groups in AFR-PEPA-4 oligomer $[A]_0 = 1$, the concentration of phenylethynyl groups at cure time t $[A]_t = 1-\alpha_t$. Assume the cure reaction follows n^{th} order kinetics, the rate equation can be written as:

$$-\frac{d[A]}{dt} = k[A]^n \tag{10}$$

If n=1, the equation (10) can be integrated as:

$$\ln[A]_t = \ln[A]_0 - kt \qquad \ln[1-\alpha] = -kt \tag{11}$$

where $\ln[A]_0 = 0$, $[A]_t = 1-\alpha_t$, α_t is reaction conversion at cure time t, and k is rate constant.

A plot ln $[1-\alpha_t]$ versus t for the cure reaction of AFR-PEPA-4 oligomer at 350°C in 1h yields a straight line, which is shown in Figure 55. Therefore, the cure kinetic

obeys first order during the first 1h at 350°C. The kinetic rate constant, k, derived from the slopes of the line, is listed in Table 10.

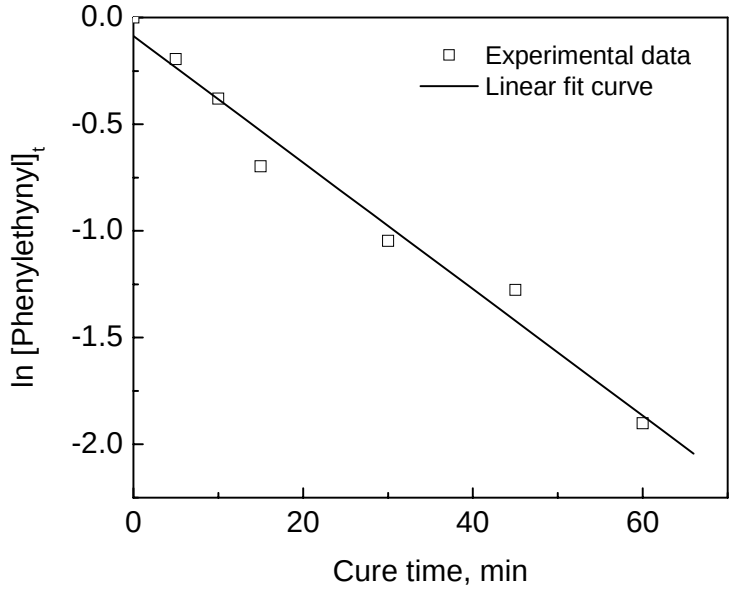

Figure 55 Reaction kinetic plot of ln C≡C vs. time for thermal cure of AFR-PEPA-4 at 350°C (calculated from FT-IR).

TABLE 10
Kinetic Analysis of the Thermal Cure of AFR-PEPA-4 Oligomer by FT-IR

Temperature, °C	Reaction order	Rate constant, min^{-1}	Regression coefficient
350	1	0.02967	0.988

The kinetic description of chainwise polymerizations requires a set of rate equations for initiation, inhibition, propagation, termination, and chain transfer steps. The polymerization rate is usually given by the propagation steps because they consume functional groups more frequently than any other involved steps. In most common cases, the free-radical cure reactions of thermosetting polymer follow n^{th} order kinetics in propagation steps. However, a significant decrease in the reaction rate is observed after the system vitrifies, which is due to diffusion restrictions.

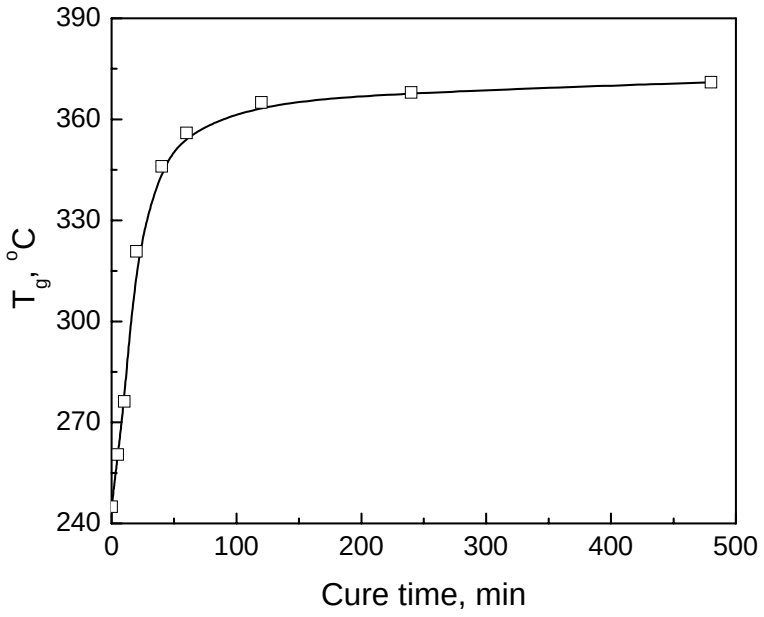

Figure 56 T_g vs. cure time of AFR-PEPA-4 oligomer cured at 350°C in 1h.

The plot of T_g vs. cure time of AFR-PEPA-4 oligomer cured at 350°C is shown in Figure 56. The increase of T_g is almost linear in the first 1 hour of curing. After 1h,

the increase of T_g has a remarkable drop due to diffusion restriction. There are many equations to model the relationships between T_g and cure extent of thermosetting polymers [137]. The original DiBedetto Equation (12) was modified to calculate the reaction extent x by determine the T_g for a highly crosslinked network, as follows [143, 144]:

$$\frac{T_g - T_{g0}}{T_{g\infty} - T_{g0}} = \frac{\lambda x}{1-(1-\lambda)x} \tag{12}$$

where T_{g0} and $T_{g\infty}$ are the glass transition temperature before and after fully cure, respectively. T_g is the glass transition temperature of the sample after isothermal cure at a cure temperature for specified cure time. λ is the ratio of isobaric heat specified time of the fully cured material, $\Delta C_{p\infty}$, to that of uncured material, ΔC_{p0}. The isobaric heat capacities can be determined by DSC.

Even if the selected $T_{g\infty}$ does not correspond to the theoretically ideal fully cured state, the extent of cure, x is still valid for kinetic analysis according to the modified DiBenedetto equation [144]. In this case, $T_{g\infty}$, λ, and x can be substituted by T_{gM}, λ', and x' respectively, where T_{gM} is the T_g of a network, λ' is the ratio of ΔC_{pM} to ΔC_{p0}, and x' refers to x/x_M, a relative reaction content.

Based on this modified DiBenedetto equation, the dependence of T_g on reaction conversion of phynylethynyl C≡C in AFR-PEPA-4 oligomers can be simulated, which is shown in Figure 57, indicating that good agreement between simulated curve and experimental data. The predicted $T_{g\infty}$ based on the simulation is 437.2°C. In the experiments, the highest T_g of cured AFR-PEPA-4 was 418°C obtained by thermal

curing of AFR-PEPA-4 oligomer at 410°C for 8h. Lincoln obtained the highest T_g of cured AFR-PEPA-4 with 422°C [19]. Therefore, this simulation method is reliable to be utilized to calculate the reaction conversions based on measured T_gs.

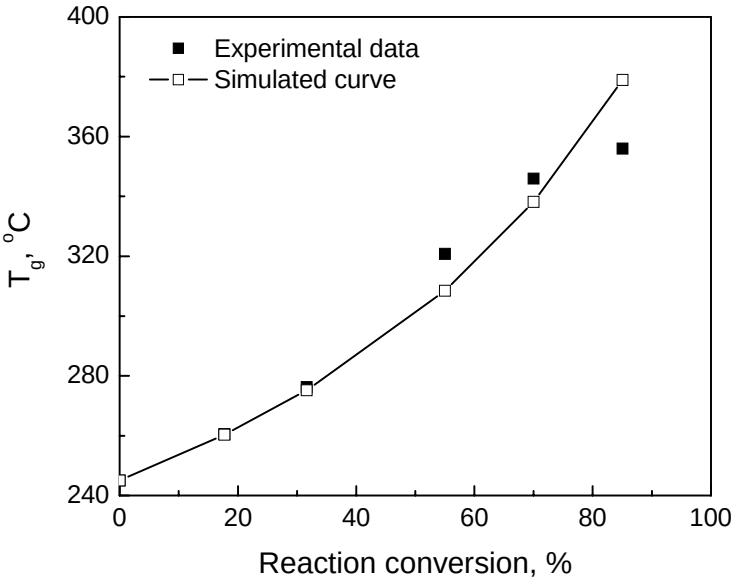

Figure 57 T_g vs. reaction conversion of AFR-PEPA-4 oligomer cured at 350°C in 1h.

The dependences of T_g of cured oligomers on cure time at various cure temperatures in air are shown in Figure 57. The T_g of the cured oligomer increases with the increase of cure time and cure temperature. The cure temperature 410°C gave the highest cure reaction rate at the beginning of the curing, at which sample's T_g went to 381°C with only 5 min curing. The cure reaction rate tends to be stable after the curing reaches certain extent due to the diffusion control. The T_gs of cured oligomers after 8h

curing at 350°C, 370°C, 390°C and 410°C are 371°C, 385°C, 398°C and 418°C, respectively.

Since FT-IR cannot detect the absorption of residue phenylethynyl group in highly crosslinked AFR-PEPA-4 polyimide, the reaction conversion of AFR-PEPA-4 oligomer cured at various temperatures can be calculated from the T_g of cured samples by using modified DiBenedetto equation obtained earlier. T_gs as a function of reaction conversion are shown in Figure 58. The reaction conversions vs. cure time of AFR-PEPA-4 oligomer cured at various cure temperatures calculated from DSC T_g are shown in Figure 59.

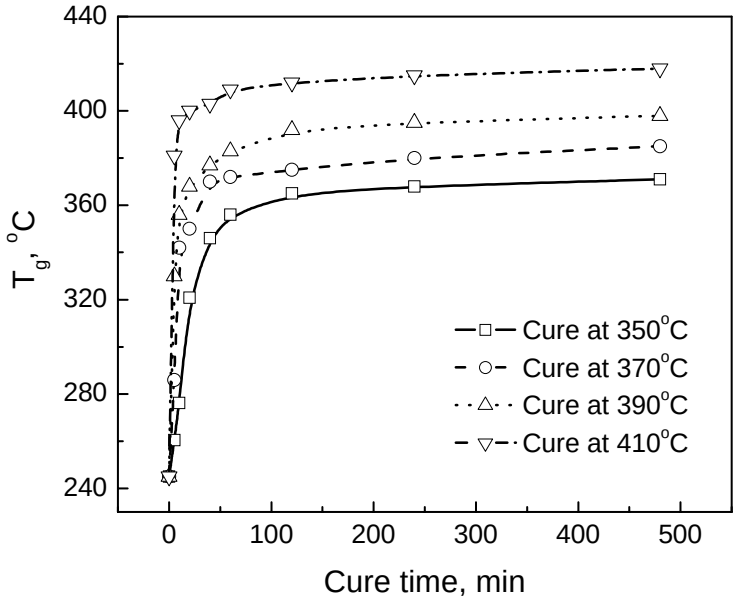

Figure 58 T_g vs. cure time of AFR-PEPA-4 oligomer cured at various temperatures.

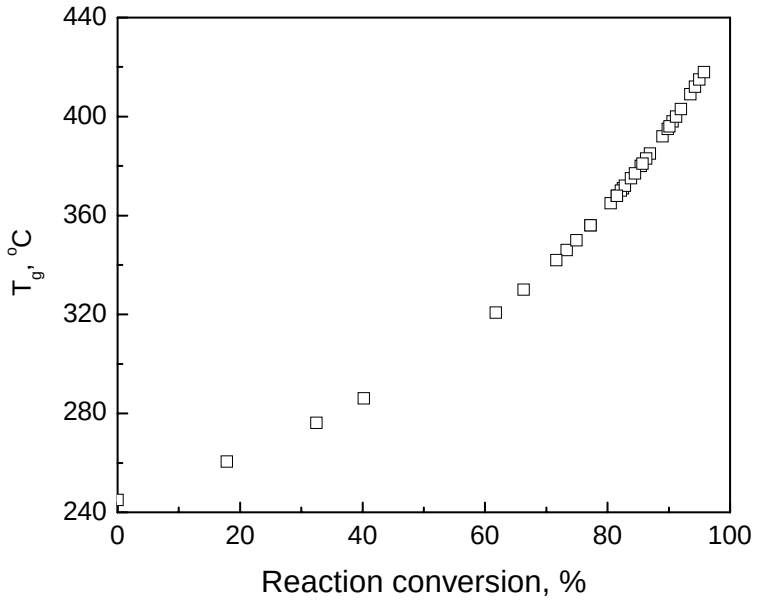

Figure 59 T_g as a function of reaction conversion of cured AFR-PEPA-4 oligomer.

TABLE 11
Kinetic Analysis of the Thermal Cure of AFR-PEPA-4 by DSC (Below 80% Cure)

Temperature, °C	Rate constant, min^{-1}	Regression coefficient
350	0.0339	0.973
350[a]	0.02967	0.988
370	0.06952	0.911
390	0.14797	0.965
410	0.3893	1

a: Analysis by reaction conversion data from FT-IR

A plot of the ln (1-α) vs. cure time (Figure 60) for a first-order reaction shows that significant deviation from linearity once the reaction conversion α excesses 80%. If the experimental points just below 80% cure are selected, first order kinetics better simulates the kinetic data (Table 11).

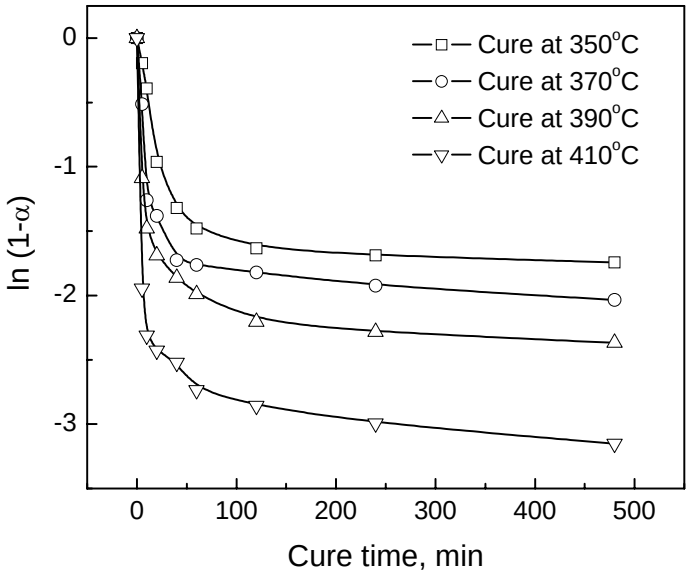

Figure 60 Kinetic plot of ln (1-α) vs. time from DSC T_g data.

The rate constant k is a function of cure temperature by the Arrhenius equation (13):

$$k(T) = A\exp\left(-\frac{E_{act}}{RT}\right) \tag{13}$$

where A is the pre-exponential factor, R is gas constant 8.3145 J mol^{-1} K^{-1}, and E_{act} is the activation energy. Equation (13) can be written as:

$$\ln k(T) = \ln A - \left(\frac{E_{act}}{R}\right)\frac{1}{T} \tag{14}$$

Thus, the activation energy E_{act} can be obtained by plot ln k vs. 1/T (Figure 61). The analysis results are listed in Table 12.

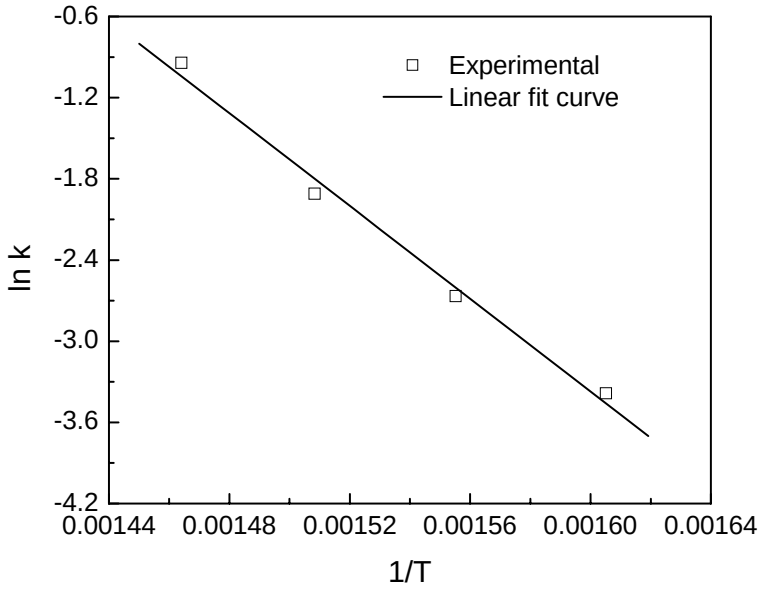

Figure 61 Kinetic plots of ln k vs 1/T of the cure reaction of AFR-PEPA-4 oligomer for first order (below 80% cure).

Sastri et al. [145] studied the cure kinetics of several phenylethynyl substituted benzene compounds by using the dynamic DSC method and found the activation

energies are from 125.2 to 148.6 kJ/mol, which is higher than ethynyl substituted compounds (97.1 kJ/mol). This implies that electro donating effects of a phenyl group may be less important than the steric factors from bulk phenyl groups, and therefore results in decreased reactivity over the ethynyl substituted compounds. Fang et al. [146] investigated the cure kinetics of PETI-5 and found it follows the first or 1.5 order kinetics. The activation energy of PETI-5 was found to be 170.4 kJ/mol [146].

TABLE 12
Activation Energy of Thermal Cure Reaction of AFR-PEPA-4 Oligomer

E_{act}, kJ/mol	A, min^{-1}	Regression coefficient
142.6 ± 10.0	2.81×10^{10}	0.995

However, this reaction order failed to describe the data over the whole range of conversion values for complete cure. The heats of reaction data do not adequately define the reaction for complete cure. The crosslinking occurs through the phenylethynyl addition reaction in the earlier stages of the cure reaction by simple first order kinetics. The continued reactions such as intramolecular and bimolecular double bond addition reactions that form more highly crosslinked polymer need to be investigated.

Thermal Stability of Cured AFR-PEPA-4 Polyimide

Cured AFR-PEPA-4 samples (390^{o}C for 1h) were heated at 100^{o}C under vacuum till weight did not change. They were then heated at rates of 10^{o}C/min under air and N_2 to 800^{o}C in TGA. The temperatures for various weight losses of cured AFR-PEPA-4 calculated from TGA are list in Table 13. In nitrogen atmosphere, the temperatures for 1%, 2%, 5%, 10% and 20% weight losses of cured AFR-PEPA-4 polyimide are higher that those in air. The polyimide has less than 2% weight loss in both air and N_2 when the temperature is lower than 510^{o}C.

TABLE 13
TGA Results of Cured AFR-PEPA-4 Polyimide (Heating Rate: 10^{o}C/min)

Weight loss (%)	Temperature (^{o}C)	
	Air	N_2
1	496.6	504.5
2	513.9	520.0
5	531.3	540.4
10	548.7	559.6
20	567.7	595.5

4.3.3 Characterization of N-phenyl-[4-(phenylethynyl) phthalimide]

The results for element analysis of synthesized model compound N-phenyl-[4-(phenylethynyl) phthalimide] are listed in Table 14. The contents of C, H, N in

synthesized N-phenyl-[4-(phenylethynyl) phthalimide] are very close to theoretical value. The errors are less than 2%.

TABLE 14
Element Analysis Results of N-Phenyl-[4-(phenylethynyl) phthalimide]

Element	Theoretical content, %	Measured content, %	Error, %
C	81.72	81.66	0.07
H	4.05	4.02	0.74
N	4.33	4.26	1.62

The mass spectrum of N-phenyl-[4-(phenylethynyl) phthalimide] is shown in Figure 62. The sample's molecular weight obtained from mass spectrum is 323.096, which is same as the theoretical value.

The ^{1}H n.m.r. ($CDCl_3$) spectrum showed peaks at δ = 8.06, 7.90, and 7.53 ppm, which are from protons in the benzene rings. The ^{13}C n.m.r. ($CDCl_3$) spectrum showed peaks at 166.62, 137.17, 132.20, 131.84, 131.52, 130.33, 129.27, 129.12, 128.52, 126.53, 126.49, 123.72, 122.03, 94.19 and 87.70 ppm. The ^{1}H n.m.r. spectrum and ^{13}C n.m.r. spectrum are shown in Figure 63 and Figure 64, respectively.

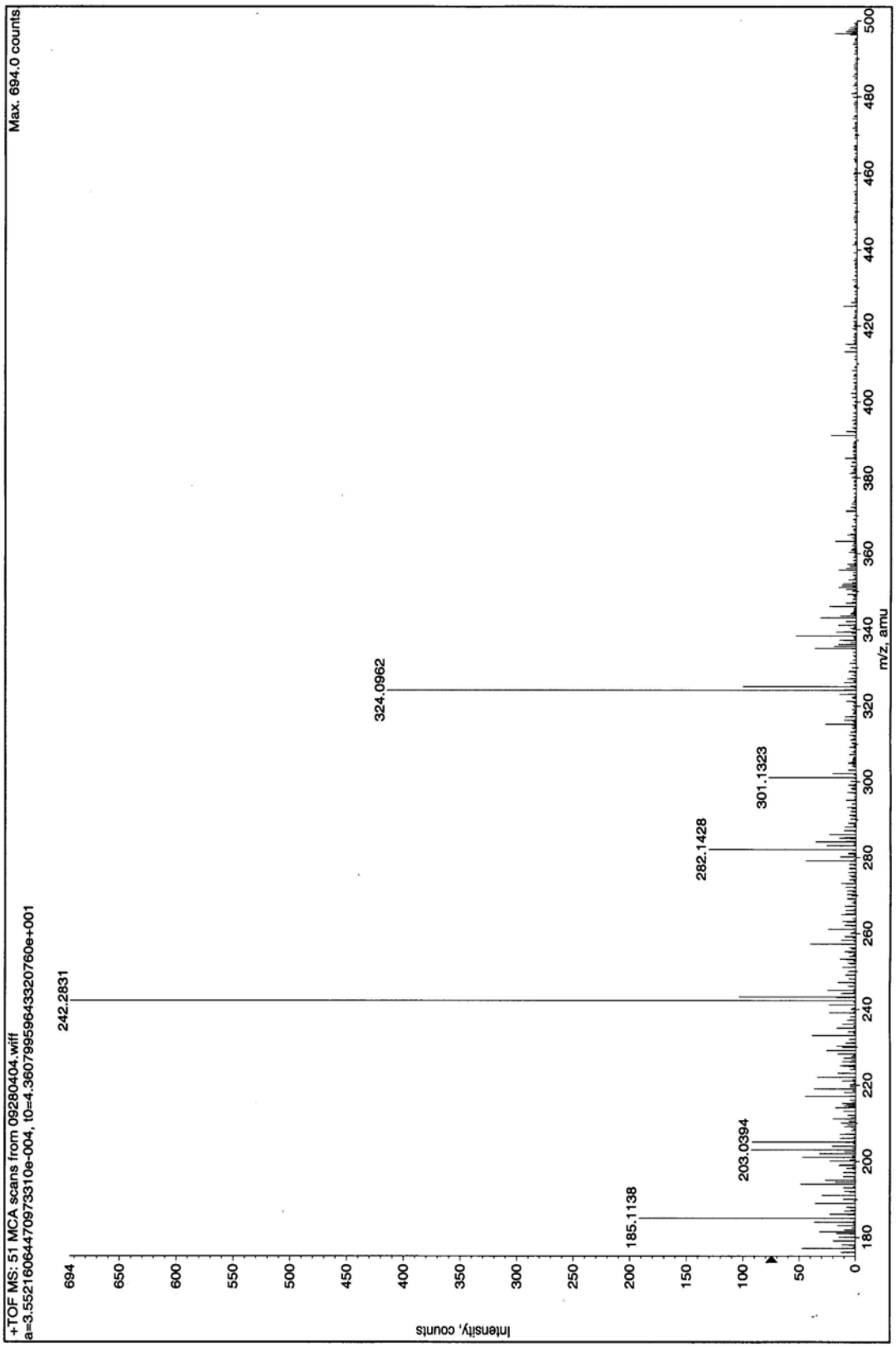

Figure 62 Mass spectrum of N-phenyl-[4-(phenylethynyl) phthalimide].

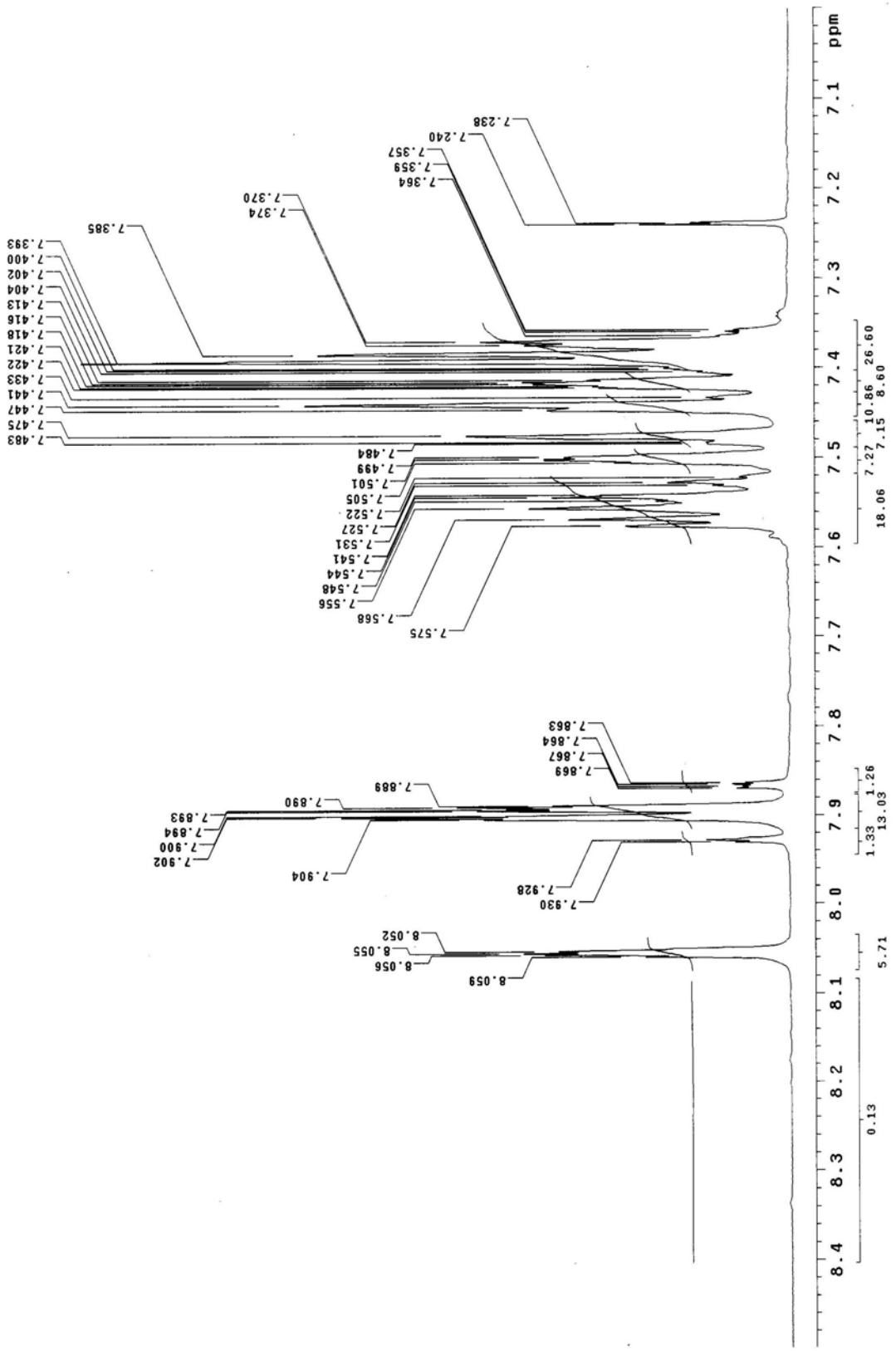

Figure 63 ^{1}H n.m.r. spectrum of N-phenyl-[4-(phenylethynyl) phthalimide].

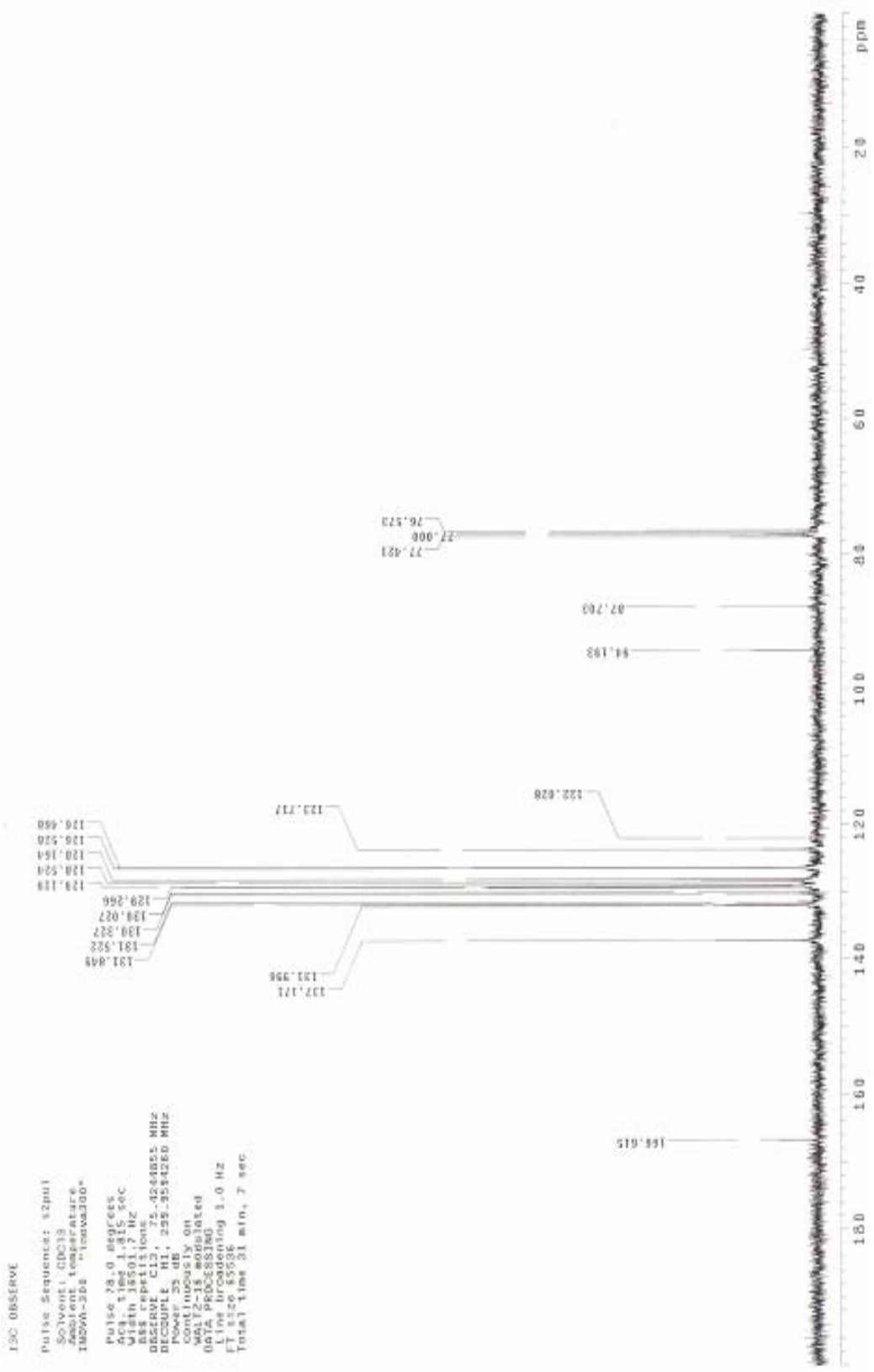

Figure 64 ^{13}C n.m.r. spectrum of N-phenyl-[4-(phenylethynyl) phthalimide].

The FT-IR spectrum of N-phenyl-[4-(phenylethynyl) phthalimide] is shown in Figure 65. Similar to the absorptions of AFR-PEPA-4 oligomer, the absorptions around 1713 cm^{-1} and 1780 cm^{-1} are attributed to symmetric stretching and asymmetric stretching of imide C=O bond, respectively. 1385 cm^{-1} is attributed to imide C-N stretching. 1611 cm^{-1} is from the conjugated bonds. The triple bond C≡C has absorption around 2216 cm^{-1}.

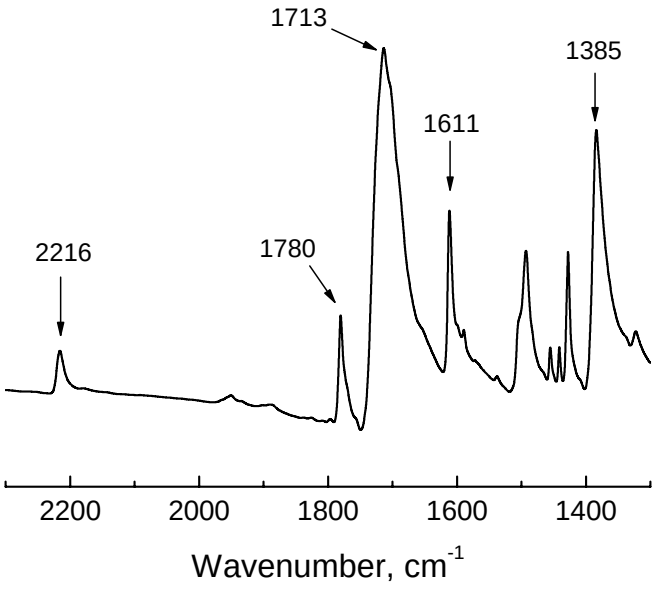

Figure 65 FT-IR spectrum of N-phenyl-[4-(phenylethynyl) phthalimide].

The melting point of N-phenyl-[4-(phenylethynyl) phthalimide] is 210-212^{o}C, which was determined by a capillary melting point apparatus. The DSC curve of N-phenyl-[4-(phenylethynyl) phthalimide] (Figure 66) also showed a sharp peak for the

melting at 209.8°C with ΔH of 128.4 J/g. As shown in Figure 66, the reaction of N-phenyl-[4-(phenylethynyl) phthalimide] starts from 320.3°C with the onset and peak reaction temperature of 360.8°C and 396.8°C, respectively. The reaction heat ΔH is 421.9 J/g.

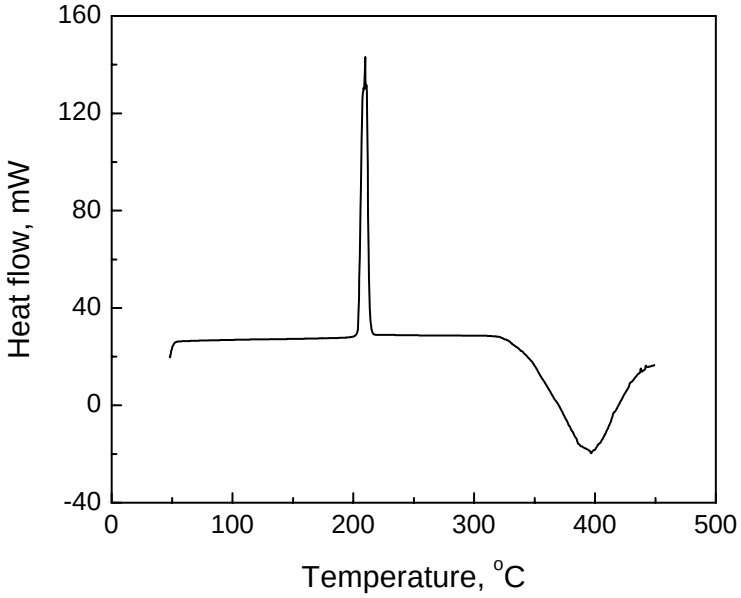

Figure 66 DSC curve of N-phenyl-[4-(phenylethynyl) phthalimide].

4.3.4 Cure Kinetics of N-phenyl-[4-(phenylethynyl) phthalimide]

Based on the reaction peak in DSC results, the cure temperatures at 330, 350, 370, and 390°C were chosen for thermal cure kinetic study of N-phenyl-[4-(phenylethynyl) phthalimide].

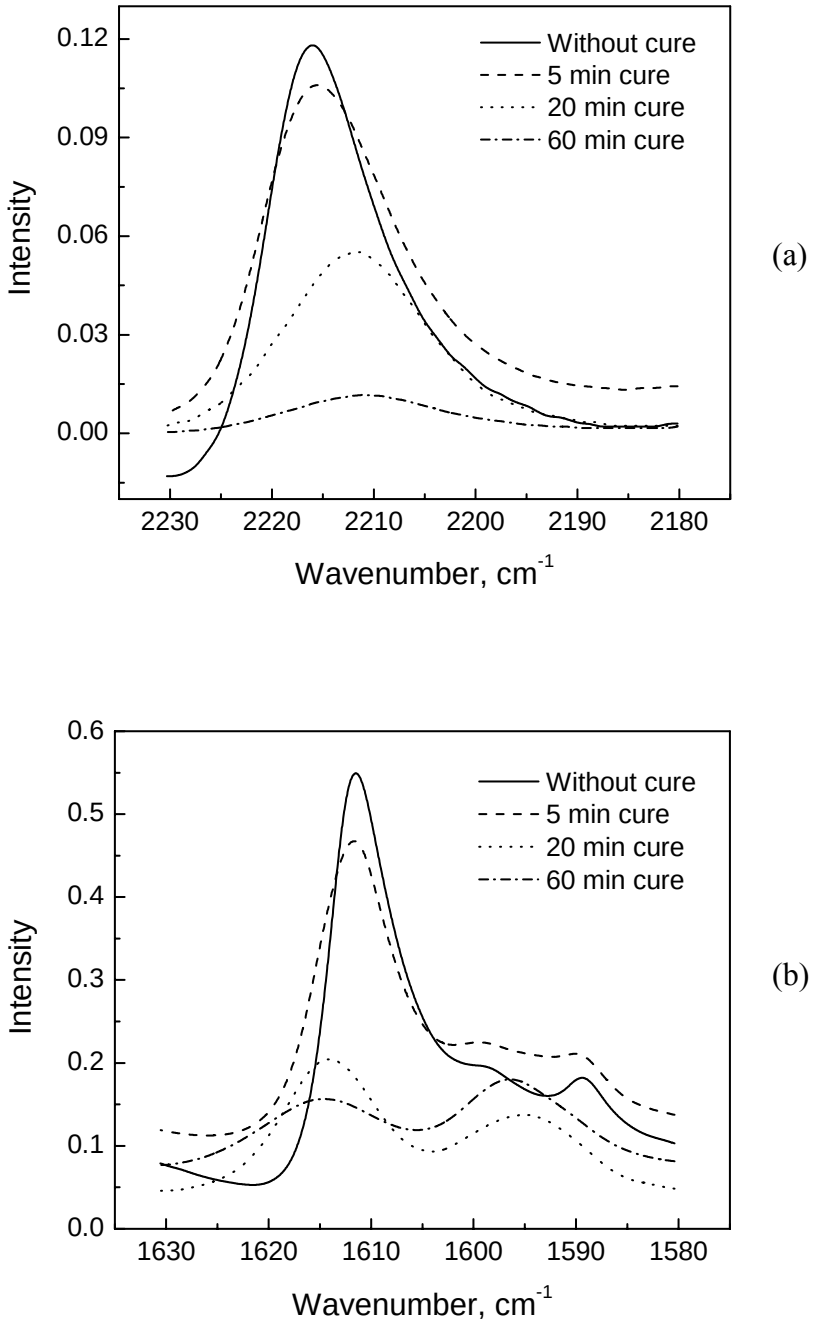

Figure 67 The dependence of IR intensity on cure time for thermal curing of N-phenyl-[4-(phenylethynyl) phthalimide] at 330°C in air (a) phenylethynyl group at 2216 cm^{-1}; (b) conjugate bonds at 1611 cm^{-1}.

The cure reactions of N-phenyl-[4-(phenylethynyl) phthalimide] can be monitored by FT-IR. Since the absorption around 2216 cm^{-1} is attributed to $\nu_{C\equiv C}$ in ethynyl group and the absorption around 1611 cm^{-1} is attributed to $\nu_{C=C}$ in conjugated bonds, the reaction conversion of N-phenyl-[4-(phenylethynyl) phthalimide] during the curing can be given by the consumption of C≡C triple bonds and conjugated double bonds through the calculation of the decreased intensities of the bands at 2216 and 1611 cm^{-1} (Figure 67). From Figure 67, the peak intensities of 2216 and 1611 cm^{-1} decrease with the increase of cure time. Moreover, the absorption band of phenylethynyl group switches to lower wavenumbers and that of conjugated bonds switches to higher wavenumbers with the increase of cure time. Therefore, the crosslinking through both the phenylethynyl addition reaction and intramolecular or bimolecular double bond addition reactions can be monitored. The absorption of imide C=O stretching around 1713 cm^{-1} and 1780 cm^{-1}, inert from the reactions, can be used as internal standard. The reaction conversion can be calculated by Equation (9).

The quantitative results are shown in Figure 68. The reaction conversion of N-phenyl-[4-(phenylethynyl) phthalimide] increased with the increase of cure time and cure temperature. However, the consumption of phenylethynyl C≡C triple bonds and that of conjugated double bonds are not same during the cure reaction. In the case of 330^{o}C cure temperature, even though the reaction conversion of phenylethynyl C≡C triple bonds reaches 90% after 1h cure, the reaction conversion of conjugated bonds is only 75%.

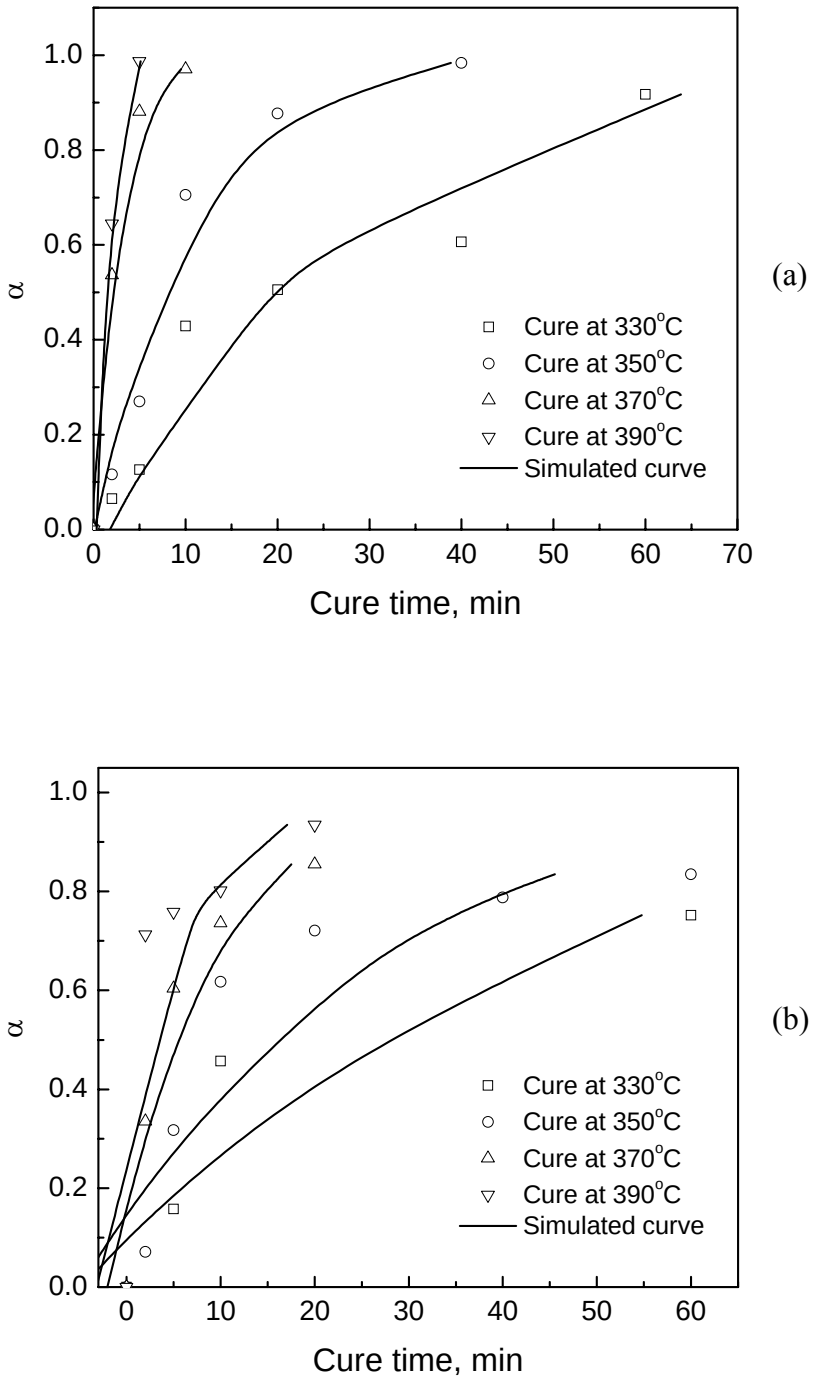

Figure 68 Reaction conversion α vs. cure time of N-phenyl-[4-(phenylethynyl) phthalimide] cured at various temperatures from FT-IR results (a) phenylethynyl group at 2216 cm^{-1}; (b) conjugate bonds at 1611cm^{-1}.

TABLE 15
Kinetic Analysis of the Thermal Cure of N-Phenyl-[4-(phenylethynyl) phthalimide] by FT-IR 2216 cm^{-1}

Cure temperature, ^{o}C	Reaction order	k
330	0.95	0.03775
350	0.95	0.09557
370	0.95	0.3303
390	0.95	0.8110

TABLE 16
Kinetic Analysis of the Thermal Cure of N-Phenyl-[4-(phenylethynyl) phthalimide] by FT-IR 1611 cm^{-1}

Cure temperature, ^{o}C	Reaction order	k
330	0.94	0.02241
350	0.94	0.03364
370	0.94	0.09343
390	0.94	0.1250

Assume the cure reaction follows n^{th} order kinetics, the rate equation can be written as:

$$-\frac{d[A]}{dt} = k[A]^n \tag{10}$$

By simulating the cure reactions as n^{th} order kinetics from reaction conversion data, the kinetics data can be obtained, which are listed in Table 15 and Table 16.

The activation energy E_{act} can be obtained by plot ln k vs. 1/T (Figure 69) from the equation (14). The analysis results are listed in Table 17.

TABLE 17
Activation Energy of Thermal Cure Reaction of N-Phenyl-[4-(phenylethynyl) phthalimide] from FT-IR Calculation

IR band, cm^{-1}	E_{act}, kJ/mol	A, min^{-1}	Regression coefficient
2216	173.5 ± 8.2	3.81×10^{13}	0.998
1611	102.7 ± 15.9	1.67×10^{7}	0.977

From kinetic analysis, the thermal crosslinking of N-phenyl-[4-(phenylethynyl) phthalimide] through phenylethynyl addition reaction has a reaction order of 0.95 and an activation energy of 173.5 ± 8.2 kJ/mol. It can be noticed that the conjugated bond addition reactions has a lower reaction order of 0.94 and lower activation energy (102.7 ± 15.9 kJ/mol). Meanwhile, phenylethynyl addition reaction in the system provides a better kinetic simulation. The cure reaction of N-phenyl-[4-(phenylethynyl) phthalimide] can be described as two stages:

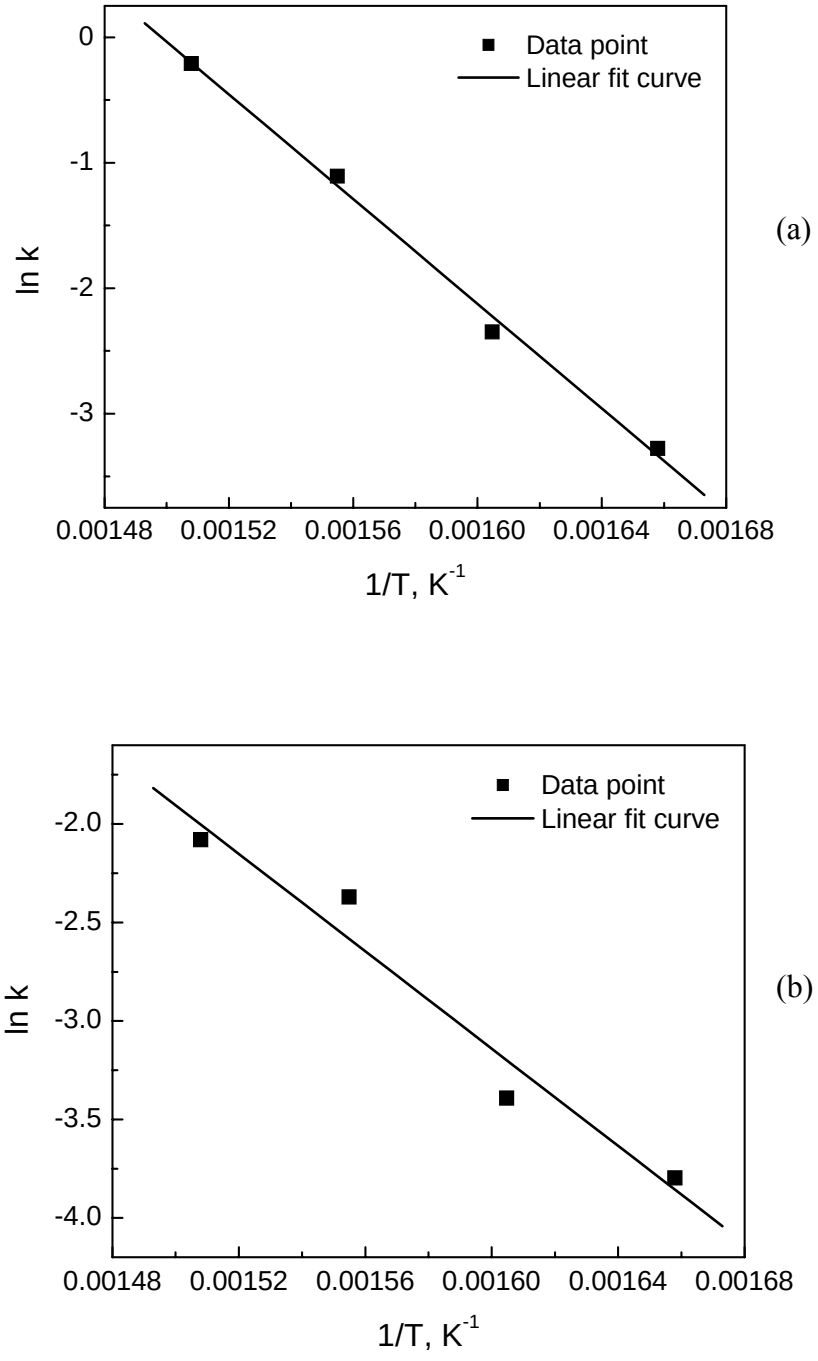

Figure 69 Kinetics plots of ln k vs 1/T of the cure reaction of N-phenyl-[4-(phenylethynyl) phthalimide] calculated from FT-IR conversion (a) phenylethynyl group at 2216 cm^{-1}; (b) conjugate bonds at 1611 cm^{-1}.

(i) A fast stage. First-order fast reaction kinetically controlled at short times to form a high molecular weight gel. Both phenylethynyl addition reaction and intramolecular or bimolecular double bond addition reactions occur in this stage.

(ii) A slow second stage. Crosslinking reaction kinetically controlled by diffusion with the reaction order close to 1. The double bond addition reactions mainly occur in this stage.

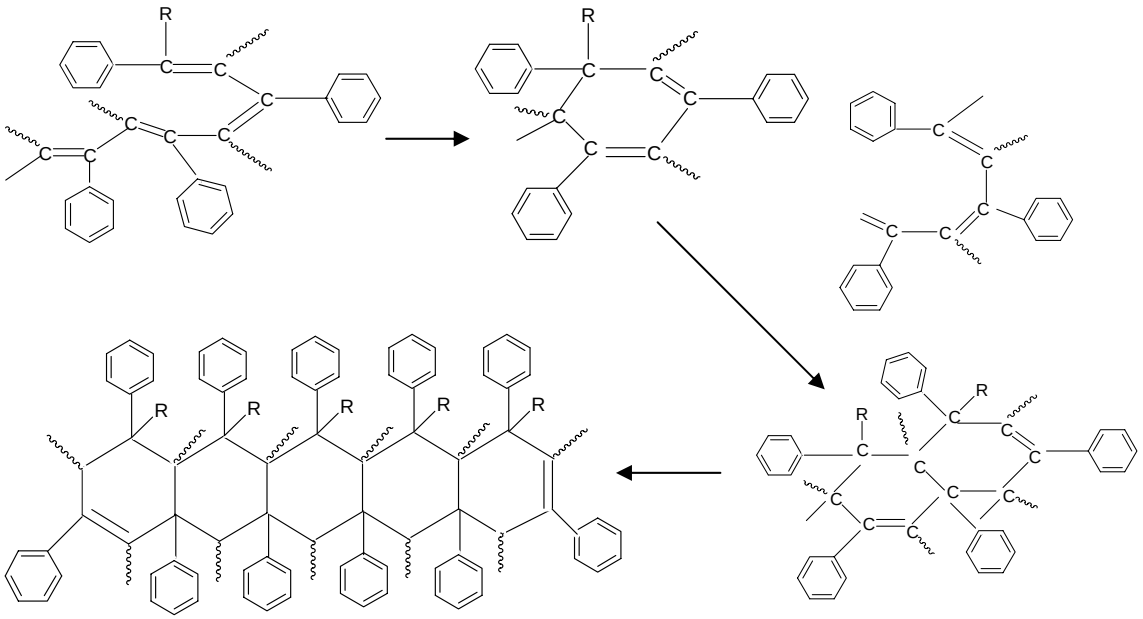

Figure 70 Proposed cure products of N-phenyl-[4-(phenylethynyl) phthalimide].

At the beginning the cure reaction occurs by simple ethynyl to ethynyl addition reactions to form linear and crosslinked polyene structures. Furthermore, the fused ring crosslinking system is formed from a series of reactions (Figure 70) such as Diel-Alder, Friedel-Crafts, Straus and Glaser coupling reactions as suggested by Fang et al. [146].

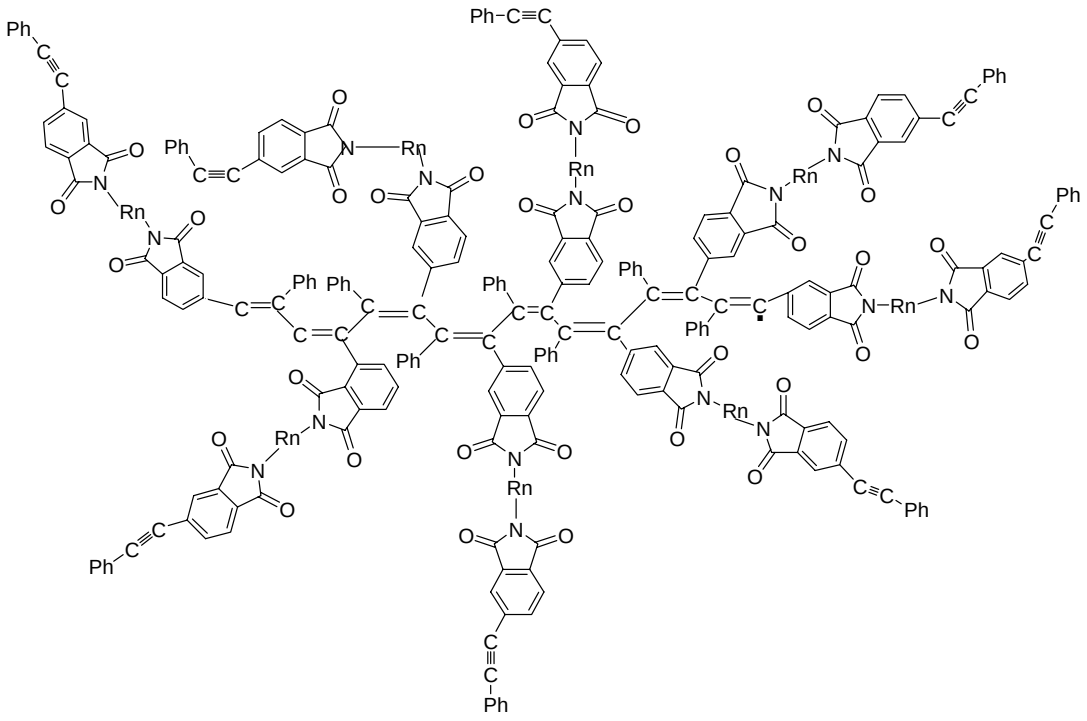

Figure 71 Proposed structure of cured AFR-PEPA-4.

For AFR-PEPA-4 oligomer, the crosslinked structure with highly steric hindrance can be obtained by ethynyl addition reactions (Figure 71). Therefore, the cure product is difficult to be further crosslinked via double bond addition reactions.

4.4 Conclusions

AFR-PEPA-4 oligomer and an imide model compound N-phenyl-[4-(phenylethynyl) phthalimide] were synthesized and characterized for cure reaction study.

DSC was used in determining the cure kinetics of AFR-PEPA-4 oligomer by following the increase in T_g as a function of cure. The predicted ultimate T_g of cured AFR-PEPA-4 polyimide is 437.2^oC. The activation energy of thermal cure reaction of AFR-PEPA-4 oligomer is 142.6 ± 10.0 kJ/mol with the kinetic order of 1 when the reaction conversion is less than 80%. However, the first order reaction failed to describe the data over the whole range of conversion values for complete cure.

Cured AFR-PEPA-4 polyimide shows excellent thermal stability. The cured polyimide has less than 2% weight loss in both air and N_2 when the temperature is lower than 510^oC.

The kinetics analysis of the thermal cure of N-phenyl-[4-(phenylethynyl) phthalimide] was determined by FT-IR spectroscopy by following the absorbance of the phenylethynyl triple bond and conjugated bonds. The thermal crosslinking of N-phenyl-[4-(phenylethynyl) phthalimide] through phenylethynyl addition reaction has a reaction order of 0.95 and an activation energy of 173.5 ± 8.2 kJ/mol. The conjugated bond addition reactions have a lower reaction order of 0.94 and lower activation energy (102.7 ± 15.9 kJ/mol) than phenylethynyl addition reaction. However, phenylethynyl addition reaction in the system provides a better kinetic simulation. The cure reaction of N-phenyl-[4-(phenylethynyl) phthalimide] can be described as two stages: (i) A fast stage. First-order fast reaction kinetically controlled at short times to form a high molecular

weight gel. Both phenylethynyl addition reaction and intramolecular or bimolecular double bond addition reactions occur in this stage. (ii) A slow second stage. Crosslinking reaction kinetically controlled by diffusion with the reaction order is close to 1. The double bond addition reactions mainly occur in this stage.

CHAPTER V

CONCLUSIONS

5.1 Conclusions

The E-beam curable BMI resin systems and phenylethynyl terminated AFR-PEPA-4 oligomer together with an imide model compound N-phenyl-[4-(phenylethynyl) phthalimide] were synthesized and characterized.

E-beam exposure cannot propagate the polymerization of BMI system until the temperature goes up to 100^{o}C. However, solid-state cure reaction of BMI does occur to some extent and a small amount of oligomers may be generated under low E-beam intensity radiation, though the reaction conversion was low. Higher intensity E-beam at 40 kGy per pass can give high reaction conversion of BMI above 75%. However, the temperature of BMI reached up to 250^{o}C, which induced normal thermal cure mechanism.

NVP is a good reactive diluent for BMI resin. It decreases the viscosity of BMI resin so that the reactivity of the system is increased significantly. The cure extents of BMI/NVP increase with the increase of the dosage and applied dosage per pass. The reaction rate is much higher at the beginning of the E-beam cure and slows down after 2 or 3 dose passes due to diffusion control. Free radical initiator dicumyl peroxide can accelerate the reaction rate at the beginning of E-beam cure reaction but doesn't affect final cure conversion very much. According to the results from FT-IR, 200 kGy total dosage E-beam exposure at 10 kGy per pass can give 70% reaction conversion of

BMI/NVP with the temperature rise no more than 50°C. The product has a T_g of 180°C. NVP shows the great potential to be utilized as the reactive diluent for phenylethynyl terminated imide.

The effect of higher intensity E-beam radiation on BMI system is much more significant than that on BMI/NVP system, which indicates that thermal cure is the dominant process in BMI system during high intensity E-beam exposure. As to BMI/NVP system, E-beam induced cure rather than the normal thermal cure is dominant, which makes low intensity E-beam curing at low temperature possible. The increase of the concentration of NVP in the system increases the reaction conversions almost linearly. The dilution and activation effects of NVP play the most important role in the interaction between BMI and NVP and make BMI have a more active response on E-beam radiation.

DSC was used in determining the cure kinetics of AFR-PEPA-4 oligomer by following the increase in T_g as a function of cure. The predicted ultimate T_g of cured AFR-PEPA-4 polyimide is 437.2°C. The activation energy of thermal cure reaction of AFR-PEPA-4 oligomer is 142.6 ± 10.0 kJ/mol with the kinetic order of 1 when the reaction conversion is less than 80%. However, the first order reaction failed to describe the data over the whole range of conversion values for complete cure.

Cured AFR-PEPA-4 polyimide shows excellent thermal stability. The cured polyimide has less than 2% weight loss in both air and N_2 when the temperature is lower than 510°C.

The kinetics analysis of the thermal cure of N-phenyl-[4-(phenylethynyl) phthalimide] was determined by FT-IR spectroscopy by following the absorbance of the phenylethynyl triple bond and conjugated bonds. The thermal crosslinking of N-phenyl-[4-(phenylethynyl) phthalimide] through phenylethynyl addition reaction has a reaction order of 0.95 and an activation energy of 173.5 ± 8.2 kJ/mol. The conjugated bond addition reactions have a lower reaction order of 0.94 and lower activation energy (102.7 ± 15.9 kJ/mol) than phenylethynyl addition reaction. However, phenylethynyl addition reaction in the system provides a better kinetic simulation. The cure reaction of N-phenyl-[4-(phenylethynyl) phthalimide] can be described as a fast first-order reaction stage followed by a slow second stage that is kinetically controlled by diffusion with the reaction order less than 1. At the beginning the cure reaction occurs by simple ethynyl to ethynyl addition reactions to form linear and crosslinked polyene structures. Furthermore, the fused ring crosslinking system is formed from a series of reactions such as Diel-Alder, Friedel-Crafts, Straus and Glaser coupling reactions. For AFR-PEPA-4 oligomer, the crosslinked structure with highly steric hindrance can be obtained by ethynyl addition reactions, which is difficult to be further crosslinked via double bond addition reactions.

5.2 Suggestions for Future Research

It was found that the thermal history affected T_g and reaction conversion of E-beam cured BMI resins. E-beam radiation energy absorption will raise the temperature of the samples together with the resin cure exotherm. The heat formation during the cure

is mainly governed by the enthalpy of polymerization, the E-beam energy absorption and the heat dissipation to the environment of the mold. The modeling approach to describe the heat transfer and temperature change involved in the E-beam process is necessary to understand and predict the E-beam induced cure kinetics, local temperature, and T_g as a function of dose and time.

The fundamental parameters that control imide oligomer synthesis, molecular weight, morphology, rheology and cure reaction mechanisms need to be further identified and characterized, such as the synthesis conditions of imide oligomer formation in terms of solvent concentration-temperature-time conditions and gaseous environment for imidization and cure reactions. To investigate how such parameters affect the network structure, deformation and failure modes and mechanical properties of the fully cured polyimide resin is critical to understand the fundamental of process-structure-properties relations of high temperature polyimides.

The cure mechanism of crosslinking of phenylethynyl terminated imide monomers and oligomers need to be further studied. The characterization of the crosslinking reaction mechanism of the imide acetylene end caps and how these cure reactions are modified by imide oligomer chemistry, air, free radical initiation, and radiation (such as electron beam) exposure-time characteristics. Meanwhile, the modification of imide oligomer chemistry and the utilization of reactive diluent for developing E-beam curable high temperature imide materials need to be investigated.

REFERENCES

1. Meador, M. A. Annu Rev Mater Sci 1998, 28, 599-630.

2. Chandra, R.; Rajabi, L. J Macromol Sci R M C 1997, C37(1), 61-96.

3. Morgan, R. J.; Shin, E. E.; Lincoln, J.; Zhou, J. SAMPE J 2001, 37(2), 102-107.

4. Saunders, C.; Lopata, V.; Barnard, J.; Stepanik, T. Radiat Phys Chem 2000, 57 (3-6), 441–445.

5. Janke, C. J.; Lopata, V. J.; Havens, S. J.; Dorsey, G. F.; Moulton, R. J. US Patent 1999, 5,877,229.

6. Cleland, M. R.; Parks, L. A.; Cheng, S. Nucl Instrum Methods Phys Res B 2003, 208, 66-73.

7. Berejka A. J.; Eberle, C. Radiat Phys Chem, 2002, 63(3-6), 551-556.

8. Bhattacharya, A. Prog Polym Sci 2000, 25(3), 371-401.

9. Glauser, T.; Johansson, M.; Hult, A. Polymer 1999, 40(19), 5297-5302.

10. Korenev, S. Vacuum 2001, 62(2-3), 233-236.

11. Nho, Y. C.; Kang, P. H.; Park, J. S. Radiat Phys Chem 2004, 71(1-2), 243-246.

12. Degrand H.; Cazaux, F.; Coqueret, X.; Defoort, B.; Boursereau, F.; Larnac, G. Radiat Phys Chem 2003, 68(5), 885-891.

13. Sui, G.; Zhang, Z. G.; Liang, Z. Y.; Chen, C. Q. Mat Sci Eng A-Struc 2003, 342(1-2), 28-37.

14. Mascioni, M.; Sands, J. M.; Palmese, G. R. Nucl Instrum Methods Phys Res B 2003, 208, 353-357.

15. Grenier-Loustalot, M. F.; Denizot, V.; Beziers, D. High Perform Polym 1995, 7, 181-217.

16. Hoyt, A. E. Proc of 46th International SAMPE Symp 2001, 46, 2526-2535.

17. Papathanasiou, T. D.; Ingber, M. S.; Mondy, L. A.; Graham, A.L., J Compo Mater 1994, 28(4), 288.

18. Ghosh, M. K.; Mittal, K. L. Polyimide: Fundamentals and Applications. Marcel Dekker, Inc., New York, 1996.

19. Lincoln, J. Structure-property-processing relationships and the effects of physical structure on the hygrothermal durability and mechanical response of polyimides. *Ph.D. Dissertation*, Michigan State University, 2001.

20. Cai, Y.; Liu, P.; Hu, X.; Wang, D.; Xu, D. Polymer 2000, 41(15), 5653-5660.

21. Jiang, B.; Hao, J.; Wang, W.; Jiang, L.; Cai, X. Eur Polym J 2001, 37(3), 463-470.

22. Reghunadhan Nair, C. P. Prog Polym Sci 2004, 29(5), 401-498.

23. AECL Technologies Inc., Electron curing of composite structures for space applications. Executive summary submitted to Phillips Laboratory, June 1997. www.ms.ornl.gov/researchgroups/composites/new%20orccmt%20pages/pdf/summary.pdf

24. Curliss, D. B. Air Force Research Laboratory Internal Report AFR 700B Polyimide, 1994.

25. Morgan, R. J.; Shin, E. E.; Zhou, J. Proc of 44th International SAMPE Symp 1999, 44, 1098-1110

26. Shin, E. E.; Morgan, R. J.; Zhou, J. Proc of 45th SAMPE Symp 2000, 45, 389-401.

27. Rice, B. P. Proc of High Temple Workshop XXVII, 1997.

28. Farmer, J. D.; Janke, C. J.; Lopata, V. J. Proc of the 43rd International SAMPE Symp 1998, 43, 1647.

29. Roylance, M. E.; Janke, C. J.; Tuss, J. M. Proc of the 43rd International SAMPE Symp 1998, 43, 1660.

30. Roylance, M. E.; Kirn, P. I Proc of the 46th International SAMPE Symp 2001, 46, 2515-2525.

31. Wilenski, M. S.; Aiken, R.; Gerzeski, R. Proc of the 47th International SAMPE Symp 2002, 47, 109-123.

32. Hay, J. N.; Hamerton, I.; Howlin, B. J.; Howgate, G. J.; O'Gara, P. M. Proc of the 46th International SAMPE Symp 2001, 46, 2140-2146.

33. Morgan, R. J.; Li, D.; Lu, J.; Ribeiro, R.; Moon, S.-W. Proc of the 47th International SAMPE Symp 2002, 47, 585-599.

34. Sroog, C. E; Endry, A. L.; Abramo, S. V.; Berr, C. E.; Edwards, W. M.; Oliver, K. L. J Polym Sci 1965, A3, 1373-90.

35. Sroog, C. E. Prog Polym Sci 1991, 16, 561-694.

36. Volksen, W. Adv Polym Sci 1994, 117, 111-164.

37. Gibbs, H. H. J Appl Polym Sci Appl Polym Symp 1979, 5, 207-222.

38. Serafini, T. T.; Delvigs, P.; Lightsey, G. R. J Appl Polym Sci 1972, 16, 905-915.

39. Hay, J. N.; Boyle, J. D.; Parker, S. F.; Wilson, D. Polymer 1989, 30, 1032-1040.

40. Landis, A. L.; Bilow, N.; Boschan, R. H.; Lawrence, R. E.; Aponyi, T. Polym Prepr, 1974, 15, 537-541.

41. Harris, F. W.; Pamidimukkala, A.; Gupta, R.; Das, S.; Wu, T.; Mock, G. J Macromol Sci 1984, A21, 1117-1135.

42. Smith, J. G.; Hergenrother, P. M. Polym Prepr 1994, 35, 353-354.

43. Smith, J. G.; Hergenrother, P. M. Polymer 1994, 35, 4857-4864.

44. Meyer, G. W.; Glass, T. E.; Grubbs, H. J.; McGrath, J. E. J Polym Sci Polym Chem 1995, 33, 2141-2149.

45. Lincoln, J. E.; Morgan, R. J.; Shin, E. E. J Polym Sci Phys 2001, 39, 2947-2959.

46. Vancraeynest, V.; Stille, J. K. Macromolecules 1980, 13, 1361-1367.

47. Droske, J. P.; Gaik, U. M.; Stille, J. K. Macromolecules 1984, 17, 10-14.

48. Takeichi, T.; Stille, J. K. Macromolecules 1986, 19, 2103-2108.

49. Stoessel, S.; Takeichi, T.; Stille, J. K.; Alston, W. B. J Appl Poly Sci 1988, 36, 1847-1864.

50. Alhakimi, G.; Klemm, E. J Polym Sci Polym Chem 1995, 33, 767-770.

51. Kuramoto, K.; Hayashi, K.; Nagai, K. J Polym Sci Polym Chem 1994, 32, 2501-2504.

52. Patel, H. S.; Patel, H. D. High Perform Polym 1992, 4, 19-33.

53. Hodgin, J. H. J Polym Sci Pol Chem 1976, 14, 409.

54. Dine-Hart, R. A.; Wright, W. W. Macromol Chem 1972, 153, 237.

55. Chang, G. E.; Jones, R. J. Proc of 28th National SAMPE Symp 1983, 728.

56. Wilson, D.; Stenzenberger, H. D.; Hergenrother, P. M. Polyimides, Blackie & Sons Ltd., 1990.

57. Clair, A. K. St.; Clair, T. L. St. Polym Eng Sci 1982, 22, 9.

58. Russell, J. D.; Kardos, J. L. Polym Compos 1997, 18, 64.

59. Shin, E. E.; Morgan, R. J.; Zhou, J. Proc of 45th International SAMPE Symp 2000, 45, 389-401.

60. Morgan, R. J.; Shin, E. E.; Lincoln J. E. Proc of High Temple Workshop XXI, Paper I, Clearwater Beach, FL, February, 2001.

61. Kreuz, J. A.; Hsiao, B. S.; Renner, C. A.; Goff, D. L. Macromolecules 1995, 28, 6926.

62. Srinivas, S.; Caputo, F. E.; Graham, M.; Gardner, S.; Davis, R. M.; McGrath, J. E.; Wilkes, G. L. Macromolecules 1997, 30, 1012.

63. Ratta, V.; Stancik, E. J.; Ayambem, A.; Pavatareddy, H.; McGrath, J. E.; Wilkes, G. L. Polymer 1999, 40, 1889.

64. Murphy, L. A. Morphological investigation of AFR-PEPA-N imide oligomers and their cured polyimides and the remodification of AFR-PEPA-N to achieve liquid-crystalline behavior, M.S. Thesis, Texas A&M University, 2003

65. Li, F.; Fang, S.; Ge, J. J.; Honigfort, P. S.; Chen J. C.; Harris, F. W.; Cheng, S. Z. D. Polymer 1999, 40, 4571.

66. Eastmond, G. C.; Paprotny, Macromolecules 1995, 28, 2140.

67. Eastmond, G. C.; Paprotny, Macromolecules 1995, 29, 1382.

68. Hsio, S. H.; Yang, C. P.; Yang, C. Y. J Polym Sci Pol Chem 1997, 35, 1487.

69. Hsio, S. H.; Li, C.T. J Polym Sci Pol Chem 1999, 37, 1435.

70. Tamai, S.; Yamashita, W.; Yamaguchi, A. J Polym Sci Pol Chem 1998, 36, 971.

71. Jensen, B.J., Polym Prepr 1996, 37, 222-223.

72. Mikroyannidis, J. A. J Macromol Sci 1992, A29, 137.

73. Pritchard, G.; Swan, M. Eur Polym J 1993, 29, 357.

74. Cubbon, R. C. P. Polymer 1965, 6, 419.

75. Wagner-Jauregg, T. H. Tetrahedron Lett 1967, 13, 1175–1176.

76. Gu, A. J.; Liang, G. Z.; Lan, L. W. J Appl Polym Sci 1996, 62(5), 799-803.

77. Hawthorne, D. G.; Hodkin, J. H.; Jakson, M. B.; Mortoncisro, T. C. High Perform Polym 1994, 6, 249.

78. Watson, K. A.; Bass, R. G. Polym Prepr 1979, 38(2), 237.

79. Ben Romdhane, H.; Chaâbouni, M. R.; Grenier-Loustalot, M. F.; Delolme, F.; Mison, P.; Sillion, B. Polymer 2000, 41(4), 1633-1639.

80. Harris, F. W.; Norris, S. O. J Polym Sci Pol Chem 1973, 11, 2143.

81. Kottner, N.; Klemm, E. Angew Makromol Chem 1998, 254, 39.

82. Dix, L. R.; Ebdon, J. R.; Flint, N. J.; Hodge, P.; O'Dell, R. Eur Polym J 1995, 31(7), 647-652.

83. Dix, L. R.; Ebdon, J. R.; Hodge P. Eur Polym J 1995, 31(7), 653-658.

84. Wang, C.-S.; Hwang, H.-J. Polymer 1996, 37(3), 499-503.

85. Lin, K.-F.; Lin, J.-S.; Cheng, C.-H. Polymer 1996, 37(21), 4729-4737.

86. Wu, C. S.; Liu, Y. L.; Chiu, Y.-S. Polymer 2002, 43(6), 1173-1179.

87. Vanaja, A.; Rao, R. M. V. G. K. Eur Polym J 2002, 38(1), 187-193.

88. Dinakaran, K.; Alagar, M.; Suresh Kumar, R. Eur Polym J 2003, 39(11), 2225-2233.

89. Liu, Y.-L.; Chen, Y.-J. Polymer 2004, 45(6), 1797-1804.

90. Hamerton, I.; Barton, J. M.; Chaplin, A.; Howlin, B. J.; Shaw, S. J. Polymer 2001, 42(6), 2307-2319.

91. Lin, R.-H.; Lu, W.-H.; Lin, C.-W. Polymer 2004, 45(13), 4423-4435.

92. Morgan, R. J.; Shin, E. E.; Rosenberg, B.; Jurek, A. Polymer 1997, 38(3), 639-646.

93. Rosenberg, B. A.; Boiko, G. N.; Morgan, R. J.; Shin, E. E. Polymer Science Ser. A 2001, 43(4), 389-399. Translated from Vysokomolekulyarnye Soedineniya Ser. A 2001, 43(4), 630-645.

94. Phelan, J. C.; Sung, C. S. P. Macromolecules 1997, 30(22), 6837-6844.

95. Phelan, J. C.; Sung, C. S. P. Macromolecules 1997, 30(22), 6845-6851.

96. Mijović, J.; Andjelić, S. Macromolecules 1996, 29, 239-246.

97. Farhataziz; Rodgers, M. A. J. Radiation Chemistry, Principles and Applications, VCH Publishers, Inc., New York, 1987

98. Bhattacharya, A. Prog Polym Sci 2000, 25(3), 371-401.

99. Spadaro, G.; Calderaro, E.; Tomarchio, E.; Dispenza, C. Radiat Phys Chem 2004, Available online 5 March 2004.

100. Dennis, G. R.; Garnett, J. L.; Zilic, Elvis. Radiat Phys Chem 2004, 71(1-2), 217-221.

101. Bajpai, M.; Shukla, V.; Kumar, A. Prog Org Coat 2002, 44 (4), 271-278.

102. Deans, J.; Kögl, M. Inter J Therm Sci 2000, 39(7), 762-769.

103. Chan, C. M.; Ko, T. M.; Hiraoka, H. Surf Sci Rep 1996, 24(1-2), 3-54.

104. Zhou, S.; Hawley, M. C. Compos Struct 2003, 61(4), 303-309.

105. Zhou, J.; Shi, C.; Mei, B.; Yuan, R.; Fu, Z. J Mater Process Tech 2003, 137(1-3), 156-158.

106. Nightingale, C.; Day, R. J. Compos Part A-Appl Sci 2002, 33(7), 1021-1030.

107. Al-Sheikhly, M.; McLaughlin, W. L. Radiat Phys Chem 1996, 48, 201.

108. Janke, C. J.; Dorsey, G. F.; Havens, S. J.; Lopata, V. J. Proc of 41st International SAMPE Symp 1996, 196-205.

109. Lopata, V. J.; Chung, M.; Janke, C. J.; Havens, S. J. Proc of 28th International SAMPE Tech Conf 1996, 901-910.

110. Drzal, L. T.; Rich, M. J.; Drown, E. K. Proc of 44th International SAMPE Symp 1999, 44, 633-646.

111. Janke, C. J.; Yarborough, K. D.; Drzal, L. T. Proc of 44th International SAMPE Symp 1999, 44, 47-657.

112. Lorenz D. H.; Azorlosa J. L.; Tu R. S. Radiat Phys Chem 1977, 9, 843-849.

113. Ali K. M. I.; Khan M. A.; Zaman M. M.; Hossain M. A. J Appl Polym Sci 1994, 54, 309-315.

114. Valette L.; Pascault J. P.; Magny B. Macromol Mater Eng 2002, 287, 52-61.

115. Wang, Z.; Deng, P.; Gao, L.; Ding M. J Appl Polym Sci 2004, 93(6), 2879-2882.

116. Joshi, S. C.; Liu, X. L.; Lam Y. C. Composite Sci Technol 1999, 59, 1003-1013.

117. Baoursereau, F.; et al. Proc of 45th International SAMPE Symp 2000, 45, 2235-2245.

118. Moon, S.; Morgan, R. J.; Lau, S. C. J Comp Mater 2004, 38, 357.

119. Seris, A.; Feve, M.; Mechin F.; Pascault, J. P. J Appl Polym Sci 1993, 48, 257-269.

120. Curliss, D. B.; Cowans, B. A.; Caruthers, J. M. Macromolecules 1998, 31, 6776-6782.

121. Grenier-Loustalot, M. F.; Da Cunha, L. Polymer 1998, 39, 1833-1843.

122. Yuan Q. L.; Huang F. O.; Jiao Y. S. J Appl Polym Sci 1996, 62, 459-464.

123. Shibahara, S.; Yamamoto, T.; Motoyoshiya, J.; Hayashi, S. Polym J 1998, 30, 410-413.

124. Wang, C. S.; Leu, T. S. Polymer 1999, 40, 5407-5413.

125. Boey, F. Y. C.; Song, X. L.; Yue, C. Y.; Zhao, Q. J Polym Sci Pol Chem 2000, 38, 907-913.

126. Hopewell, J. L.; George, G. A.; Hill, D. J. T. Polymer 2000, 41, 8231-8239.

127. Sunitha, M.; Reghunadhan, N. C. P.; Krishnan, K.; Ninan, K. N. Thermochim Acta 2001, 374, 159-169.

128. Chian, K. S.; Du, X. Y.; Goy, H. A.; Feng, J. L.; Yi, S.; Yue, C. Y. J Appl Polym Sci 2002, 84, 2935-2945.

129. Boey, F. Y. C.; Song, X. L.; Rath, S. K.; Yue, C. Y. J Appl Polym Sci 2002, 85, 227-235.

130. Tungare, A. T.; Martin, G. C. Polym Eng Sci 1993, 33, 614-621.

131. Morgan, R. J.; Jurek, R. J.; Yen, A.; Donnellan, T. Polymer 1993, 34, 835-842.

132. Hamerton, I. High Perform Polym 1996, 8, 83-95.

133. Lincoln, J. E.; Morgan, R. J.; Shin, E. E. Polym Composite 2001, 22, 397-419.

134. Wei, G. X.; Sue, H. -J. J Appl Polym Sci 1999, 74, 2539-2545.

135. Bao, L. R.; Yee, A. F.; Lee, C. Y. C. Polymer 2001, 42, 7323-7333.

136. Li, Y. M.; Miranda, J.; Sue, H.-J. Polym Eng Sci 2002, 42, 375-381

137. Pascault, J. P.; Sautereau, H.; Verdu, J.; Williams, R. J. J. Thermosetting Polymers; Marcel Dekker Inc: New York, 2002; Chapter 8

138. Tamura, H.; Tanake, M.; Murata, N. Bull Chem Soc Japan 1970, 73, 844.

139. Decker, C. Acta Polym 1994, 45, 333.

140. Chandra, R.; Son, R. K. Prog Polym Sci 1994, 19, 137-169.

141. Young, J. S.; Kannurpatti, A. R.; Bowman, C. N. Macromol Chem Phys 1998, 199, 1043.

142. Anseth, K. S.; Decker, C.; Bowman, C. N. Macromolecules 1995, 28, 4040.

143. Defoort, B.; Defoort, D. Coqueret, X. Macromol Theory Simul 2000, 9(9), 725-734.

144. Pascault, J. P.; Williams, R. J. J. J Polym Sci Pol Phys 1990, 28, 85.

145. Sastri, S. B; Keller, T. M.; Jones, K. M.; Armistead, J. P. Macromolecules 1993, 26, 6171.

146. Fang, X.; Rogers, D. F.; Scola, D. A.; Stevens, M. P. J Polym Sci Pol Chem 1998, 36, 461-470.

VITA

Yuntao Li was born in Lanzhou, China, on June 5th, 1975. He received his Bachelor of Science degree in chemistry from Lanzhou University in China in July 1994. He went on to receive his Master of Science degree in polymer chemistry from Lanzhou University in July 1997. That same year he went to The State Key Laboratory of Polymer Materials Engineering at Sichuan University in China for his polymer research. In 2001, he began his Ph.D. studies at Texas A&M University in mechanical engineering. In 2003, he changed his major from mechanical engineering to materials science and engineering.

His permanent address:

100 Datong Road Room 401, Hai Shi Wan Honggu District

Lanzhou, Gansu 730084

CHINA

His e-mail address:

liytus@yahoo.com